UNIVERSITY OF
KWAZULU-NATAL
INYUVESI
YAKWAZULU-NATALI

# Delivery of F*luc*-mRNA using functionalised gold nanoparticles *in vitro*

**Shandré Pillay**

A thesis submitted to the School of Life Sciences, University of KwaZulu-Natal, Westville in fulfilment of the degree of Master of Science in Biochemistry

*Supervisor*

**Professor Moganavelli Singh**

**2016 DURBAN**

# Delivery of F*luc*-mRNA using functionalised gold nanoparticles *in vitro*

**Shandré Pillay**

**2016**

A thesis submitted to the School of Life Sciences, University of KwaZulu-Natal, Westville, for the degree of Master of Science in Biochemistry.

This thesis is comprised of chapters written as research papers with an overall introduction, literature review and a final conclusion.

As the candidates supervisor I have approved this thesis for submission.

Supervisor: Professor Moganavelli Singh

Signature: ……

This is to certify that this thesis is the original work of Miss Shandré Pillay

Signature: …….

# ABSTRACT

Nanomedicine, a branch of nanotechnology which includes the use of nanoparticles, is set to revolutionize the area of gene therapy. Gold nanoparticles (AuNPs) have steadily gained favour as promising gene and drug delivery agents in clinical medicine for diagnostics and the treatment of diseases such as cancer. Cancer is a chronic disease with mortality rates increasing steadily. It has been highlighted as a genetic disease with a rising need for the development of innovative gene therapy strategies and, thus, the development of safe and effective gene delivery vehicles. AuNPs feature unique properties which includes small size, high dispersity, stability and surface plasmon resonance with a capacity for ease-of-synthesis and parametric control *via* chemical methods. Characteristics which favour gene delivery include their biocompatibility, voluntary cellular uptake and low core toxicity. Functionalisation with cationic polymers enhances the properties of AuNPs in terms of condensation of nucleic acids, cellular internalisation, protection against nucleases and release of the therapeutic gene for expression. Over the years, gene therapy applications have routinely utilized therapeutic plasmid DNA (pDNA) for treatment. However, pDNA expression is associated with many limitations hindering cellular trafficking and nuclear entry. As a promising alternative, mRNA molecules overcome these intracellular barriers with no risk of insertional mutagenesis. In this study, the unique properties of AuNPs, cationic polymers and mRNA molecules were exploited and optimized to provide effective gene delivery vehicles for the intracellular release of mRNA for future cancer gene therapy applications, an area of research which until recently has not been investigated. AuNPs were synthesized and functionalised with chitosan (CS) and poly-l-lysine (PLL), respectively. All nanoparticles and their nanocomplexes were characterized using UV-vis spectrophotometry, ICP, FTIR, transmission electron microscopy (TEM) and Nanoparticle tracking analysis (NTA). Functionalised AuNP:F*luc*-mRNA binding, compaction and nuclease protection were assessed using the gel retardation, dye displacement and nuclease protection assays, respectively. The effects of these nanocomplexes *in vitro* were assessed on three human cell lines, embryonic kidney (HEK293), colorectal adenocarcinoma (Caco-2) and breast adenocarcinoma (MCF-7). The cytotoxicity profile of the nanocomplexes was evaluated using the MTT assay and mRNA transfection efficiency assessed using the luciferase reporter gene assay in the three human cell lines. The AO/EB apoptosis assay was employed to confirm the mechanism of cell death as being either apoptotic or necrotic.

Results show that both functionalised nanocomplexes exhibit suitable and favourable properties such as small size (CS-AuNP nanocomplex: 95.0 nm and PLL-AuNP nanocomplex: 89.4 nm), colloidal stability (zeta potential: CS-AuNP nanocomplex: 25.9 mV and PLL-AuNP nanocomplex: -97.1 mV), efficient binding and protection against nucleases, low cytotoxicity (<40%) and significant transgene expression. Furthermore, these functionalised nanocomplexes exhibited apoptosis induction selective to cancer cells when compared to the non-cancer cell line. Functionalised AuNPs proved to be more efficient than their respective cationic polymers by themselves, indicating that AuNPs improve cationic polymer properties and functions. Overall, these characteristics highlight the potential of these AuNPs as suitable carriers of mRNA *in vitro* and with further studies can be extended to biomedical applications, especially in cancer and immuno-therapy.

**Keywords:** cancer, cytotoxicity, F*luc*-mRNA, poly-l-lysine, chitosan, gene expression, gold nanoparticles, immuno-therapy

# DECLARATION 1 - PLAGIARISM

I, Shandré Pillay declare that

1. The research reported in this thesis is original, except where otherwise stated.
2. This thesis has not been submitted for any degree or examination at any other university.
3. This thesis does not contain other persons' data, pictures, graphs, or other information unless specifically acknowledged as being sourced from other persons.
4. This thesis does not contain other persons' writing, unless specifically acknowledged as being sourced from other researchers. Where other written sources have been quoted, then:
    a. Their words have been re-written but the general information attributed to them has been referenced.
    b. Where their exact words have been used, then their writing has been placed in italics and inside quotation marks, and referenced.
5. This thesis does not contain text, graphics or tables copied and pasted from the internet, unless specifically acknowledged, and then source being detailed in the thesis and in the References sections.

Signature: ……

## DECLARATION 2 – PUBLICATIONS

### Manuscripts in preparation

### Manuscript 1

S. Pillay and M. Singh. Chitosan functionalised gold nanoparticle mediated delivery of F*luc*-mRNA *in vitro*: synthesis, characterization, cytotoxicity and transfection efficiency.

### Manuscript 2

S. Pillay and M. Singh. Poly-l-lysine functionalised gold nanoparticle mediated delivery of F*luc*-mRNA *in vitro*: synthesis, characterization, cytotoxicity and transfection efficiency.

### Conference Presentations

1. Poster presentation - Delivery of F*luc*-mRNA using functionalised gold nanoparticles *in vitro* - 25$^{th}$ South African Society of Biochemistry and Molecular Biology (SASBMB) congress, East London, Eastern Cape 10$^{th}$-14$^{th}$ July 2016. Awarded 1$^{st}$ prize.

2. Poster presentation - Delivery of F*luc*-mRNA using functionalised gold nanoparticles *in vitro* - University of KwaZulu-Natal, postgraduate research day 29$^{th}$ November 2016.

# ACKNOWLEDGEMENTS

I wish to express my sincere gratitude and appreciation to the following persons and institutions:

- To the Lord, for blessing me with the opportunity of furthering my education and seeing me through this course of study.

- My supervisor, Professor Moganavelli Singh, for giving me excellent guidance and advice, being patient and supportive, all of which has ensured the completion of this degree.

- The UKZN Research office, Durban and National Research Foundation (NRF), Pretoria, South Africa for the financial assistance.

- My fellow laboratory members, Lorenzo, Vareessh, Fiona, Aliscia, Geraldine, Saffiya, Nirasha, Nicolisha, Adhika, Zoe, Londi, Rose as well as other post-graduates at UKZN for their assistance and moral support during this study.

- My father, the late Mr S. Pillay and my mother Mrs S. Pillay for their love, support and motivation.

- To my family Jade, Natasha, Deric, Ivan and Alwyn for their moral support and assistance in this study.

- My nephews and nieces Jordan, Caden, Jiran, Aria and Tamzin for inspiring me to be a great role model by furthering my education.

# DEDICATION

*This thesis is dedicated to my late father, Mr. Samuel Pillay whose endless love, support, encouragement and sacrifice have paved the way for my future.*

# TABLE OF CONTENTS

**ABSTRACT**.....**ii**
**DECLARATION 1 – PLAGIARISM**.....**iv**
**DECLARATION 2 – PUBLICATIONS** .....**v**
**ACKNOWLEDGEMENTS** .....**vi**
**DEDICATION**.....**vii**
**TABLE OF CONTENTS** .....**viii**
**LIST OF TABLES** .....**xiii**
**LIST OF FIGURES** .....**xiv**
**ABBREVIATIONS** .....**xix**

**CHAPTER ONE**.....**1**
**INTRODUCTION**.....**1**
**1.1** Aim and Objectives.....**2**
**1.2** Outline of thesis.....**3**

**CHAPTER TWO**.....**5**
**LITERATURE REVIEW**.....**5**
**2.1** Cancer……..…….**5**
**2.1.1** The burden of cancer, causes and risk factors…….……...**5**
**2.1.2** The development and genetics of cancer…….……..**6**
**2.2** Gene therapy……..……..…**8**
**2.2.1** Viral gene delivery methods…..……**8**
**2.2.2** Non-viral gene delivery methods……**10**
**2.2.2.1** Physical methods…….……..……..**10**
**2.2.2.2** Chemical methods……**11**
**2.2.3** Chitosan…….……...**12**
**2.2.4** Poly-l-lysine……**13**
**2.3** Inorganic Nanoparticles : Gold nanoparticles (AuNPs)……..…….....**14**
**2.3.1** Properties of AuNPs ……....**15**
**2.3.2** AuNP Synthesis ……...**17**
**2.3.2.1** Chemical methods……....**17**

**2.3.2.2** Physico-Chemical methods ……**19**
**2.3.2.3** Biological methods……..……..**19**
**2.3.3** Functionalisation of AuNPs with Cationic Polymers (CPs)……**20**
**2.3.4** Gene delivery and Gold Nanoparticles ……..…….**22**
**2.3.4.1** Intracellular Trafficking……...**23**
**2.3.4.2** Cellular uptake……**26**
**2.3.4.3** Transfection Efficiency……**29**
References……**30**

**CHAPTER THREE**……...…**38**

**CHITOSAN FUNCTIONALISED GOLD NANOPARTICLE MEDIATED DELIVERY OF F*luc*-mRNA *IN VITRO*: SYNTHESIS, CHARACTERIZATION, CYTOTOXICITY AND TRANSFECTION EFFICIENCY**……...……**38**

Abstract……**39**
**3.1** Introduction……**40**
**3.2** Materials and methods……...**42**
**3.2.1** General materials and reagents……...……..**42**
**3.2.2** Experimental methods…….…**43**
**3.2.2.1** Colloidal AuNP synthesis by citrate reduction……**43**
**3.2.2.2** Functionalisation of AuNPs with chitosan……..……**44**
**3.2.2.3** Elemental verification of synthesized nanoparticle solutions…….**45**
**3.2.2.3.1** Inductively Coupled Plasma (ICP) analysis……..……**45**
**3.2.2.3.2** Fourier Transformed Infrared Spectroscopy (FTIR) analysis……..……..**46**
**3.2.2.3.3** Qualitative ninhydrin test for amino acids…….**46**
**3.2.2.4** Formation of mRNA:NP complexes…….……..…….**46**
**3.2.2.5** Characterization of nanoparticle and nanocomplexes……..……**47**
**3.2.2.5.1** UV-Vis optical spectrophotometry analysis……...……**47**
**3.2.2.5.2** Transmission Electron Microscopy (TEM)……...…**47**
**3.2.2.5.3** Nanoparticle Tracking Analysis (NTA)…….....**47**
**3.2.2.6** Assessment of CS and CS-AuNP binding to F*luc*-mRNA……..……**48**
**3.2.2.6.1** Gel retardation assay……...…**48**

**3.2.2.6.2** Dye displacement/Intercalation assays……...……**49**
**3.2.2.6.2.1** Ethidium bromide dye displacement…….……**49**
**3.2.2.6.2.2** SYBR green dye displacement……...……**50**
**3.2.2.7** Nuclease Protection assay……..…..**50**
**3.2.3** *In Vitro* cell culture studies……..……**51**
**3.2.3.1** Cell culture materials and reagents…….……**51**
**3.2.3.2** Reconstitution of frozen cells and routine cell culture maintenance……..…..**52**
**3.2.3.3** Trypsinization of cells and cell counts……...……..**53**
**3.2.3.4** Cryopreservation……..**53**
**3.2.3.5** MTT cytotoxicity assay……**53**
**3.2.3.6** Luciferase reporter gene assay……...…..**54**
**3.2.3.7** Acridine Orange/Ethidium Bromide (AO/EB) apoptosis assay……..….**55**
**3.2.3.8** Statistical analysis……...…….**57**
**3.3** Results and Discussion……...……..…**57**
**3.3.1** Characterization of Nanoparticles and Nanocomplexes…….....**57**
**3.3.1.1** Chemical analysis…….……**57**
**3.3.1.2** UV-Vis optical spectrophotometry analysis and dialysis……..……...…**58**
**3.3.1.3** Qualitative Ninhydrin test for amine groups…….……...…**60**
**3.3.1.4** Transmission electron microscopy……...…**60**
**3.3.1.5** Nanoparticle tracking analysis (NTA)…….……**61**
**3.3.2** Assessment of CS and CS-AuNP binding to F*luc*-mRNA……..……**63**
**3.3.2.1** Gel retardation assay……**63**
**3.3.2.2** Dye Displacement/Intercalation assays…...……**65**
**3.3.3** Nuclease Protection assay……**67**
**3.3.4** *In Vitro* cell culture studies……..……**68**
**3.3.4.1** Reconstitution and cell culture maintenance……**68**
**3.3.4.2** MTT cytotoxicity assay……**69**
**3.3.4.3** Luciferase reporter gene assay…….……**72**
**3.3.4.4** Acridine Orange/Ethidium Bromide (AO/EB) apoptosis assay…..……**75**
**3.4** Conclusion…….……**79**
References…….……...……**80**

**CHAPTER FOUR**……..……**86**

**POLY-L-LYSINE FUNCTIONALISED GOLD NANOPARTICLE MEDIATED DELIVERY OF F*luc*-mRNA *IN VITRO*: SYNTHESIS, CHARACTERIZATION, CYTOTOXICITY AND TRANSFECTION EFFICIENCY**……..……**86**

Abstract……..……..……**87**

**4.1** Introduction……..……..…**88**

**4.2** Materials and methods……...…**90**

**4.2.1** Materials……...……**90**

**4.3** Synthesis, Characterisation and Nanocomplex Evaluation…….……...……**90**

**4.3.1** Synthesis of citrate reduced colloidal AuNP solution……..……**90**

**4.3.2** Functionalisation of AuNPs with poly-l-lysine (PLL)…….……**91**

**4.3.3** Inductively Coupled Plasma (ICP) analysis…….....……**91**

**4.3.4** Fourier Transformed Infrared Spectroscopy (FTIR) analysis……..……**91**

**4.3.5** Qualitative ninhydrin test for amino groups…….……**91**

**4.3.6** Formation of mRNA:PLL-AuNP complexes……...……**92**

**4.3.7** UV-Visible spectrophotometry analysis……..…**92**

**4.3.8** Transmission electron microscopy (TEM)…….…….……**92**

**4.3.9** Nanoparticle Tracking Analysis (NTA)……. ……**93**

**4.3.10** Gel retardation assay……**93**

**4.3.11** Dye displacement/Intercalation assays…….……**94**

**4.3.11.1** Ethidium bromide dye displacement…….…….……**94**

**4.3.11.2** SYBR Green dye displacement…….…….……**95**

**4.3.12** Nuclease Protection assay……**95**

**4.4** *In Vitro* cell culture studies……**96**

**4.4.1** Cell culture materials and reagents……..……**96**

**4.4.2** Cell culture maintenance……..……**97**

**4.4.3** MTT cytotoxicity assay…….……...……**98**

**4.4.4** Luciferase reporter gene assay…….……**98**

**4.4.5** Acridine Orange/Ethidium Bromide (AO/EB) apoptosis assay……...……**99**

**4.4.6** Statistical analysis……..……**100**

**4.5** Results and Discussion…….……..……**100**

**4.5.1** Characterization of nanoparticles and complexes…….……..…**100**

**4.5.1.1** Chemical analysis……..……**100**
**4.5.1.2** UV-Vis optical spectrophotometry analysis……..…….……**101**
**4.5.1.3** Qualitative ninhydrin test for amine groups……..…….……**103**
**4.5.1.4** Transmission electron microscopy (TEM)…… ……**103**
**4.5.1.5** Nanoparticle tracking analysis (NTA)…...……**104**
**4.5.2** Assessment of PLL and PLL-AuNP binding to F*luc*-mRNA……**106**
**4.5.2.1** Gel retardation assay…….…….……**106**
**4.5.2.2** Dye displacement/Intercalation assays..…..……**107**
**4.5.3** Nuclease protection assay……..……**109**
**4.5.4** *In Vitro* cell culture studies……..……..……**110**
**4.5.4.1** Cell culture maintenance…….……...**110**
**4.5.4.2** MTT cytotoxicity assay……..……**110**
**4.5.4.3** Luciferase reporter gene assay……..…..……**113**
**4.5.4.4** Acridine Orange/Ethidium Bromide (AO/EB) apoptosis assay..……...……**116**
**4.6** Conclusion…….……..……**119**
References…….…….……**121**

**CHAPTER FIVE**……..……**126**
**CONCLUSION**…….……**126**
**5.1** Future recommendations……..……**127**

**Appendix A1: ICP results**…….……..…..……**128**
**Appendix A2: FTIR spectra**…….……..…..……**129**
**Appendix B: NTA results**……**130**
**Appendix C: Conference presentation**……...……**135**

# LIST OF TABLES


| | | |
|---|---|---|
| **Table 2.1** | Examples of viral vectors, properties, advantages and disadvantages | **9** |
| **Table 3.1** | Preparation of complexes for the gel retardation assay | **49** |
| **Table 3.2** | Preparation of complexes for the nuclease digestion assay | **51** |
| **Table 3.3** | Preparation of complexes for the AO/EB apoptosis assay | **56** |
| **Table 3.4** | Size, zeta potential and concentration of the nanoparticle solutions obtained from nanoparticle tracking and zeta potential analysis | **63** |
| **Table 3.5** | Apoptotic index values for each complex on each cell line | **78** |
| **Table 4.1** | Nanocomplex preparations for gel retardation assay | **94** |
| **Table 4.2** | Preparation of complexes for the nuclease protection assay | **95** |
| **Table 4.3** | Composition of complexes used in the AO/EB apoptosis assay | **100** |
| **Table 4.4** | Size, zeta potential and concentration of the nanoparticle solutions obtained from nanoparticle tracking and zeta potential analysis | **105** |
| **Table 4.5** | Apoptotic index values for each nanocomplex in the three cell lines | **119** |

# LIST OF FIGURES


| | | |
|---|---|---|
| **Figure 2.1** | Cancer-causing factors and their related incidences worldwide | **6** |
| **Figure 2.2** | Morphological differences between normal and cancer cells | **7** |
| **Figure 2.3** | Various colours of colloidal AuNP solutions in relation to their size | **15** |
| **Figure 2.4** | Diagram depicting the various shapes of synthesized AuNPs | **16** |
| **Figure 2.5** | Reaction for the synthesis of AuNPs by sodium citrate reduction of $HAuCl_4$ using the Turkevich method | **18** |
| **Figure 2.6** | Electrostatic interactions between citrate capped AuNPs and PLL | **21** |
| **Figure 2.7** | Hydrogen bonding between PLL and citrate capped AuNPs | **22** |
| **Figure 2.8** | mRNA structure and components | **23** |
| **Figure 2.9** | Mechanism of cationic polymer-based nanoparticle gene delivery and expression | **24** |
| **Figure 2.10** | DNA and mRNA gene expression pathways | **25** |
| **Figure 2.11** | Representation of passive and active cellular uptake of AuNPs | **27** |
| **Figure 3.1** | Diagram depicting the formation of a citrate reduced AuNP core resulting from the Turkevich method | **43** |
| **Figure 3.2** | Schematic representation of the colour transitions observed during the synthesis of AuNPs | **44** |

| | | |
|---|---|---|
| **Figure 3.3** | Image of CS functionalised AuNP (CS-AuNP) solution | **45** |
| **Figure 3.4** | Mechanism depicting the reduction of MTT to Formazan by mitochondrial reductase present in living cells | **54** |
| **Figure 3.5** | Mechanism of the bioluminescence exhibited upon oxidation of the substrate D-Luciferin by the luciferase enzyme present in transfected cells | **55** |
| **Figure 3.6** | UV-Vis spectrum of AuNP, CS-AuNP before dialysis and CS-AuNP after dialysis indicating a shift in SPR absorbance after functionalization | **59** |
| **Figure 3.7** | UV-Vis spectrum of the CS-AuNP:F*luc*-mRNA complex indicating an absorbance at 540 nm | **59** |
| **Figure 3.8** | Image of the light purple CS-AuNP solution after the ninhydrin test indicating a positive reaction | **60** |
| **Figure 3.9** | Transmission electron micrographs depicting the morphology of (A) AuNPs, (B) CS-AuNP and (C) CS-AuNP:F*luc*-mRNA at a magnification of 50 000× | **61** |
| **Figure 3.10** | Gel retardation study of (A) CS-AuNP:F*luc*-mRNA and (B) CS:F*luc*-mRNA complexes. Incubation mixtures (10 µl) in 20 mM HEPES, 150 mM NaCl (pH 7.5) contained varying amounts of (A) CS-AuNP and, (B) CS in lanes 1–8 (0, 0.025, 0.05, 0.075, 0.1, 0.125, 0.15, 0.175 µg) and F*luc*-mRNA (0.25 µg) | **64** |
| **Figure 3.11** | Comparison of relative fluorescence between the CS-AuNP and CS complexes using the Ethidium Bromide intercalation assay | **66** |

| | | |
|---|---|---|
| **Figure 3.12** | Comparison of the relative fluorescence between CS-AuNP and CS complexes using the SYBR Green intercalation assay | **66** |
| **Figure 3.13** | Nuclease digestion of CS-AuNP:F*luc*-mRNA and CS:F*luc*-mRNA complexes. Incubation mixtures (10 µl) in 20 mM HEPES, 150 mM NaCl (pH 7.5) contained a constant amount of F*luc*-mRNA (0.25 µg) in all lanes and varying amounts of CS-AuNP, lanes 1-3 (0.075, 0.1, 0.125 µg) and CS, lanes 4-6 (0.075, 0.1, 0.125 µg). C1 contained undigested F*luc*-mRNA and C2 contained FBS-digested F*luc*-mRNA | **68** |
| **Figure 3.14** | Images of confluent cell lines (A) HEK293, (B) Caco-2 and (C) MCF-7 using phase contrast microscopy at a 10 000× magnification | **69** |
| **Figure 3.15** | MTT cytotoxicity assay of complexes in cell lines: (A) HEK293, (B) Caco-2 and (C) MCF-7. Data represented as means ± SD (n=3), * $p<0.05$, ** $p<0.01$ and ** $p<0.001$ were considered statistically significant as determined by the Dunnet test | **71** |
| **Figure 3.16** | Luciferase gene expression activity of complexes measured in RLU/mg protein assayed in cell lines: (A) HEK293, (B) Caco-2 and (C) MCF-7. Data represented as mean ± SD (n=3), * $p<0.05$, ** $p<0.01$ and *** $p<0.001$ were considered statistically significant as determined by the Tukey-Kramer test | **74** |
| **Figure 3.17** | Fluorescence images obtained from the AO/EB apoptosis assay on HEK293, Caco-2 and MCF-7 cell lines at 20× magnification. A= apoptotic cells, N= necrotic | **77** |

| | | |
|---|---|---|
| **Figure 3.18** | Fluorescence intensity (FI) of cell lines HEK293, Caco-2 and MCF-7 with and without treatment of the complexes. Data represented as mean ± SD (n=3) | **78** |
| **Figure 4.1** | UV-Vis spectrum of AuNPs, PLL-AuNPs before and after dialysis indicating the shift in SPR absorbance after functionalization | **102** |
| **Figure 4.2** | UV-Vis spectrum of the PLL-AuNP:F*luc*-mRNA nanocomplex indicating a red shift to 620 nm | **102** |
| **Figure 4.3** | The positive dark purple PLL-AuNP reaction produced in the ninhydrin test | **103** |
| **Figure 4.4** | Transmission electron micrographs of (A) AuNPs, (B) PLL-AuNPs at 50 000 ×, and (C) PLL-AuNP:F*luc*-mRNA at a magnification of 500 000 ×. Bar = 50 nm | **104** |
| **Figure 4.5** | Gel retardation study of (A) PLL-AuNP:F*luc*-mRNA and (B) PLL:F*luc*-mRNA complexes. Incubation mixtures (10 µl) in 20 mM HEPES, 150 mM NaCl (pH 7.5) contained varying amounts of (A) PLL-AuNP and (B) PLL in lanes 1–8 (0, 0.025, 0.05, 0.075, 0.1, 0.125, 0.15, 0.175 µg) and F*luc*-mRNA (0.25 µg) | **106** |
| **Figure 4.6** | Comparison of the relative fluorescence between the PLL-AuNP and PLL complexes using the EtBr intercalation assay. Arrows indicate the point of inflection | **108** |
| **Figure 4.7** | Comparison of the relative fluorescence between PLL-AuNP and PLL complexes using the SYBR Green intercalation assay. Arrows indicate the point of inflection | **108** |

| | | |
|---|---|---|
| **Figure 4.8** | Nuclease digestion of PLL-AuNP:F*luc*-mRNA and PLL:F*luc*-mRNA complexes. Incubation mixtures (10 µl) in 20 mM HEPES, 150 mM NaCl (pH 7.5) contained a constant amount of F*luc*-mRNA (0.25 µg) in all lanes and varying amounts of PLL-AuNP, lanes 1-3 (0.15, 0.175, 0.2 µg) and PLL, lanes 4-6 (0.125, 0.15, 0.175µg). C1 contained undigested F*luc*-mRNA and C2 contained FBS-digested F*luc*-mRNA | **109** |
| **Figure 4.9** | Images of cell lines (A) HEK293, (B) Caco-2 and (C) MCF-7 using phase contrast microscopy at a 10 000× magnification | **110** |
| **Figure 4.10** | MTT cytotoxicity assay of complexes in cell lines: (A) HEK293, (B) Caco-2 and (C) MCF-7. Data represented as means ± SD (n=3), * $p<0.05$, ** $p<0.01$ and ** $p<0.001$ were considered statistically significant as determined by the Dunnet test | **112** |
| **Figure 4.11** | Luciferase gene expression activity of nanocomplexes in RLU/mg protein in cell lines: (A) HEK293, (B) Caco-2 and (C) MCF-7. Data represented as mean ± SD (n=3), * $p<0.05$, ** $p<0.01$ and *** $p<0.001$ were considered statistically significant as determined by the Tukey-Kramer test | **116** |
| **Figure 4.12** | Fluorescence images obtained for the AO/EB apoptosis assay on HEK293, Caco-2 and MCF-7 cell lines at 20× magnification. A= apoptotic cells, N= necrotic cells, L= live cells | **118** |
| **Figure 4.13** | Fluorescence intensity (FI) in cell lines HEK293, Caco-2 and MCF-7 with and without treatment of the complexes. Data represented as mean ± SD (n=3) | **119** |

# ABBREVIATIONS

| | |
|---|---|
| **ζ potential** | Zeta potential |
| **Abs** | Absorbance |
| **ANOVA** | One-way analysis of variance |
| **AO/EB** | Acridine orange/Ethidium bromide |
| **ATCC** | American tissue culture collection |
| **ATR** | Attenuated Total Reflectance |
| **Au** | Gold |
| **AuNPs** | Gold nanoparticles |
| **BCA** | Bicinchoninic acid |
| **C3A** | Primary rat hepatocyte cell line |
| **Caco-2** | Colorectal adenocarcinoma cell line |
| **CP-AuNPs** | Cationic polymer functionalised gold nanoparticles |
| **CPs** | Cationic polymers |
| **CS** | Chitosan |
| **CS-AuNPs** | Chitosan functionalised gold nanoparticles |
| **CTAB** | Cetyltrimethyl ammonium bromide |
| **DMSO** | Dimethylsulphoxide |
| **DNA** | Deoxyribonucleic acid |
| **EDTA** | *N*, *N*, *N'*, *N'*-ethylenediaminetetra acetic acid |
| **EMEM** | Eagle's Minimum essential medium |
| **EtBR** | Ethidium bromide |

| | |
|---|---|
| **FBS** | Fetal bovine serum |
| **F*luc*:mRNA** | Fluorescent luciferase-encoded messenger ribonucleic acid |
| **FTIR** | Fourier transformed infrared radiation spectroscopy |
| **$HAuCl_4$** | Hydrochloroauric acid |
| **HBS** | Hepes buffered solution |
| **HEK293** | Human embryonic kidney cells cell line |
| **HepG2** | Human hepatocyte cell line |
| **ICP** | Inductively coupled plasma |
| **ICP-OES** | Inductively coupled plasma-Optical emission spectroscopy |
| **IR** | Infrared radiation |
| **L1210** | Lymphoid leukaemia cell line |
| **M** | Molar |
| **MCF-7** | Human breast adenocarcinoma cell line |
| **mg** | Milligram |
| **miRNA** | Micro ribonucleic acid |
| **ml** | Millilitre |
| **mM** | Milli mole |
| **MPS** | Mononuclear phagocyte systems |
| **mRNA** | Messenger ribonucleic acid |
| **MTT** | 3-(4, 5-dimethylthiazol-2-yl)-2, 5-diphenyltetrazolium bromide |
| **mV** | Millivolt |
| **Mw** | Molecular weight |

| | |
|---|---|
| **$NaBH_4$** | Sodium borohydride |
| **nm** | Nanometre |
| **NP** | Nanoparticle |
| **NTA** | Nanoparticle tracking analysis |
| **P38** | macrophage derived tumour cell line |
| **P388** | Erythro-leukaemia cell line |
| **PBS** | Phosphate buffered saline |
| **pDNA** | Plasmid DNA |
| **PEG** | Polyethylene glycol |
| **PLL** | Poly-l-lysine |
| **PLL-AuNPs** | Poly-l-lysine functionalised gold nanoparticles |
| **PMT** | Photo Multiplier Tube |
| **RAW264.7** | Murine monocyte-macrophage cell line |
| **rev/min** | Revolutions per minute |
| **RLU** | Relative light units |
| **SD** | Standard deviation |
| **SDS** | Sodium dodecyl sulphate |
| **SEM** | Scanning electron microscopy |
| **siRNA** | Small interfering RNA |
| **SPR** | Surface plasmon resonance |
| **TEM** | Transmission electron microscopy |
| **THP-1** | Monocytic cell line |

| | |
|---|---|
| **TPE** | Tris-phosphate-ethylenediamine tetra acetic acid |
| **UV-vis** | Ultraviolet-visible spectroscopy |
| **V** | Volts |
| **v/v** | Volume to volume ratio |
| **w/v** | Weight to volume ratio |
| **w/w** | Weight to weight ratio |
| **µg** | Micrograms |
| **µl** | Microliters |
| **µM** | Micromole |

# CHAPTER ONE

## Introduction

Cancer is a leading global health concern, claiming more than 8 million deaths annually which is expected to rise to 23.6 million deaths by 2030 (International Agency for Research on Cancer and World Health Organization, 2014). The basic hallmark of cancer is uncontrolled cell proliferation which is coupled with invasion and metastasis, induction of angiogenesis, resistance to apoptosis, altered differentiation, self-sufficient in-growth signals, resistance to anti-growth factors and secretion of growth factor molecules (Hanahan and Weinberg, 2011). These molecular mechanisms render many of the conventional cancer treatments such as chemotherapy and radiotherapy inefficient due to a lack of target cell specificity, multi-drug resistance, poor drug penetration and unpleasant side-effects (Pedrosa *et al*., 2015). The pathophysiological and genetic processes contributing to cancer cell transformation and tumorigenesis require much investigation and the development of novel innovative cancer treatment strategies is crucial.

Gene therapy is the delivery of therapeutic nucleic acids for the treatment of genetic diseases including cancer (Shan *et al*., 2012). The challenge facing gene therapy is the development of an ideal gene delivery system which can safely, efficiently and selectively deliver the nucleic acid cargo to the intended cells (Verma *et al*., 2014), in addition to overcoming the various intracellular barriers encountered (Elsabahy *et al*., 2011). The use of non-viral delivery systems has gained favour due to their unlimited clone capacity, low immunogenicity, low cytotoxicity and ability for repeated application, in comparison to viral methods (Gardlík *et al*., 2005).

Inorganic nanoparticles have recently emerged as attractive nanocarriers in comparison to the traditional lipid-based vectors due to their numerous advantages such as tuneable size and surface properties, multifunctional capabilities and the capacity to translate the metal core's physical properties to the delivery vehicle (Ding *et al*., 2014). In particular, gold nanoparticles (AuNPs) provide a suitable platform for the development of efficient gene delivery vehicles due to characteristics such as their inert core, small size, colloidal stability, high dispersity and surface plasmon resonance. AuNPs possess a high surface-to-volume ratio which allows for facile modification with various functional moieties such as cationic

polymers which include chitosan and poly-l-lysine, thus controlling their reactivity, degree of toxicity and cellular uptake (Sivaramakrishnan *et al*., 2014).

These cationic polymer functionalised AuNPs possess additional advantages such as low toxicity, biodegradability, bio-adhesiveness ensuring localized concentration of nucleic acid molecules *via* electrostatic interactions, protection against nuclease degradation, possibility of receptor-mediated endocytosis and release of the therapeutic cargo *via* the "proton-sponge effect" (Pedrosa *et al*., 2015).

To date, plasmid DNA (pDNA) has been commonly used in gene therapy strategies. However, the use of pDNA faces many challenges such as the requirement for transportation across the nuclear membrane, cell-cycle dependency and the use of large quantities to elicit gene expression. This has been identified as a rate-limiting step in gene transfection (Ding *et al*., 2014). In addition, pDNA carries the risk of insertional mutagenesis and induction of immune responses due to their viral promoter components. In comparison, mRNA is able to overcome these endosomal barriers, does not require nuclear uptake, produces rapid gene expression as protein translation occurs within the cytoplasm, has no risk of insertional mutagenesis, is cell-cycle independent and is suitable for hard-to-transfect-cells (Matsui *et al*., 2015).

This study is novel in that it exploits the unique properties of cationic polymer functionalised AuNPs as delivery vehicles for mRNA molecules encompassing a luciferase gene (F*luc*-mRNA) to investigate gene delivery and expression in three mammalian cell lines. This study will serve to provide a platform for determining the feasibility of these mRNA nanocomplexes in future genetic vaccination and immunotherapy in cancer treatment, an area of research which until recently has not been fully investigated.

### 1.1 Aim and objectives

This study aims to design, synthesize, functionalise and fully characterize the AuNPs, functionalised AuNPs and their nanocomplexes with F*luc*-mRNA. Functionalisation of AuNPs will be carried out using the cationic polymers, chitosan and poly-l-lysine. Furthermore, their cytotoxicity, transgene expression and apoptosis induction will be examined on selected mammalian cell lines *in vitro*.

The main objectives will include:

1. To synthesize AuNPs using the sodium citrate reduction method.
2. To functionalise AuNPs with chitosan (CS) and poly-l-lysine (PLL).
3. To fully characterize the synthesized AuNPs, functionalised AuNPs and nanocomplexes.
4. To assess the binding and protection ability of the functionalised AuNPs, CS and PLL to F*luc*-mRNA using the gel retardation, dye displacement and nuclease protection assays.
5. To finally investigate the biological activity of these nanocomplexes with regards to cytotoxicity using the MTT assay gene expression using the Luciferase reporter gene assay, and apoptosis induction using the acridine orange-ethidium bromide (AO/EB) dual staining method *in vitro*.

### 1.2 Outline of thesis

This thesis is written in the format of two research papers and is divided into five chapters.

**Chapter 1** includes a basic introduction highlighting the need for this research, together with the aim and objectives of the study.

**Chapter 2** provides a detailed and up to date review of literature and contextual information on the various areas of interest in this study, including cancer, gene therapy, cationic polymers and AuNPs.

**Chapter 3** is presented in the format of a research paper which includes a brief introduction, methods and materials, results, discussion and a conclusion. The title of the paper is 'Chitosan functionalised gold nanoparticle mediated delivery of F*luc*-mRNA *in vitro*: synthesis, characterization, cytotoxicity and transfection efficiency.'

**Chapter 4** is also presented in the format of a research paper which includes a brief introduction, methods and materials, results, discussion and a conclusion. The title of the paper is 'Poly-l-lysine functionalised gold nanoparticle mediated delivery of F*luc*-mRNA *in vitro*: synthesis, characterization, cytotoxicity and transfection efficiency.'

**Chapter 5** provides the concluding remarks, summarizing and highlighting the results obtained in addition to future recommendations.

## REFERENCES


Ding, Y., Jiang, Z., Saha, K., Kim, C. S., Kim, S. T., Landis, R. F., and Rotello, V. M. (2014). Gold nanoparticles for nucleic acid delivery. *Molecular Therapy*, *22*(6), 1075.

Elsabahy, M., Nazarali, A., and Foldvari, M. (2011). Non-viral nucleic acid delivery: key challenges and future directions. *Current drug delivery*, *8*(3), 235-244.

Gardlík, R., Pálffy, R., Hodosy, J., Lukács, J., Turna, J., and Celec, P. (2005). Vectors and delivery systems in gene therapy. *Medical Science Monitor*, *11*(4), RA110-RA121.

Hanahan, D., and Weinberg, R. A. (2011). Hallmarks of cancer: the next generation. *Cell*, *144*(5), 646-674.

International Agency for Research on Cancer and World Health Organization. (2014). World Cancer Report. (Vol. 505). Lyon, France: International Agency for Research on Cancer Press.

Matsui, A., Uchida, S., Ishii, T., Itaka, K., and Kataoka, K. (2015). Messenger RNA-based therapeutics for the treatment of apoptosis-associated diseases. *Scientific reports*, *5*.

Pedrosa, P., Vinhas, R., Fernandes, A., and Baptista, P. V. (2015). Gold nanotheranostics: proof-of-concept or clinical tool? *Nanomaterials*, *5*(4), 1853-1879.

Shan, Y., Luo, T., Peng, C., Sheng, R., Cao, A., Cao, X., Shi, X. (2012). Gene delivery using dendrimer-entrapped gold nanoparticles as nonviral vectors. *Biomaterials*, *33*(10), 3025-3035.

Sivaramakrishnan, C., Jositta, S. J., and Yadavalli, T. (2014). Surface functionalization of gold nanoparticles for targeted drug delivery. *International Journal of ChemTech Research*, *7*(3), 1198-1205.

Verma, H. N., Singh, P., and Chavan, R. (2014). Gold nanoparticle: synthesis and characterization. *Veterinary world*, *7*(2), 72-77.

# CHAPTER TWO

# LITERATURE REVIEW

## 2.1 Cancer

The global health impact of cancer has been a continuous cause for concern with mortality rates increasing steadily every year. Despite the extensive progress in research and development of many treatment strategies including surgery, hormone therapy, chemotherapy and radiotherapy, numerous side effects such as risk of toxicity and non-specificity (Deb *et al*., 2011) persist, reducing their effectiveness. In this regard, the complexity and heterogeneity of cancer have contributed to the difficulty of developing a single effective therapeutic solution. However, the knowledge of the genetics and molecular biology associated with the development of cancer has expanded tremendously over the past few decades and can now be exploited in the search of an effective treatment to eradicate the burden of this disease.

### 2.1.1 The burden of cancer, causes and risk factors

The burden and incidence of cancer is alarmingly high and is predicted to increase substantially on a global scale in the next few years. Of all diagnosed cases, 40% were associated with lung, breast, colorectal and stomach cancer, with 34.2% of reported lung cancer cases occurring in men and 43.3% of women being diagnosed with breast cancer. Developing countries which includes South Africa, account for more than 70% of all reported cancer-associated deaths with a 15% rise predicted by 2050 (Bray and Møller, 2006).

In South Africa, the commonly occurring cancers include breast, lung, oesophageal, colorectal, liver, prostate, cervical, lymphoma, oral, pancreatic, skin, bladder, stomach and leukaemia (Cancer Association of South Africa, 2016). Cancer can be caused by several risk factors or a combination thereof, including age, sex, environment, lifestyle, dietary choices, physical inactivity, genetics, carcinogens, physical agents, weak immune systems, infections and other diseases (Figure 2.1).

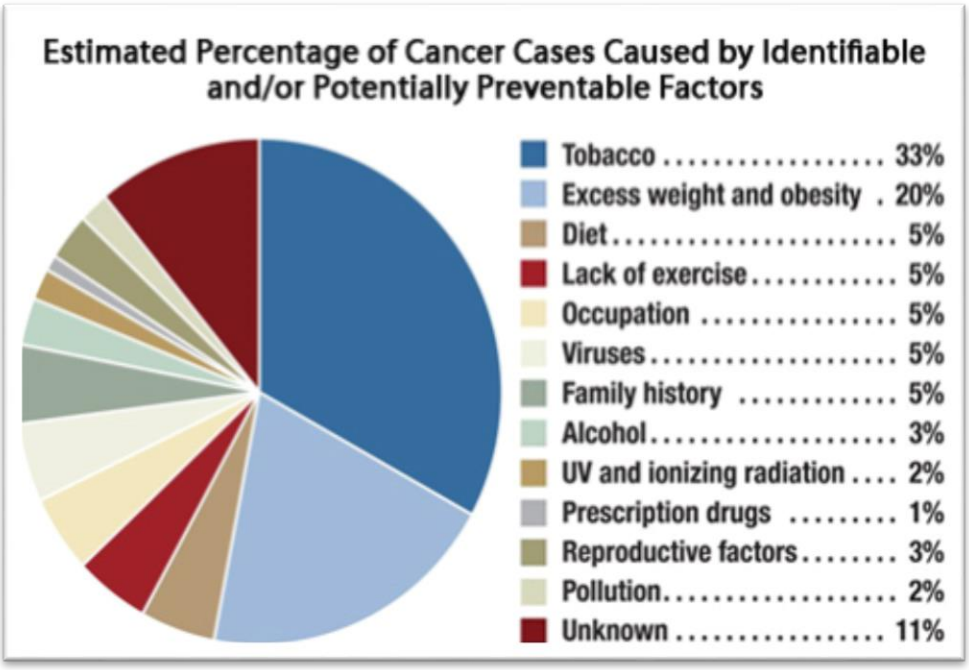


**Figure 2.1:** Cancer-causing factors and their related incidences worldwide (Cantley *et al*., 2012).

### 2.1.2 The development and genetics of cancer

The development of cancer is associated with many abnormalities such as the uncontrolled proliferation of cancer cells and the lack of response to multiple normal regulatory growth signals leading to the formation of masses or tumours. These abnormalities are reflected in their properties and behaviour which distinguishes them from normal cells (Figure 2.2). Ultimately, cancer cells invade normal cells and spread throughout the body to other tissues and organs in a process termed metastasis. Malignant tumours formed secrete hormones to induce the formation of new blood vessels which invade the tissues of the tumour by means of capillary buds and sprouts in a process termed angiogenesis (Adair and Montani, 2010), providing a continuous blood supply for nourishment and growth.

The understanding of the underlying genetic mechanisms and their roles in cancer development are crucial in the designing of suitable therapeutic strategies. A balance between cell proliferation and programmed cell death (apoptosis) has to be maintained to ensure tissue and organ integrity and functionality. Mutations of cellular genetic elements are indicated as one of the causes of cancer development (Lodish *et al*., 2000). The inheritance of a genetic mutation predisposes an individual to a specific type of cancer.

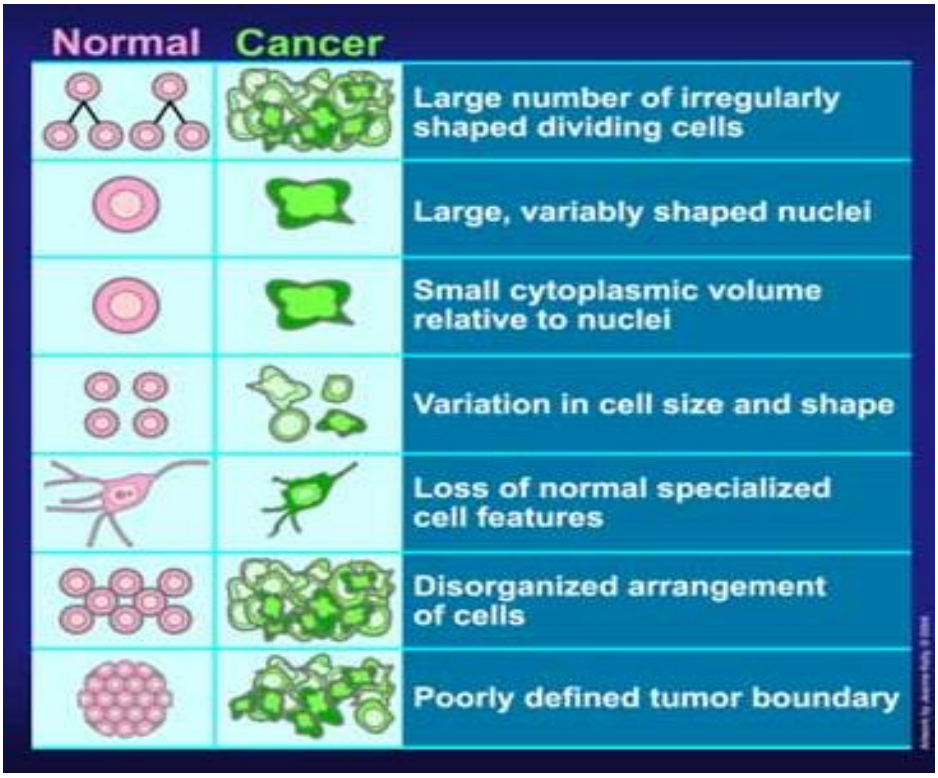


**Figure 2.2:** Morphological differences between normal and cancer cells (Fadjari, 2011). In comparison to normal cells, cancer cells grow and divide at an abnormally rapid rate, poorly differentiate, possess abnormal membranes, cytoskeletal proteins and various other morphological characteristics.

The multi-hit model theory states that a substantial number of different gene mutations give rise to the transformation of normal cells to cancer cells (Chial, 2008). Mutations of cell division, cell death and DNA repair genes have been implicated in the loss of cell proliferation control. Hence, cancer can be considered as a genetic disease due to the accumulation of genetic mutations that affect normal cellular processes. To date, more than 100 different genes and their gene products have been identified in promoting carcinogenesis (Fogar *et al*., 2005). These genes can be proto-oncogenes that become activated or tumour suppressor genes that are inactivated, giving rise to the development of cancer.

Common genetic alterations that occur are point mutations, gene amplification and chromosomal rearrangements which alter the encoded amino acid sequence for a specific protein (Pelengaris, 2013). Conventional therapies using drugs treat the symptoms of cancer but do not eliminate the underlying genetic causes leading to limited efficacy often due to multidrug resistance, poor drug penetration into tumours and damage to normal tissues (Ashworth *et al*., 2011). The use of gene therapy has emerged as a promising strategy for the treatment of the underlying genetic mutations in cancer development.

## 2.2 Gene therapy

Gene therapy, the use of nucleic acids as therapeutic agents in the hope of curing human diseases, was initially devised as a strategy to treat monogenic inherited diseases but has since expanded to include other diseases such as cancer (Gardlík *et al*., 2005). The therapeutic gene, also known as a transgene, is designed to augment, suppress or repair the defective gene (Ramamoorth and Narvekar, 2015). Nucleic acids are limited by size and physiochemical properties in the sense that they cannot diffuse directly through to the plasma membrane, thus giving rise to the development of delivery strategies and vehicles to overcome these limitations. The therapeutic gene is loaded onto a delivery vehicle or vector which transports the gene to the target cell.

The challenge facing gene therapy is for the gene to be successfully transferred into the target cell through the cytoplasm and into the nucleus, transcribed into mRNA and translated into a protein to induce its therapeutic effect (Rivera-Gil *et al*., 2012). The optimal vector and method of delivery are designed based on the type of target cells, their characteristics, expression, duration and the size of the therapeutic gene to be transported (Ramamoorth and Narvekar, 2015). Therefore, the choice of vector and delivery method is a critical step in achieving gene delivery. In addition, vectors are required to carry genetic material into the cells due to their sensitivity to nuclease degradation, hydrophilic poly-anionic nature and large size that limit passive penetration of the cell membrane (Ibraheem *et al*., 2014). There are two broad classes of gene delivery methods, viz. viral and non-viral methods.

### 2.2.1 Viral gene delivery methods

Viral vectors such as the retrovirus, lentivirus, herpes simplex virus, adenovirus and adeno-associated virus have been used in more than 70% of human clinical trials to date (Cotrim and Baum, 2008). A brief description of some of the commonly used viral vectors, their advantages and disadvantages and nucleic acid loading capacity are provided in Table 2.1. Viral vectors have the natural tendency to enter cells through receptor-mediated endocytosis and initiate expression of their own proteins using the cells biosynthetic machinery due to their strong promoters (Lundstrom and Boulikas, 2003). Thus, their rate of transfection is high and transcription of their foreign material occurs rapidly.

**Table 2.1.** Examples of viral vectors, properties, advantages and disadvantages adapted from (Bolhassani and Rafati, 2011; Lundstrom and Boulikas, 2003; Ponder, 2001).

| Virus | Description | Loading capacity | Advantages | Disadvantages |
|---|---|---|---|---|
| **Adenovirus** | Non-enveloped, icosahedral-shaped, linear dsDNA genome | High (36 kb) | Broad host range, long-term expression, transfection of non-dividing and dividing cells, production of high titres | Insertional mutagenesis, slow transient expression, strong immunogenicity, requires a helper virus |
| **Adeno-associated virus** | Non-enveloped, icosahedral-shaped, linear dsDNA genome | Medium (7.5 kb) | Broad host range, transfection non-dividing and dividing cells, establishes latent infection | Transient expression, strong immunogenicity, inefficient large-scale production, pre-existing immunity in humans |
| **Herpesvirus** | Enveloped, spherical-shaped, linear dsDNA genome. Example: Herpes simplex virus type 1 | High (30 kb) | Broad host range, long-term expression, establishes latent infection | Cytotoxicity in various cells |
| **Retrovirus** | Enveloped, linear ssRNA genome. Example: Vesicular stomatitis virus | Medium (7-12 kb) | Long-term expression, high titre production. | Restricted host range, insertional mutagenesis, transfection of dividing cells only |
| **Lentivirus** | Enveloped, spherical, linear dsRNA. Example: Simian immunodeficiency virus | Medium (8 kb) | Broad host range, high transduction efficiency, transfects non-dividing cells, long-term expression, high titre production | Insertional mutagenesis |

The use of viral vectors raises many health concerns such as immune responses, toxicity, inflammatory responses, degeneration of tissues, toxin production and insertional mutagenesis which may disrupt the expression of tumour suppression genes or activate oncogenes leading to the formation of malignant tumours. In addition, these vectors are only able to carry small sequences of nucleic acid in their genome, making large-scale production difficult. They are difficult to construct and some viruses require the use of a helper virus. Due to these reasons, researchers have had to study and develop alternative methods such as non-viral gene delivery.

### 2.2.2 Non-viral gene delivery methods

Non-viral methods include the physical and chemical based delivery methods. Non-viral methods possesses many advantages over viral methods such as unlimited clone capacity, low immunogenicity, low cytotoxicity and the ability of repeated application (Gardlík *et al*., 2005). Some of these methods are briefly discussed below.

#### 2.2.2.1 Physical methods

Physical methods allow for the direct penetration of genes into the cytosol by fine needle punctures, electric impulses or high-pressure gas, thereby avoiding all the limitations associated with viral and chemical methods. Direct injection of nucleic acids into tissues is the simplest method of gene therapy to date (Mansouri *et al*., 2004) but gene expression is much lower than viral or liposomal vectors. Naked nucleic acid delivery is faced with challenges such as degradation by serum nucleases and clearance by the mononuclear phagocyte systems (MPS), reducing their gene transfection efficiency (Gascón *et al*., 2013). Hence, this method is limited to injection to accessible tissues such as the muscle, skin, cardiac muscle, liver and solid tumours (Ramamoorth and Narvekar, 2015).

**Particle bombardment/ gene gun method** involves the coating of nucleic acids onto metal micro-particles such as gold or tungsten which are then fired at high velocity into tissues or cells through a perforated plate using a ballistic gun. This method has been used to transfer therapeutic genes with transient expression to mammalian cells *in vitro* and *in vivo* (Ibraheem *et al*., 2014). Advantages include safety, simplicity and the ability of crossing physical barriers such as the skin and muscle layer. Disadvantages include inefficiency of gene transfer, low stability of the nucleic acid and damage to cells.

**Electroporation** exploits the electrical conductivity and the permeability properties of a cell membrane which can be altered by the application of a high voltage external electric field. (Ramamoorth and Narvekar, 2015). Pores are formed in the cell membrane through which exogenous molecules such as nucleic acids are taken up by the cells. The high cell death, inability to access large portions of tissue and the implantation of electrodes into internal organs have limited the use of this method. The transfection efficiency is dependent on both physical and biological properties such as field intensity, pulse duration, electrode geometry, size, shape and density of cells (Ibraheem *et al*., 2014).

**Sonoporation,** an extension from electroporation results in acoustic cavitations induced by the ultrasound frequencies that disrupt and permeate the cell membrane allowing nucleic acids to be delivered into cells (Ibraheem *et al*., 2014). This method is non-invasive and site-specific. Therapeutic genes are commonly incorporated into a microbubble, administered systemically and, thereafter, the application of ultrasound is conducted allowing for the deposition of the transgene. Microbubbles consist of a biocompatible outer shell and a gas filled core (nitrogen or air) conjugated with sulphur hexafluoride and perfluorocarbon to obtain a high molecular weight (Ramamoorth and Narvekar, 2015). This method is dependent on the frequency, time of ultrasound, the use of a contrast factor, size and the concentration of the nucleic acid.

**Magnetofection** is a process involving the use of magnetic particles complexed with nucleic acids brought into contact with the cell monolayer by placing a magnet under the tissue culture dish or they are introduced intravenously and brought towards the target using high gradient external magnets. The magnetic field gradient generated increases sedimentation of these complexes and increases transfection speed (Ramamoorth and Narvekar, 2015). The therapeutic gene is released by charge interaction, enzymatic cleavage of cross linking molecules or degradation in the matrix. This method has been successfully applied to a variety of cell lines, primary and hard-to-transfect cell lines (Nayerossadat *et al*., 2012).

#### 2.2.2.2 Chemical methods

Chemical based gene delivery vectors have the potential to overcome the limitations associated with viral and physical methods. Gene transfection efficiency and cytotoxicity can be controlled by manipulating their physical and chemical properties such as size, surface composition and surface potential. These vectors can interact with nucleic acids to form nano-sized conjugates suitable for transport through the cell membrane. The most popular chemical based gene delivery systems are discussed briefly below.

**Liposomes** are vesicles made up of synthetic lipid bilayers, closely resembling the structure of biological membranes. These vesicles spontaneously self-assemble upon dispersal of the lipids into aqueous solutions (Ibraheem *et al*., 2014). Liposomes can be anionic, neutral or cationic. The former two require entrapment of the macromolecule while cationic liposomes

can spontaneously interact with negatively charged nucleic acids to form ‘lipoplexes’ (Wheeler *et al*., 1999).

Cationic liposomes can also favourably interact with the negatively charged cell membrane *via* electrostatic binding, allowing for fusion and direct delivery of the nucleic acid across the plasma membrane (Zelphati *et al*., 2001). Advantages associated with cationic liposomes are ease of preparation, biocompatibility, low immunogenicity, transfection of many cell types and high nucleic acid loading capacity. Disadvantages include cytotoxicity *in vivo*, requirement of helper lipids, non-specific interactions with serum proteins and enzymes, decreased cell adhesion, haemolysis and low transfection compared to viral vectors (Mansouri *et al*., 2004).

**Cationic polymers (CPs**), comprising natural or synthetic polymers are regarded as being stable and better able to condense nucleic acids than cationic liposomes. Natural polymers include chitosan, pol-l-lysine, gelatin, sodium alginate and albumin. Synthetic CPs include polyethyleneimine, polyethylene glycol, poly-lactide co-glycolides and poly-glutamic acid. CPs possess characteristics such as structural variability, versatility, efficient binding of therapeutic molecules without comprising their function, biodegradability, low cytotoxicity, efficient nucleic acid release and the ability to elicit long-term expression without insertional oncogenesis (Nayerossadat *et al*., 2012). The size and charge density of these vectors determine their transfection efficiency, the longer the cationic polymer chain the higher the condensation of nucleic acids and their protection against nuclease degradation (Gardlík *et al*., 2005). The cationic polymers chitosan and poly-L-lysine used in this study will be discussed further.

### 2.2.3 Chitosan

Chitosan belongs to a family of linear polysaccharides comprising β (1-4) linked units of N-acetyl glucosamine (N-acetyl-2-amino-2-deoxy-D-glucose) and glucosamine (2-amino-2-deoxy-D-glucose) and is commonly used in gene and drug delivery. It is derived from the deacetylation of chitin, found in crustacean shells, fungi and bacteria (Andersen *et al*., 2015). The degree of deacetylation determines the biodegradability, biocompatibility, cytotoxicity, viscosity, crystallinity and solubility of chitosan (Hsu *et al*., 2011). Chitosan is readily degraded into water and carbon dioxide in the body, eliminating any toxicity problems.

Chitosan-DNA polyplexes possess mucoadhesive properties and, hence, are utilized in many nasal and oral gene therapy applications (Ramamoorth and Narvekar, 2015). Chitosan is soluble at pH <6 with the amine groups displaying a high density of positive charges, thereby increasing chitosan's metal chelating properties (Narayanan *et al*., 2014) and stability. Hence, it has been used as a stabilizer contributing to steric hindrance and electrostatic repulsion in gold nanoparticles (AuNPs) (Mohd and Johan, 2014). Chitosan functionalised AuNPs (CS-AuNPs) will be discussed in section 2.3.3.

The molecular weight of chitosan strongly influences its transfection efficiency, the higher the molecular weight the higher the transfection due to strong stabilization of chitosan-nucleic acid complexes *in vitro* (Köping-Höggård *et al*.,2003). However, high molecular weight chitosan has shown low solubility at neutral pH, large aggregated shapes, high viscosity and slow release of nucleic acids while low molecular weight chitosan has been associated with low complexation ability but better intracellular release of nucleic acids (Jin *et al*., 2014). Hence, the choice of chitosan of an optimal molecular weight is crucial for gene-delivery studies. The polycationic nature of chitosan results in strong electrostatic interactions with anionic nucleic acids, resulting in efficient complexation, condensation and protection of the nucleic acids from nuclease degradation. Chitosan also acts as a permeator, opening tight intercellular junctions in the cellular membrane and ensuring its delivery into the cell (Gascón *et al*., 2013).

### 2.2.4 Poly-l-lysine

Poly-l-lysine (PLL) is an extensively used cationic polymer and one of the first cationic polymers to be used in gene therapy (Jin *et al*., 2014) due to its ability to electrostatically interact with nucleic acids and cells. PLL is derived from polymerisation of the N-carboxy-anhydride component of lysine (Gascón *et al*., 2013). The different conformations of PLL's secondary structure are influenced by temperature and pH. At 25°C, PLL exhibits a β-sheet conformation and at neutral pH forms an extended random coil due to the presence of repulsion forces as a result of protonation of the $NH_3^+$ (Smirnovas *et al*., 2005). PLL has a large number of protonable amine groups and as the positive charge density of PLL increases so does the binding and formation of stable nucleic acid complexes (Nayerossadat *et al*., 2012).

In addition, the increase in the length of the polymer directly influences gene delivery efficiency and cytotoxicity (Segura and Shea, 2001). In normal cellular processes, PLL was found to stimulate immunoglobulin (interferon-β) production without hindering cellular proliferation (Stobiecka and Hepel, 2011). PLL has been shown to exhibit anti-tumour effects in L1210 lymphoid leukaemia, erythro-leukaemia, P388, Lewis lung, Ehrlich carcinoma and P38 macrophage derived tumour cell lines (Szende *et al*., 2002).

Intravenous injection of PLL-DNA complexes conjugated to various targeting ligands of the asialoglycoprotein receptor and exhibited successful transient transgene expression in the liver of animal models (Wu *et al*., 2002). PLL functionalised AuNPs (PLL-AuNPs) will be discussed further in section 2.3.3.

## 2.3 Inorganic Nanoparticles : Gold nanoparticles (AuNPs)

Nanomedicine is the use of nanotechnology in medicine and is globally a fast-growing area for the treatment of various diseases, including cancer. It is a new and exciting branch of nanotechnology and utilizes nanosized particles or nanoparticles as carriers of genes or drugs. This application of nanoparticles, of which inorganic nanoparticles play a major role, is still under development and promises to revolutionize medicine. Over the years, an array of inorganic nanoparticles have emerged as potential genes and drug delivery systems having a dual function for imaging and therapeutics, giving rise to the intriguing area of theranostics. These inorganic nanoparticles that include carbon nanotubes, iron oxide, quantum dots and gold are being investigated in cancer therapy, bioengineering and gene therapy. Gold nanoparticles were used in this study and are hence discussed further in detail.

Since the history of time, gold has captured the interest of scientists. Soluble gold was popular in Egypt and China in the $4^{th}$ - $5^{th}$ century B.C. with the first report of colloidal gold being the creation of ruby glass, ceramic and silk staining methods that are still in use today. In the middle ages, soluble gold was used for curative purposes to treat dysentery, heart disease, venereal problems, syphilis, epilepsy, ulcerative skin conditions and tumours (Pedrosa *et al*., 2015). It has been reported that reduction of aqueous chloroaurate using phosphorous in a two-phase system of $CS_2$ produced a deep red AuNP solution which changed to blue-purple and to green upon drying (Faraday, 1857).

The first *in vivo* applications of AuNPs was in mice during the 1980's and involved the use of 27 nm PEGylated AuNPs functionalised with the recombinant human tumour necrosis factor alpha which displayed anti-tumour effects by apoptosis, cytolysis or cytostasis (Pedrosa *et al*., 2015). Subsequently, the first human clinical trials were conducted using these AuNPs (Libutti *et al*., 2010). During the 1990's, various AuNPs formulations were shown as effective treatments for diseases such as rheumatism, tuberculosis and *Lupus vulgaras* (Does *et al*., 2003). The applications of AuNPs in nanomedicine have since expanded immensely.

### 2.3.1 Properties of AuNPs

One of the reasons that AuNPs have attracted favourable attention is due to their unique properties that include small size, different shapes, large surface-to-volume ratio, high stability, biocompatibility, oxidation resistance, intense surface plasmon resonance, high photothermal conversion rate and low toxicity (Deb *et al*., 2011). A distinctive physical property of AuNPs is their surface plasmon resonance (SPR) absorbance. The colour of a colloidal AuNP solution varies based on the size of AuNPs in solution with yellow to purple having a size range of 1-100 nm (Figure 2.3). The size of AuNPs influences their cellular uptake, release and clearance pathways, biodistribution and cytotoxicity.

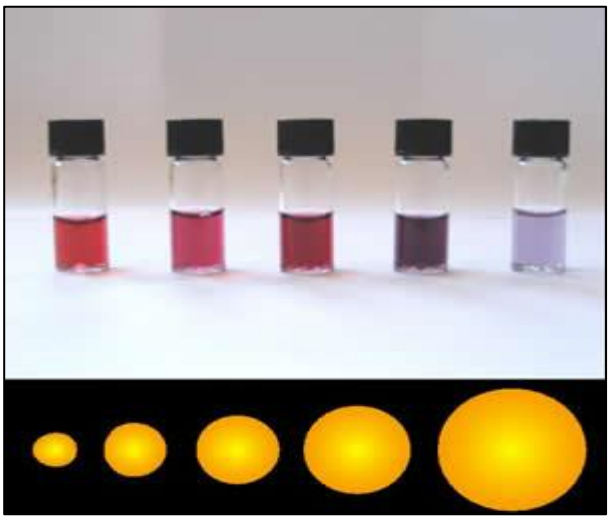

**Figure 2.3:** Various colours of colloidal AuNP solutions in relation to their size (Douma, 2008). The size of AuNPs determines the wavelengths of SPR absorption and consequently, the colour of the AuNP solution.

Generally, a size-relative absorption peak is observed in the 500-550 nm range, with an increase in size of the AuNPs causing an increase in the scattering, absorption wavelength

and total extinction, resulting in a change of colour of the solution (Jain *et al*., 2006). The SPR absorbance of colloidal AuNPs enhances their scattering and absorption optical properties (Long *et al*., 2009). Aggregation of AuNPs in solution due to a shift in the SPR absorbance of larger particles is indicated visually by a colour transition of the AuNP solution.

AuNPs can be solids or a hollow shell and spherical, triangular, octahedral, sub-octahedral, tetrahedral, decahedral, multiple twined, icosahedral multiple twined, prisms, rods or hexagonal in shape (Figure 2.4). Each shape comes with its own set of properties and applications eg. gold nanorods are suitable for bio-sensing, photo thermal therapy and gene delivery while gold nanocages coated with temperature-sensitive polymers have been used as drug carriers (Guo *et al*., 2010).

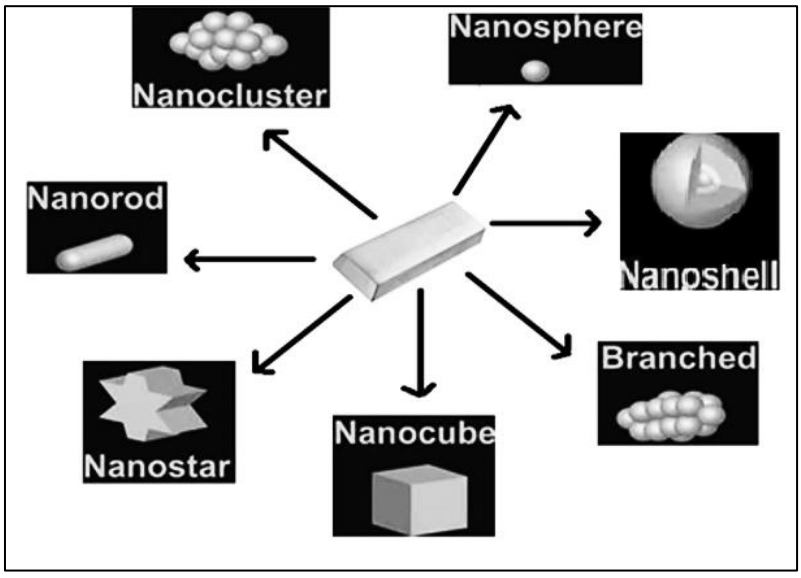


**Figure 2.4:** Diagram depicting the various shapes of synthesized AuNPs (Khan *et al*., 2014).

The surface of AuNPs consist of negative or positive charges, making them highly receptive to surface modifications by oppositely charged molecules *via* electrostatic interactions to either cations or anions (Pillay *et al*., 2010). The surface charge of AuNP-nucleic acid complexes influence their stability, intracellular uptake, cytotoxicity and release of the therapeutic cargo (Pedrosa *et al*., 2015). The stability of AuNPs is vital for their use as therapeutic agents as they are required to maintain their stability in the cellular environment and bloodstream. The chemical stabilization of AuNPs with sodium citrate and functionalisation with ligands imparts electrostatic and steric repulsion towards colloidal stability. Importantly, undesired interactions and the formation of protein coronas on the

surface of AuNPs may influence colloidal stability in biological systems. Colloidal stability of AuNPs can be manipulated by adjusting the pH of the solution, increasing electrolyte concentration, changing the stabilizing agent or medium and adding inorganic salts (Dukhin and Goetz, 2010).

### 2.3.2 AuNP Synthesis

Various methods for the synthesis of AuNPs have been employed and include physical, chemical and biological methods, producing AuNPs of desired size, shape and monodispersity.

#### 2.3.2.1 Chemical methods

Chemical methods are most commonly utilized for the synthesis of AuNPs in liquid form. The basic principle of the chemical method is the conversion of $Au^{3+}$ ions to $Au^{0}$ (neutral) atoms by a reducing agent and, thereafter, a stabilizing agent is added to prevent aggregation of the resulting AuNPs. The most common reducing agents are sodium citrate and sodium borohydride. Stabilizing agents such as block co-polymers, peptide-biphenyl hybrids, polyvinyl pyrrolidine, bovine serum albumin, 1-octadecanethiol, 1, 5-pentanediol and cetyltrimethyl ammonium bromide (CTAB) are associated with the AuNP surface, providing charge, solubility and stability.

The simplest and most popular method for colloidal AuNP synthesis is the Turkevich method (Turkevich *et al*., 1951) and adaptations, thereof, that produce 10-20 nm monodisperse colloidal AuNPs. This method utilizes hydrochloroauric acid ($HAuCl_4$) reduced with sodium citrate which acts as an electrostatic stabilizing agent to prevent particle aggregation. This results in sub-nanometer particles in solution evidenced by a colour transition of the solution from yellow to wine-red (Figure 2.5). The size of the AuNPs are controlled by the reaction time and the amount of stabilizing agent used while its dispersion properties are controlled by the temperature of the reaction.

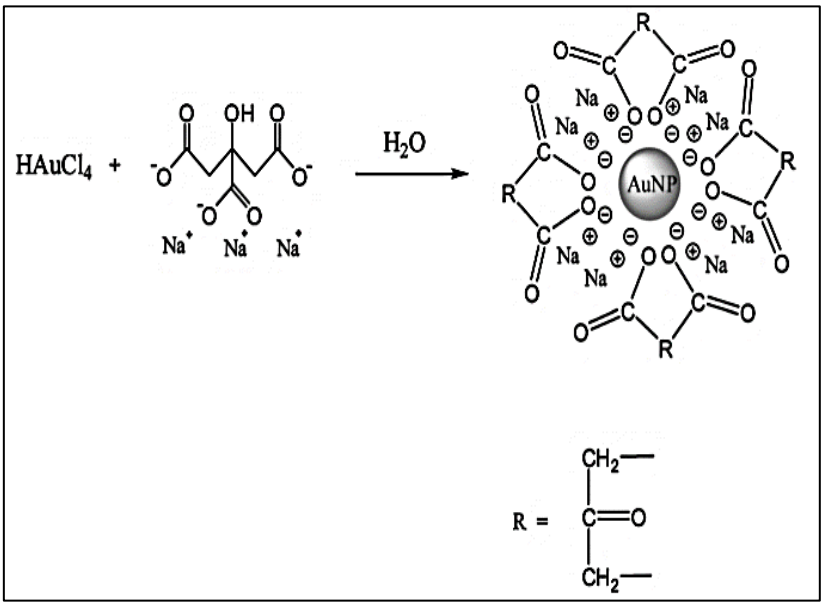


**Figure 2.5:** Reaction for the synthesis of AuNPs by sodium citrate reduction of $HAuCl_4$ using the Turkevich method (Herizchi *et al*., 2016).

The Brust-Schiffrin method produces thermal and air stable AuNPs of controlled size (5-6 nm) and low dispersity in organic liquids such as toluene which are not miscible in water (Brust and Schiffrin, 1994). Reduction is achieved by sodium borohydride ($NaBH_4$) which additionally acts as an anti-coagulant and initiates a colour transition of the organic phase from orange to deep brown. However, this method is laborious and requires several steps of purification.

The seeding growth approach involves the reduction of previously synthesized AuNPs using the Turkevich method but reduced by hydroquinone producing AuNPs in the 30-300 nm range (Perrault and Chan, 2009). Modifications of this method have since been made, reducing the size distribution to 5-40 nm (Stanglmair *et al*., 2014).

The ionic liquid synthesis method has more recently been introduced for the synthesis and stabilization of metal nanoparticles (Richter *et al*., 2013). These media, in addition to acting as reducing and stabilizing agents, have several advantages such as low melting points, non-volatility, thermal stability and designable miscibility. A simple one-pot synthesis method of AuNPs utilizing N-(2-hydroxyethyl)-N-methylmorpholinium tetrafluoroborate has been developed (Herizchi *et al*., 2016).

#### 2.3.2.2 Physico-Chemical methods

These include photochemical, sonochemical and electrochemical methods. In photochemical synthesis, microwave irradiation using citric acid as a reducing agent, CTAB as a binding agent (Murawala *et al*., 2014) and gamma irradiation using bovine serum albumin. The natural polysaccharide alginate as a stabilizing agent and have been used to synthesize 5-40 nm AuNPs of controllable size and high purity (Rezende *et al*., 2010). Sonochemical synthesis using ultrasound produce AuNPs smaller than 10 nm in size (Baigent and Müller, 1980). Adaptations on this method using reducing agents such as hydroxyl radicals and sugar pyrolysis radicals produced 30-50 nm nanoribbons which are extremely flexible and can bend at angles greater than $90^0$. A disadvantage of this method is the production of AuNPs with a broad size distribution. The electrochemical production of nanoparticles producing size selective nanoscale transition metal particles, stabilized by tetra alkyl ammonium salts, have been reported (Reetz and Helbig, 1994).

This method has advantages such as low cost, modest equipment, high quality, lower temperatures and ease of controlling the yield of the product (Herizchi *et al*., 2016).

#### 2.3.2.3. Biological methods

Recently, biological synthesis termed the 'green synthesis' of nanoparticles was developed as an alternative eco-friendly method using non-toxic regents, cost-effective and renewable materials. This method is not energy consuming and does not require the need for the disposal of hazardous chemicals. Biological methods entail the use of microorganisms, enzymes, plants and plant extracts (Mohanpuria *et al*., 2008). Natural biomaterials such as egg-shell membranes, chitosan and edible mushrooms have been used to synthesize AuNPs. Sun light irradiation has additionally been used as a reducing agent with the aid of 6-mercaptourine and folic acid as stabilizing agents (Lan *et al*., 2013). Although these biological methods are environmentally friendly, they are associated with many disadvantages such as non-uniform shapes, poor mono-dispersity, random aggregation and low scale-up, rendering them unappealing for use in comparison to the chemical methods (Narayanan and Sakthivel, 2010).

### 2.3.3 Functionalisation of AuNPs with Cationic Polymers (CPs)

The purpose of nanoparticle surface functionalization is to modulate the reactivity, toxicity, stability, shape and size to enhance the rate of uptake and tissue biocompatibility in a biological environment (Sivaramakrishnan *et al*., 2014). For *in vivo* applications, surface modification regulates the circulation half-time and systemic clearance of these nanoparticles with enhanced bioavailability, low immunogenicity and target specific accumulation (Baptista *et al*., 2015). AuNPs allow for easy functionalization and binding with targeting agents and drugs in therapeutic applications due to their high surface-to-volume ratio (Yeh *et al*., 2012). The strong binding efficiency of AuNPs to ligands such as thiols, disulphides and amines also facilitate their conjugation with biomolecules such as DNA, RNA and antibodies (Balasubramanian *et al*., 2010).

AuNP nanocarriers allow for the protection of their therapeutic cargo by the prevention of degradation before the biological target is reached (Pedrosa *et al*., 2015). The interactions involved during functionalisation include covalent and non-covalent conjugation to AuNPs. The loading efficiency is dependent on the quantity of functional ligands and the reaction time. Non-covalent conjugation involves different interactions such as electrostatic interactions, specific binding affinity and hydrophobic interaction. It is the simplest way of conjugation. Although, covalent conjugation is known to produce stable constructs (Yeh *et al*., 2012), non-covalent conjugation reduces the risk of altering the structure and function of the AuNPs or the therapeutic cargo (De Long *et al*., 2010).

For the transport of nucleic acids such as mRNA which is negatively charged there is a requirement for the electrostatic complexation of the nucleic acid with a positively charged agent for cellular internalization. Cationic polymers (CPs) are considered most suitable for the functionalization of the neutral AuNPs due to their abundance of positively charged groups in their structure. Polymers are used to functionalise AuNPs interact and overlap each other in solution giving rise to repulsive osmotic forces by the compressed polymer segments associated with unfavourable entropy (Cosgrove, 2005). This type of force is also referred to as steric repulsion and prevents the AuNPs from aggregating. Chitosan (CS) and poly-l-lysine (PLL) functionalization of AuNPs are employed in this study and will be briefly discussed.

As a metal chelator, chitosan can reduce gold precursors and stabilize the resulting AuNPs. CS-AuNPs offer a platform for cross-linking due to chitosans' cationic properties and amino groups and can be functionalised further with various biomolecules for gene delivery. CS-

AuNP conjugates have been developed into useful tools as antibacterial and antifungal agents, for gene and drug delivery, bio-sensing and tumour targeting and have been recommended for insulin delivery by oral and nasal administration (Boyles *et al*., 2015). It has been reported that CS-AuNPs maintain and enhance treatment efficacy, extends systemic circulation time, enhances cellular uptake efficiency, widens intracellular distribution and prevents undesired degradation of the therapeutic gene through various uptake mechanisms such as micropinocytosis (Nam *et al*., 2009). These properties bode well for use of CS-AuNPs in cancer gene therapy applications.

The gene delivery efficiency of PLL by itself is relatively low but conjugation with other vectors such as AuNPs facilitate better cellular uptake and gene expression. The direct interaction of AuNP and PLL surface stabilizes the AuNPs in solution (Joshi *et al*., 2004). PLL-AuNPs have exhibited efficient electrostatic binding of nucleic acids and penetration of eukaryotic membranes with low cytotoxicity (Stobiecka and Hepel, 2011). PLL may be adsorbed electrostatically onto the surface of AuNPs, depending on the overall charge of the AuNPs (Figure 2.6).

Citrate stabilization confers a negative charge on the AuNP surface which enhances the electrostatic binding of AuNP to PLL. Apart from electrostatic interactions, hydrogen bonding occurs between the PLL chains and citrate molecules on the surface of citrate-capped AuNPs (Figure 2.7). All these interactions result in the formation of a condensed structure which is efficient for binding and protecting nucleic acids in gene delivery applications. PLL-AuNPs have also been used to develop bactericidal and viricidal vaccines as scaffolds in tissue repair and as stem cell carriers (Ghosh *et al*., 2008).

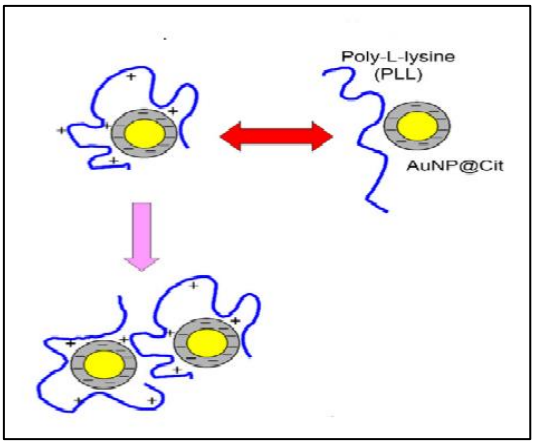


**Figure 2.6:** Electrostatic interactions between citrate capped AuNPs and PLL (Stobiecka and Hepel, 2011).

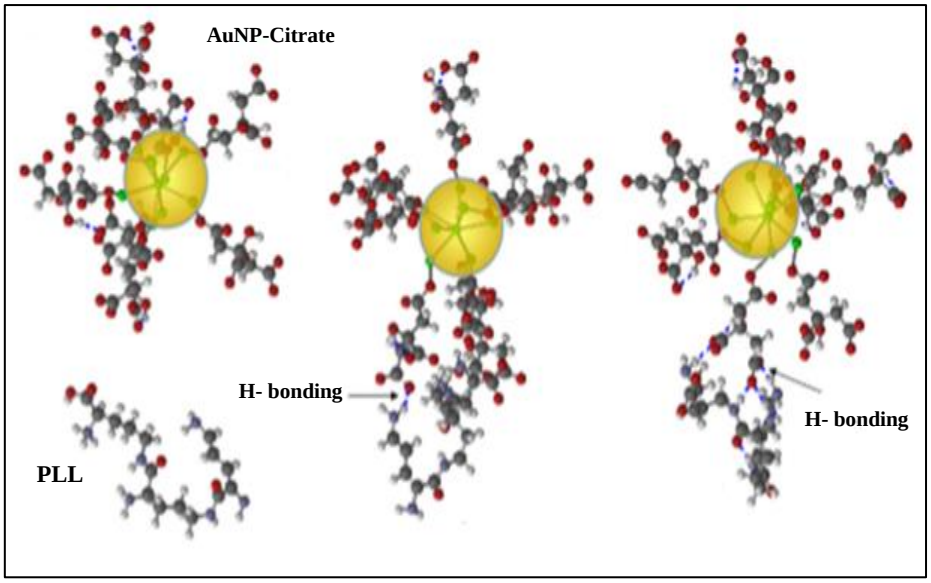


**Figure 2.7:** Hydrogen bonding between PLL and citrate capped AuNPs (Stobiecka and Hepel, 2011).

### 2.3.4 Gene delivery and Gold Nanoparticles

Plasmid DNA (pDNA), anti-sense oligonucleotides, small-interfering RNA (siRNA) and micro RNA (miRNA) are most commonly used in gene therapy applications. In the case of pDNA, it is transcribed into messenger RNA (mRNA) and translated into the desired protein as a replacement for or to supplement a faulty gene-encoded protein. Anti-sense oligonucleotides are short, single stranded nucleotide sequences (25 bases or less) that have shown potential in gene therapy applications. These oligonucleotides are designed to be complementary to a specific sequence of mRNA, bringing about inhibition. However, they have a short half-life and are rapidly degraded by nucleases. For gene silencing in gene therapy, both siRNA and miRNA can be employed. The use of these strategies are associated with high targeting specificity, coupled with a high and prolonged effect on gene silencing (Gardlík *et al*., 2005).

To date, there has been limited success in gene expression studies using the above nucleic acids, leading to the investigation of other nucleic acids such as mRNA as an alternative to pDNA. This thesis is based on the AuNP delivery of mRNA which will be elaborated upon. The use of mRNA holds promise for efficient gene expression and overcoming the cellular barriers limiting the use of pDNA and is therefore investigated in this study. mRNA are short 10 kb sequences of ssRNA consisting of five components: the 5’ cap, 5’ untranslated region, open reading frame, 3’-untranslated region and poly (A) tail (Figure 2.8) (Weide *et al*., 2008).

The non-coding 5’ untranslated region which has a high G-C content plays a role in the post-transcriptional regulation of gene expression and allows for excellent control over the protein product by modulating stability, transport, sub-cellular localization and translation efficiency of the mRNA (Tavernier *et al*., 2011). The 3’ untranslated region is A-U rich and functions in a similar manner. The poly (A) tail (± 200 A residues) and 5’ cap determine the efficiency of translation and stability of the mRNA (Yamamoto *et al*., 2009). In this study, a reporter mRNA (F*luc*-mRNA), incorporating the firefly luciferase gene in the open reading frame, is used to evaluate gene expression.

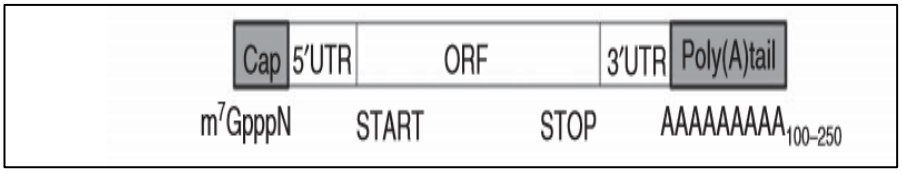


**Figure 2.8:** mRNA structure and components (Youn and Chung, 2015).

#### 2.3.4.1 Intracellular Trafficking

Effective gene delivery is dependent on the type of the carrier, its interaction with serum, circulation time, bio-distribution, evasion of immune cells and macrophages, cell surface interaction and penetration, endosomal escape, protection from degradative nucleases, transport to the nucleus, persistence as an extrachromosomal element or integration into the genome and sustained gene expression (Lundstrom and Boulikas, 2003).

CPs and polymeric nanoparticles associate with the cellular membrane *via* electrostatic interactions, resulting in internalization by receptor-mediated endocytosis, adsorptive endocytosis, clathrin-coated pits, phagocytosis or caveolae (Wiethoff and Middaugh, 2003). Once in the cells, cationic polymeric nanoparticles with protonated amine groups at a pKa close to the endosomal or lysosomal pH, utilize the proton sponge effect with an influx of $H^+$, $Cl^-$ and water causing the endosome to swell and rupture releasing its contents (Elsabahy *et al*., 2011). In addition, they electrostatically interact with the anionic structures of the endosome in the flip-flop mechanism, resulting in a lateral diffusion of CPs and the release of the nucleic acid cargo from the carrier into the cytoplasm (Figure 2.9).

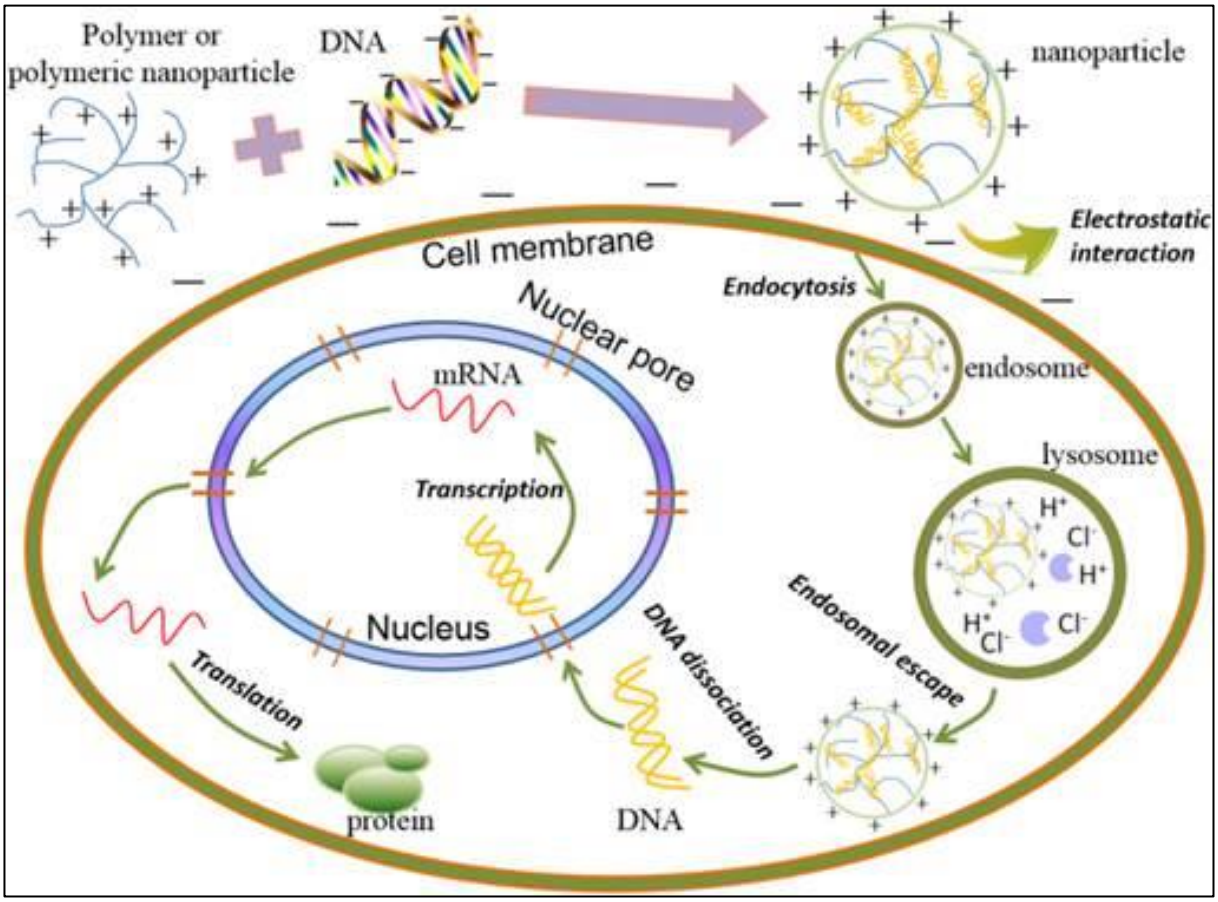


**Figure 2.9:** Mechanism of cationic polymer-based nanoparticle gene delivery and expression (Jin *et al*., 2014).

In an *in vivo* system, naked nucleic acids encounter extracellular and intracellular enzymes which rapidly degrade the nucleic acids (Yellepeddi, 2015). Polymeric nanoparticles are efficient at condensing and protecting nucleic acids, exhibiting excellent colloidal stability and shielding the therapeutic cargo from the harsh effects of biological and cellular environments. Foreign nucleic acids are known to activate immune responses, resulting in the production of inflammatory cytokines (Kreiter *et al*., 2011) which can be avoided by complexation with CPs that are biocompatible and mask the foreign characteristics of the therapeutic nucleic acids. Compared to pDNA, mRNA is devoid of immunogenic CpG motif sequences and is less toxic as it contains no viral promoters or bacterial sequences in its' structure (Tavernier *et al*., 2011).

pDNA must be first translocated from the cytoplasm to the nucleus for transcription before translation and gene expression. In contrast, mRNA molecules do not need nuclear entry for gene expression as mRNA is already in transcript form and the translation of mRNA to

protein occurs in the cytoplasm. Hence, it evades the nuclear barrier and expresses the therapeutic gene quicker than pDNA (Figure 2.10).

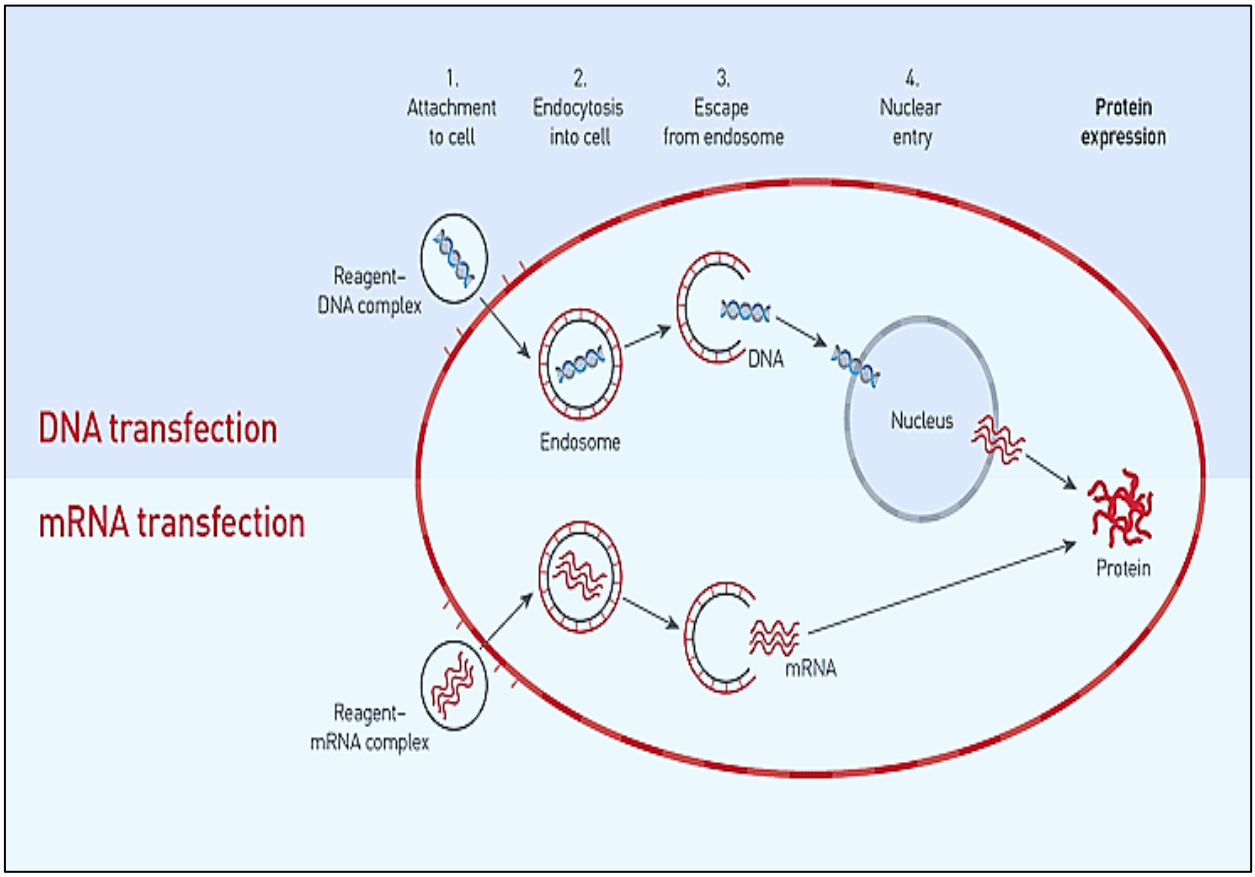


**Figure 2.10:** DNA and mRNA gene expression pathways (Thermo Fisher Scientific, 2016).

mRNA transfection is independent of the cell-cycle and can be used to transfect non-dividing and dividing cells since mRNA does not require nuclear membrane degradation during the replication cycle for translation. Hence, mRNA can be used for hard-to-transfect cells such as endothelial and dendritic cells (Yamamoto *et al.*, 2009). With mRNA transfection there is no risk of insertional mutagenesis as protein translation from mRNA occurs independently without integration into the cellular genome, resulting in transient expression of the therapeutic protein. The use of mRNA-based gene transfer in combination with CP functionalised AuNPs could be a promising new strategy for cancer gene therapy (Ding *et al.*, 2014).

#### 2.3.4.2 Cellular uptake

Cellular uptake of AuNPs depends on their physiochemical characteristics such as shape and size which ensure that absorption, penetration, circulation and distribution of AuNPs are easily achieved in bio-systems (De Jong *et al*., 2008). Passive or active targeting mechanisms can be used for the delivery of AuNP therapeutics into cells (Figure 2.11). The enhanced permeability retention factor effect (EPR) is associated with passive targeting wherein AuNPs accumulate in the tumour due to increased vasculature, allowing passage through the endothelium for delivery at the tumour site with reduced systemic toxicity (Kennedy *et al*., 2011).

Passive cellular uptake of AuNPs involves mechanisms such as endocytosis, pinocytosis, clathrin-coated pits, phagocytosis or caveolae with pinocytosis being the most dominant internalisation pathway for AuNPs in several cell lines (Huefner *et al*., 2014). These pathways follow a general process of cell membrane receptor recognition, engulfment into vesicles, penetration into cells, signal pathway activation, trafficking and storage or elimination of the AuNPs.

Active targeting is dependent on a functional surface ligand for targeting, selectivity and specificity using receptor-mediated endocytosis and cargo release inside the cell (Matsui *et al*., 2015). AuNPs functionalised with bombesin peptide was successfully used to target the gastrin-releasing peptide receptor overexpressed in the breast, prostate and small-lung carcinomas (Manjila *et al*., 2013). Other overexpressed receptors (such as the epidermal growth factor and folate receptors) on cancer cells have successfully been targeted using their respective antibody-AuNP conjugates (Rana *et al*., 2012).

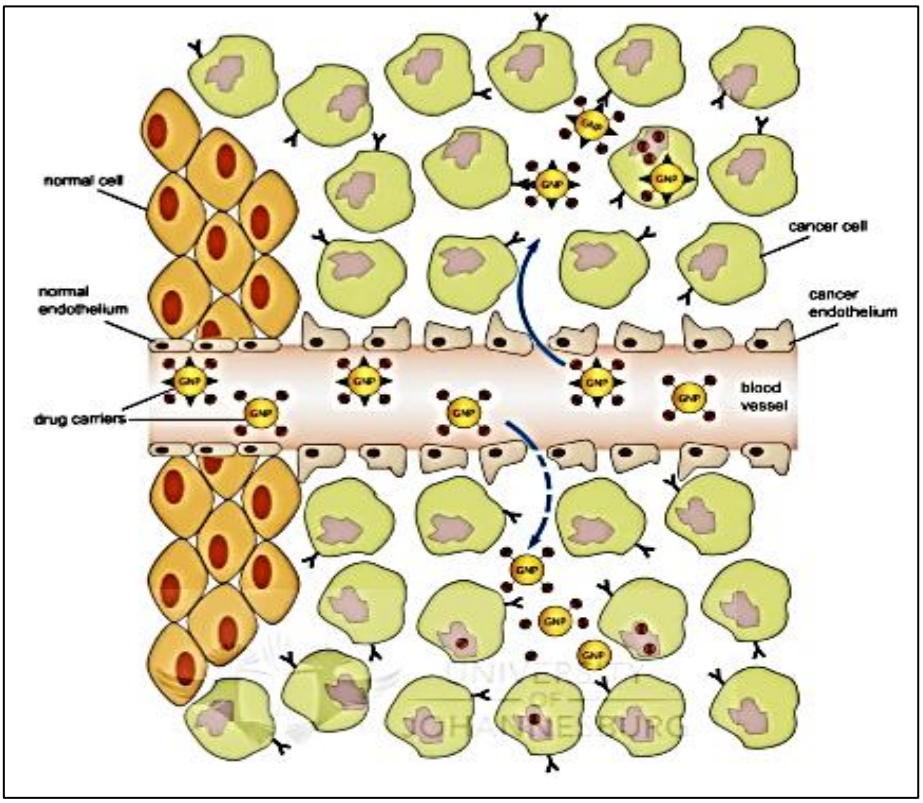


**Figure 2.11:** Representation of passive and active cellular uptake of AuNPs (Ghosh *et al*., 2008).

The prevention of aggregation of AuNPs is crucial as this increases their size, restricting easy translocation across membranes (Gosens *et al*., 2010). Furthermore, plasma proteins may adsorb onto the surface of the AuNPs, altering these properties (Vijayakumar and Ganesan, 2012). The formation of a protein corona on the AuNP surface increases their stability and may be a possible mechanism for the recognition and internalisation of AuNPs into the cells (Giljohann *et al*., 2007). The absorption of proteins may cause aggregation and opsonisation of the nanoparticles *in vivo*, shortening systemic circulation and reducing the enhanced permeation and retention effect (Kim *et al*., 2015).

The size of AuNPs influences many factors such as cellular adhesion and interaction, deposition, translocation, biodistribution, circulation time and fate, both *in vitro* and *in vivo*. AuNPs from 1-18 nm in size have been reported to easily cross the cell membrane and enter the nucleus to interact with the DNA (Gao *et al*., 2011). The cellular uptake efficiency of 20 nm polystyrene coated AuNPs in the human hepatocyte cell line (HepG2) and the primary rat hepatocyte cell line (C3A) was size and exposure-time dependent (Johnston *et al*., 2010).

AuNPs are also capable of crossing the blood-brain and placental barriers, thereby accumulating within neural tissue, placenta and foetus. Several studies have reported these observations using maternal rat models and intravenous injections of various sizes of AuNPs (Myllynen *et al*., 2008; Takahashi and Matsuoka, 1981). There are two possible mechanisms of AuNP biodistribution *in vivo*, namely transport by endocytotic-exocytotic and paracellular transport mechanisms which include the transport of molecules around cells and *via* tight junctions of epithelial cells (Mühlfeld *et al*., 2008). These mechanisms are not only influenced by the size of AuNPs but also their surface properties, type of animal models and the exposure route.

Functionalisation with ligands and various biochemical molecules influences the bodistribution of AuNPs within *in vivo* applications (Niidome *et al*., 2006). PEG is an anti-fouling polymer which prevents opsonisation by creating stealth AuNPs and extending their circulation period CS-AuNPs were found to transverse the cell membranes of Chinese hamster ovary cells by endocytosis (Boca *et al*., 2011) and the outer cell membrane of THP-1 monocytic cells and the plasma membrane of lysosomes by exocytosis (Boyles *et al*., 2015).

The surface charges present on AuNP surfaces have shown to enhance their uptake into cells. For positively charged amine functionalised AuNPs, the mechanism of internalization involves their interaction with the negatively charged cell membrane (Sandhu *et al*., 2002). Several reports have proven the superiority of positively-charged AuNP cellular uptake in comparison to negatively-charged AuNPs (Bartneck *et al*., 2012). Cationic AuNPs were seen to be internalised by THP-1 monocytic cells within 30 min whereas anionic AuNPs internalisation occurred only after 6 hours (Boyles *et al*., 2015). These findings can be attributed to the repulsive forces between negatively-charged AuNPs and the negatively-charged cell membrane. In terms of intracellular trafficking, cationic AuNPs have exhibited perinuclear arrangement whereas anionic AuNPs remain in endocytic vesicles (Shukla *et al*., 2005).

Cellular internalization of AuNPs has shown to be dependent on cell type, concentration and incubation time. Internalization is also likely to differ for different preparations of AuNPs due to their variations in size, charge and surface chemistry (Choi *et al*., 2013). It has been reported that cationic AuNPs depend on endocytosis for cellular transport and uptake (Lin *et al*., 2013). After endocytosis, the endo-lysosomal compartment facilitates the degradation of biodegradable AuNPs. Those that are non-degradable are excreted along with phagocytosing

cells (Pan *et al*., 2007). *In vivo*, this occurs by excretion in faeces or expectoration by the lung.

#### 2.3.4.3 Transfection Efficiency

Transfection efficiency and release of the therapeutic payload are improved by the hydrophobicity of the AuNPs that have been functionalised with CPs or other positively-charged biomolecules (Rana *et al*., 2012). Positively charged AuNPs have shown an overall trend of efficient nucleic acid condensation, protection, delivery and expression. Cationic AuNPs with amino-based side chains are more efficient for DNA transfection (Kim *et al*., 2006) compared to neutral and anionic AuNPs. Due to the positive charges of surface-functionalised AuNPs at physiological pH, the nanoconjugates interact strongly with negatively charged nucleic acids. The ratio of positive charges present on the amines to the negative charges present on the selected nucleic acid and the concentration and length of the amine chains are factors which have been shown to influence the efficiency of nanoparticle mediated gene delivery.

Simple cationic primary amine groups used to functionalise AuNPs can increase gene delivery and transfection efficiency (Noh *et al*., 2007) . PLL-AuNPs have been shown to be highly efficacious for the delivery of plasmid DNA and surpasses most commercial vectors (Ghosh *et al*., 2008). CS-AuNP/DNA complexes have shown enhanced transfection efficiency in murine monocyte-macrophage cells (RAW264.7 cells) which was attributed to the stability of the CS-AuNPs in serum (Zhou *et al*., 2008). To date, most investigations have covered AuNPs for pDNA, siRNA and miRNA delivery with limited reports on the use of AuNPs or CP-AuNPs for the delivery of mRNA which theoretically is a far superior nucleic acid in terms of achieving the goal of gene therapy as explained earlier.

In this study, we have evaluated the transfection efficiency and transgene expression in normal and cancer cell lines as a means to assess the potential of CP-AuNPs as vectors for the delivery of mRNA with the aim of the formulation of vaccines for the immunotherapy of cancer.

## REFERENCES


Adair, T. H, and Montani, J-P. (2010). Overview of angiogenesis.

Andersen, T., Bleher, S., Eide F. G., Tho, I., Mattsson, S., and Škalko-Basnet, N. (2015). Chitosan in mucoadhesive drug delivery: focus on local vaginal therapy. *Marine drugs, 13*(1), 222-236.

Ashworth, A., Lord, C. J., and Reis-Filho, J. S. (2011). Genetic interactions in cancer progression and treatment. *Cell, 145*(1), 30-38.

Baigent, C., and Müller, G. (1980). A colloidal gold prepared with ultrasonics. *Experientia, 36*(4), 472-473.

Balasubramanian, S. K, Yang, L., Yung, L-Y. L., Ong, C-N., Ong, W-Y., and Liya, E. Y. (2010). Characterization, purification, and stability of gold nanoparticles. *Biomaterials, 31*(34), 9023-9030.

Baptista, P., Fernandes, A., Figueiredo, S., Vinhas, R., Cordeiro, M., Carlos, F., and Mendo, S. (2015). Gold nanoparticle-based theranostics: Disease diagnostics and treatment using a single nanomaterial. *Nanobiosen. Dis. Diagn, 4*(11).

Bartneck, M., Keul, H. A., Wambach, M., Bornemann, J., Gbureck, U., Chatain, N., Zwadlo-Klarwasser, G. (2012). Effects of nanoparticle surface-coupled peptides, functional endgroups, and charge on intracellular distribution and functionality of human primary reticuloendothelial cells. *Nanomedicine: Nanotechnology, Biology and Medicine, 8*(8), 1282-1292.

Boca, S. C., Potara, M., Toderas, F., Stephan, O., Baldeck, P. L., and Astilean, S. (2011). Uptake and biological effects of chitosan-capped gold nanoparticles on Chinese Hamster Ovary cells. *Materials Science and Engineering: C, 31*(2), 184-189.

Bolhassani, A., and Rafati, S. (2011). *Non-Viral Delivery Systems in Gene Therapy and Vaccine Development*: INTECH Open Access Publisher.

Boyles, M. S. P., Kristl, T., Andosch, A., Zimmermann, M., Tran, N., Casals, E., Lütz-Meindl, U. (2015). Chitosan functionalisation of gold nanoparticles encourages particle uptake and induces cytotoxicity and pro-inflammatory conditions in phagocytic cells, as well as enhancing particle interactions with serum components. *Journal of nanobiotechnology, 13*(1), 1.

Bray, F., and Møller, B. (2006). Predicting the future burden of cancer. *Nature Reviews Cancer, 6*(1), 63-74.

Brust, M., Walker, M., Bethell, D., Schiffrin, D. J., and Whyman, R. (1994). Synthesis of thiol-derivatised gold nanoparticles in a two-phase liquid–liquid system. *Journal of the Chemical Society, Chemical Communications* (7), 801-802.

Cancer Association of South Africa. (2016). Fact Sheet on a Health Profile of South Africa and Related Information.

Cantley, L. C., Dalton, W. S., DuBois, R. N., Finn, O. J., Futreal, P. A., Golub, T. R., Nelson, W. G. (2012). AACR Cancer Progress Report 2012. *Clinical cancer research: an official journal of the American Association for Cancer Research, 18*(21 Suppl).

Chial, H. (2008). Tumor suppressor (TS) genes and the two-hit hypothesis. *Nature Education, 1*(1), 177.

Choi, C. H. J., Hao, L., Narayan, S. P., Auyeung, E., and Mirkin, C. A. (2013). Mechanism for the endocytosis of spherical nucleic acid nanoparticle conjugates. *Proceedings of the National Academy of Sciences, 110*(19), 7625-7630.

Cosgrove, T. (2005). Polymers at interfaces. *Colloid Science: Principles, Methods and Applications*, 113-142.

Cotrim, A. P., and Baum, B. J. (2008). Gene therapy: some history, applications, problems, and prospects. *Toxicologic pathology, 36*(1), 97-103.

De Jong, W. H., Hagens, W. I., Krystek, P., Burger, M. C., Sips, A. J.A.M., and Geertsma, R. E. (2008). Particle size-dependent organ distribution of gold nanoparticles after intravenous administration. *Biomaterials, 29*(12), 1912-1919.

De Long, R. K., Reynolds, C. M., Malcolm, Y., Schaeffer, A., Severs, T., and Wanekaya, A. (2010). Functionalized gold nanoparticles for the binding, stabilization, and delivery of therapeutic DNA, RNA, and other biological macromolecules. *Nanotechnol Sci Appl, 3*(1), 53-63.

Deb, S., Patra, H. K., Lahiri, P., Dasgupta, A. K. R, Chakrabarti, K., and Chaudhuri, U. (2011). Multistability in platelets and their response to gold nanoparticles. *Nanomedicine: Nanotechnology, Biology and Medicine, 7*(4), 376-384.

Ding, Y., Jiang, Z., Saha, K., Kim, C. S., Kim, S. T., Landis, R. F, and Rotello, V. M. (2014). Gold nanoparticles for nucleic acid delivery. *Molecular Therapy, 22*(6), 1075.

Does, A., Thiel, T., and Johnson, N. (2003). Rediscovering biology: molecular to global perspectives. *Annenberg Learner, Washington*.

Douma, M., curator. (2008). Causes of colour. from http://www.webexhibits.org/causesofcolor/3.html

Dukhin, A. S., and Goetz, P. J. (2010). Fundamentals of Interface and Colloid Science. *Studies in Interface Science, 24*, 21-89.

Elsabahy, M., Nazarali, A., and Foldvari, M. (2011). Non-viral nucleic acid delivery: key challenges and future directions. *Current drug delivery, 8*(3), 235-244.

Fadjari, H. (2011). Understanding cancer.

Faraday, M. (1857). The Bakerian lecture: experimental relations of gold (and other metals) to light. *Philosophical Transactions of the Royal Society of London, 147*, 145-181.

Fogar, P., Greco, E., Basso, D., Navaglia, F., Plebani, M., and Pedrazzoli, S. (2005). Killer genes in pancreatic cancer therapy. *Cell Mol Biol (Noisy-le-grand), 51*(1), 61-76.

Gao, W., Xu, K., Ji, L., and Tang, B. (2011). Effect of gold nanoparticles on glutathione depletion-induced hydrogen peroxide generation and apoptosis in HL7702 cells. *Toxicology letters, 205*(1), 86-95.

Gardlík, R., Pálffy, R., Hodosy, J., Lukács, J., Turna, J., and Celec, P. (2005). Vectors and delivery systems in gene therapy. *Medical Science Monitor, 11*(4), RA110-RA121.

Gascón, A. R., Pozo-Rodríguez, A. D., and Solinís, M. A. (2013). Non-viral delivery systems in gene therapy. *Gene therapy–tools and potential application*.

Ghosh, P., Han, G., De, M., Kim, C. K., and Rotello, V. M. (2008). Gold nanoparticles in delivery applications. *Advanced drug delivery reviews, 60*(11), 1307-1315.

Giljohann, D. A., Seferos, D. S., Patel, P. C., Millstone, J. E., Rosi, N. L., and Mirkin, C. A. (2007). Oligonucleotide loading determines cellular uptake of DNA-modified gold nanoparticles. *Nano letters, 7*(12), 3818-3821.

Gosens, I., Post, J. A., de la Fonteyne, L. J. J, Jansen, E. H. J.M., Geus, J. W., Cassee, F. R., and de Jong, W. H. (2010). Impact of agglomeration state of nano-and submicron sized gold particles on pulmonary inflammation. *Particle and fibre toxicology, 7*(1), 1.

Guo, C. X., Sheng, Z. M., Shen, Y. Q., Dong, Z. L., and Li, C. M. (2010). Thin-walled graphitic nanocages as a unique platform for amperometric glucose biosensor. *ACS applied materials and interfaces, 2*(9), 2481-2484.

Herizchi, R., Abbasi, E., Milani, M., and Akbarzadeh, A. (2016). Current methods for synthesis of gold nanoparticles. *Artificial cells, nanomedicine, and biotechnology, 44*(2), 596-602.

Hsu, S-H., Chang, Y-B., Tsai, C-L., Fu, K-Y., Wang, S-H., and Tseng, H-J. (2011). Characterization and biocompatibility of chitosan nanocomposites. *Colloids and Surfaces B: Biointerfaces, 85*(2), 198-206.

Huefner, A., Septiadi, D., Wilts, B. D., Patel, I. I., Kuan, W-L., Fragniere, A., Mahajan, S. (2014). Gold nanoparticles explore cells: Cellular uptake and their use as intracellular probes. *Methods, 68*(2), 354-363.

Ibraheem, D., Elaissari, A., and Fessi, H. (2014). Gene therapy and DNA delivery systems. *International journal of pharmaceutics, 459*(1), 70-83.

Jain, P. K., Lee, K. S., El-Sayed, I. H., and El-Sayed, M. A. (2006). Calculated absorption and scattering properties of gold nanoparticles of different size, shape, and composition: applications in biological imaging and biomedicine. *The Journal of Physical Chemistry B, 110*(14), 7238-7248.

Jin, L., Zeng, X., Liu, M., Deng, Y., and He, N. (2014). Current progress in gene delivery technology based on chemical methods and nano-carriers. *Theranostics, 4*(3), 240-255.

Johnston, H. J., Semmler-Behnke, M., Brown, D. M., Kreyling, W., Tran, L., and Stone, V. (2010). Evaluating the uptake and intracellular fate of polystyrene nanoparticles by primary and hepatocyte cell lines *in vitro*. *Toxicology and Applied Pharmacology, 242*(1), 66-78. doi: http://dx.doi.org/10.1016/j.taap.2009.09.015

Joshi, H., Shirude, P. S., Bansal, V., Ganesh, K. N., and Sastry, M. (2004). Isothermal titration calorimetry studies on the binding of amino acids to gold nanoparticles. *The Journal of Physical Chemistry B, 108*(31), 11535-11540.

Kennedy, L. C., Bickford, L. R., Lewinski, N. A., Coughlin, A. J., Hu, Y., Day, E. S., Drezek, R. A. (2011). A New Era for Cancer Treatment: Gold-Nanoparticle-Mediated Thermal Therapies. *Small, 7*(2), 169-183.

Khan, A. K., Rashid, R., Murtaza, G., and Zahra, A. (2014). Gold Nanoparticles: Synthesis and Applications in Drug *Tropical Journal of Pharmaceutical Research, 13*(7), 1169-1177.

Kim, J., Wilson, D. R., Zamboni, C. G., and Green, J. J. (2015). Targeted polymeric nanoparticles for cancer gene therapy. *Journal of drug targeting, 23*(7-8), 627-641.

Kim, K., Choi, S., Cha, J-H., Yeon, S-H., and Lee, H. (2006). Facile one-pot synthesis of gold nanoparticles using alcohol ionic liquids. *Journal of Materials Chemistry, 16*(14), 1315-1317.

Köping-Höggård, M., Mel'nikova, Y. S., Vårum, K. M., Lindman, B., and Artursson, P. (2003). Relationship between the physical shape and the efficiency of oligomeric chitosan as a gene delivery system *in vitro* and *in vivo*. *The journal of gene medicine, 5*(2), 130-141.

Kreiter, S., Diken, M., Selmi, A., Türeci, Ö., and Sahin, U. (2011). Tumor vaccination using messenger RNA: prospects of a future therapy. *Current opinion in immunology, 23*(3), 399-406.

Lan, M-Y., Hsu, Y-B., Hsu, C-H., Ho, C-Y., Lin, J-C., and Lee, S-W.. (2013). Induction of apoptosis by high-dose gold nanoparticles in nasopharyngeal carcinoma cells. *Auris Nasus Larynx, 40*(6), 563-568.

Libutti, S. K., Paciotti, G. F., Byrnes, A. A., Alexander, H. R., Gannon, W. E., Walker, M., and Tamarkin, L. (2010). Phase I and pharmacokinetic studies of CYT-6091, a novel PEGylated colloidal gold-rhTNF nanomedicine. *Clinical Cancer Research, 16*(24), 6139-6149.

Lin, J., and Alexander-Katz, A. (2013). "Cell membranes open “doors” for cationic nanoparticles/biomolecules: insights into uptake kinetics." *ACS nano, 7*(12): 10799-10808.

Lodish, H., Berk, A., Zipursky, L. S., Matsudaira, P., Baltimore, D., and Darnell, J. (2000). DNA Damage and Repair and Their Role in Carcinogenesis.

Long, N. N., Kiem, C, D., Doanh, S. C., Nguyet, C. T., Hang, P. T., Thien, N. D., and Quynh, L. M. (2009). *Synthesis and optical properties of colloidal gold nanoparticles.* Paper presented at the Journal of Physics: Conference Series.

Lundstrom, K., and Boulikas, T. (2003). Viral and non-viral vectors in gene therapy: technology development and clinical trials. *Technology in cancer research and treatment, 2*(5), 471-485.

Manjila, S. B., Baby, J. N., Bijin, E. N., Constantine, I., Pramod, K., and Valsalakumari, J. (2013). Novel gene delivery systems. *International journal of pharmaceutical investigation, 3*(1), 1.

Mansouri, S., Lavigne, P., Corsi, K., Benderdour, M., Beaumont, E., and Fernandes, J. C. (2004). Chitosan-DNA nanoparticles as non-viral vectors in gene therapy: strategies to improve transfection efficacy. *European journal of pharmaceutics and biopharmaceutics, 57*(1), 1-8.

Matsui, A., Uchida, S., Ishii, T., Itaka, K., and Kataoka, K. (2015). Messenger RNA-based therapeutics for the treatment of apoptosis-associated diseases. *Scientific reports, 5*.

Mohanpuria, P., Rana, N. K., and Yadav, S. K. (2008). Biosynthesis of nanoparticles: technological concepts and future applications. *Journal of Nanoparticle Research, 10*(3), 507-517.

Mohd S. N., and Johan, M. R. (2014). Synthesis and Ultraviolet Visible Spectroscopy Studies of Chitosan Capped Gold Nanoparticles and Their Reactions with Analytes. *The Scientific World Journal, 2014*.

Mühlfeld, C., Rothen-Rutishauser, B., Blank, F., Vanhecke, D., Ochs, M., and Gehr, P. (2008). Interactions of nanoparticles with pulmonary structures and cellular responses. *American Journal of Physiology-Lung Cellular and Molecular Physiology, 294*(5), L817-L829.

Murawala, P., Tirmale, A., Shiras, A., and Prasad, B. (2014). In situ synthesized BSA capped gold nanoparticles: Effective carrier of anticancer drug Methotrexate to MCF-7 breast cancer cells. *Materials Science and Engineering: C, 34*, 158-167.

Myllynen, P. K., Loughran, M. J., Howard, V. C., Sormunen, R., Walsh, A. A., and Vähäkangas, K. H. (2008). Kinetics of gold nanoparticles in the human placenta. *Reproductive toxicology, 26*(2), 130-137.

Nam, H. Y., Kwon, S. M., Chung, H., Lee, S-Y., Kwon, S-H., Jeon, H., and Her, S. (2009). Cellular uptake mechanism and intracellular fate of hydrophobically modified glycol chitosan nanoparticles. *Journal of Controlled Release, 135*(3), 259-267.

Narayanan, R. L., and Sivakumar, M. (2014). *Preparation and Characterization of Gold Nanoparticles in Chitosan Suspension by One-Pot Chemical Reduction Method.* Paper presented at the Nano Hybrids.

Narayanan, K. B., and Sakthivel, N. (2010). Biological synthesis of metal nanoparticles by microbes. *Advances in colloid and interface science, 156*(1), 1-13.

Nayerossadat, N., Maedeh, T., and Ali, P. A. (2012). Viral and nonviral delivery systems for gene delivery. *Advanced biomedical research, 1*(1), 27.

Niidome, T., Yamagata, M., Okamoto, Y., Akiyama, Y., Takahashi, H., Kawano, T., and Niidome, Y. (2006). PEG-modified gold nanorods with a stealth character for *in vivo* applications. *Journal of Controlled Release, 114*(3), 343-347.

Noh, S. M., Kim, W-K., Kim, S. J., Kim, J. M., Baek, K-H., and Oh, Y-K. (2007). Enhanced cellular delivery and transfection efficiency of plasmid DNA using positively charged biocompatible colloidal gold nanoparticles. *Biochimica et Biophysica Acta (BBA)-General Subjects, 1770*(5), 747-752.

Pan, Y., Neuss, S., Leifert, A., Fischler, M., Wen, F., Simon, U., and Jahnen-Dechent, W. (2007). Size-dependent cytotoxicity of gold nanoparticles. *Small, 3*(11), 1941-1949.

Pedrosa, P., Vinhas, R., Fernandes, A., and Baptista, P. V. (2015). Gold nanotheranostics: proof-of-concept or clinical tool? *Nanomaterials, 5*(4), 1853-1879.

Pelengaris, S. (2013). *The molecular biology of cancer: A bridge from bench to bedside*: John Wiley and Sons.

Perrault, S. D., and Chan, W. C. (2009). Synthesis and surface modification of highly monodispersed, spherical gold nanoparticles of 50− 200 nm. *Journal of the American Chemical Society, 131*(47), 17042-17043.

Pillay, J., Ozoemena, K. I., Tshikhudo, R. T., and Moutloali, R. M. (2010). Monolayer-protected clusters of gold nanoparticles: impacts of stabilizing ligands on the heterogeneous electron transfer dynamics and voltammetric detection. *Langmuir, 26*(11), 9061-9068.

Ponder, K. P. (2001). Vectors in gene therapy. *An introduction to molecular medicine and gene therapy*, 77-112.

Ramamoorth, M., and Narvekar, A. (2015). Non viral vectors in gene therapy-an overview. *J Clin Diagn Res, 9*(1), GE01-GE06.

Rana, S., Bajaj, A., Mout, R., and Rotello, V. M. (2012). Monolayer coated gold nanoparticles for delivery applications. *Advanced drug delivery reviews, 64*(2), 200-216.

Reetz, M. T., and Helbig, W. (1994). Size-selective synthesis of nanostructured transition metal clusters. *Journal of the American Chemical Society, 116*(16), 7401-7402.

Rezende, T. S., Andrade, G. R. S., Barreto, L. S., Costa, N. B., Gimenez, I. F., and Almeida, L. E. (2010). Facile preparation of catalytically active gold nanoparticles on a thiolated chitosan. *Materials Letters, 64*(7), 882-884.

Richter, K., Campbell, P. S., Baecker, T., Schimitzek, A., Yaprak, D., and Mudring, A-V. (2013). Ionic liquids for the synthesis of metal nanoparticles. *physica status solidi (b), 250*(6), 1152-1164.

Rivera-Gil, P., Jimenez De Aberasturi, D., Wulf, V., Pelaz, B., Del Pino, P., Zhao, Y., Liang, X-J. (2012). The challenge to relate the physicochemical properties of colloidal nanoparticles to their cytotoxicity. *Accounts of chemical research, 46*(3), 743-749.

Sandhu, K. K., McIntosh, C. M., Simard, J. M., Smith, S. W., and Rotello, V. M. (2002). Gold nanoparticle-mediated transfection of mammalian cells. *Bioconjugate chemistry, 13*(1), 3-6.

Segura, T., and Shea, L. D. (2001). Materials for non-viral gene delivery. *Annual Review of Materials Research, 31*(1), 25-46.

Shukla, R., Bansal, V., Chaudhary, M., Basu, A., Bhonde, R. R., and Sastry, M. (2005). Biocompatibility of gold nanoparticles and their endocytotic fate inside the cellular compartment: a microscopic overview. *Langmuir, 21*(23), 10644-10654.

Sivaramakrishnan, C., Jositta S. J., and Yadavalli, T. (2014). Surface functionalization of gold nanoparticles for targeted drug delivery. *International Journal of ChemTech Research, 7*(3), 1198-1205.

Smirnovas, V., Winter, R., Funck, T.r, and Dzwolak, W. (2005). Thermodynamic properties underlying the α-helix-to-β-sheet transition, aggregation, and amyloidogenesis of polylysine as probed by calorimetry, densimetry, and ultrasound velocimetry. *The Journal of Physical Chemistry B, 109*(41), 19043-19045.

Stanglmair, C., Scheeler, S. P., and Pacholski, C. (2014). Seeding growth approach to gold nanoparticles with diameters ranging from 10 to 80 nanometers in organic solvent. *European Journal of Inorganic Chemistry, 2014*(23), 3633-3637.

Stobiecka, M., and Hepel, M. (2011). Double-shell gold nanoparticle-based DNA-carriers with poly-L-lysine binding surface. *Biomaterials, 32*(12), 3312-3321.

Szende, B., Szökán, G.Y., Tyihá, E., Pál, K., Gáborjányi, R., Almás, M., and Khlafulla, A. R. (2002). Antitumor effect of lysine-isopeptides. *Cancer cell international, 2*(1), 1.

Takahashi, S., and Matsuoka, O. (1981). Cross placental transfer of 198Au-colloid in near term rats. *Journal of radiation research, 22*(2), 242-249.

Tavernier, G., Andries, O., Demeester, J., Sanders, N. N., De Smedt, S. C., and Rejman, J. (2011). mRNA as gene therapeutic: how to control protein expression. *Journal of controlled release, 150*(3), 238-247.

Thermo Fisher Scientific. (2016). Neurobiology transfection guide.

Turkevich, J., Stevenson, P. C., and Hillier, J. (1951). A study of the nucleation and growth processes in the synthesis of colloidal gold. *Discussions of the Faraday Society, 11*, 55-75.

Vijayakumar, S., and Ganesan, S. (2012). In vitro cytotoxicity assay on gold nanoparticles with different stabilizing agents. *Journal of Nanomaterials, 2012*, 14.

Weide, B., Garbe, C., Rammensee, H-G., and Pascolo, S. (2008). Plasmid DNA-and messenger RNA-based anti-cancer vaccination. *Immunology letters, 115*(1), 33-42.

Wheeler, J. J., Palmer, L., Ossanlou, M., MacLachlan, I., Graham, R. W., Zhang, Y. P., and Cullis, P. R. (1999). Stabilized plasmid-lipid particles: construction and characterization. *Gene therapy, 6*(2), 271-281.

Wiethoff, C. M., and Middaugh, R. C. (2003). Barriers to nonviral gene delivery. *Journal of pharmaceutical sciences, 92*(2), 203-217.

Wu, J., Nantz, M. H., and Zern, M. A. (2002). Targeting hepatocytes for drug and gene delivery: emerging novel approaches and applications. *Frontiers in bioscience: a journal and virtual library, 7*, d717-725.

Yamamoto, A., Kormann, M., Rosenecker, J., and Rudolph, C. (2009). Current prospects for mRNA gene delivery. *European Journal of Pharmaceutics and Biopharmaceutics, 71*(3), 484-489.

Yeh, Y-C., Creran, B., and Rotello, V. M. (2012). Gold nanoparticles: preparation, properties, and applications in bionanotechnology. *Nanoscale, 4*(6), 1871-1880.

Yellepeddi, V. K. (2015). Vectors for non-viral gene delivery–clinical and biomedical applications. *Austin Therapeutics, 2*(1), 1014.

Youn, H., and Chung, J-K. (2015). Modified mRNA as an alternative to plasmid DNA (pDNA) for transcript replacement and vaccination therapy. *Expert opinion on biological therapy, 15*(9), 1337-1348.

Zelphati, O., Wang, Y., Kitada, S., Reed, J. C., Felgner, P. L., and Corbeil, J. (2001). Intracellular delivery of proteins with a new lipid-mediated delivery system. *Journal of Biological Chemistry, 276*(37), 35103-35110.

Zhou, X., Zhang, X., Yu, X., Zha, X., Fu, Q., Liu, B., and Shan, Y. (2008). The effect of conjugation to gold nanoparticles on the ability of low molecular weight chitosan to transfer DNA vaccine. *Biomaterials, 29*(1), 111-117.

# CHAPTER THREE

# CHITOSAN FUNCTIONALISED GOLD NANOPARTICLE MEDIATED DELIVERY OF F*luc*-mRNA *IN VITRO*: SYNTHESIS, CHARACTERIZATION, CYTOTOXICITY AND TRANSFECTION EFFICIENCY

**S. Pillay[1] and M. Singh[1*]**

[1]Non-Viral Gene Delivery Laboratory, Discipline of Biochemistry, School of Life Sciences, University of Kwa-Zulu Natal, Private Bag X54001, Durban, South Africa

[*]Corresponding author: Moganavelli Singh, email: Singhm1@ukzn.ac.za

**Abstract**

Gold nanoparticles (AuNPs) have recently shown immense potential in clinical medicine and therapeutic delivery applications due to their many desirable properties that include stability, high dispersity, small size, surface plasmon resonance (SPR), low cytotoxicity and biocompatibility. Advances in clinical medicine have highlighted gene therapy as a promising technique for the treatment of numerous life threatening diseases such as cancer. In recent studies, plasmid DNA has been routinely utilized for gene therapy. However, its use has crucial limitations such as the requirement of intracellular trafficking and nuclear entry for efficacious gene delivery. In comparison, mRNA molecules possess the ability to overcome these barriers. In this study, we exploit the above mentioned desirable properties using chitosan functionalised AuNPs as vehicles for mRNA delivery and assess the degree of transgene expression in three human cell lines: embryonic kiney (HEK293), colorectal adenocarcinoma (Caco-2), and breast adenocarcinoma (MCF-7). AuNPs were synthesized and successfully functionalised with chitosan (CS). All nanoparticles (AuNPs and CS-AuNPs) and the nanocomplexes (CS-AuNP:F*luc*-mRNA) were characterized using UV-Vis spectrophotometry, Transmission Electron Microscopy (TEM) and Nanoparticle Tracking Analysis (NTA). CS-AuNP:F*luc*-mRNA binding, compaction and nuclease protection were evaluated using the band shift, dye displacement and nuclease protection assays, respectively. The degree of cytotoxicity of the complexes to the mammalian cells was evaluated using the MTT reduction assay and gene expression experiments were conducted using the luciferase reporter gene assay. In addition, these assays were also conducted on pure CS:F*luc*-mRNA complexes for a comparative analysis against the AuNP nanocomplexes. Results indicate that CS-AuNPs and their nanocomplexes exhibit suitable and favourable properties such as small size (CS-AuNP: 69 ± 15.2 nm, nanocomplexes: 95 ±9.9 nm), stability (zeta potential: CS-AuNP: 55.5 ±1.2 mV, nanocomplexes: 25.9 ±0.5 mV), excellent binding, low cytotoxicity, and effective transgene expression. In addition, CS-AuNPs proved to be more efficient than the CS polymer itself, indicating that AuNPs greatly improve the biological properties and functions of chitosan. Overall, these results bode well for the use of CS-AuNPs as potential vehicles for the delivery of mRNA in biomedical applications, especially in cancer treatment and immunotherapy.

Keywords: biomedical, cancer, chitosan, cytotoxicity, F*luc*-mRNA, gene expression, gold nanoparticles, immunotherapy

## 3.1 Introduction

Cancer is a scientific term used for the complex collection of diseases which entail a sequence of molecular events that primarily alter the normal properties of cells (Does *et al*., 2003). As a result, these altered cells divide uncontrollably and invade surrounding tissues, overcoming the normal control systems. The development of cancer may be caused by a variety of factors such as improper diet and exercise, exposure to certain physical and chemical agents, infection, radiation, inadequate hormone levels and inherited genetic defects (Cancer Association of South Africa, 2016). Progress in the study of treatments has increased immensely over the years, providing us with methods such as surgery, cryosurgery, chemotherapy, radiation, laser, hyperthermia, photodynamic, hormone, transplant, biological and targeted therapy (American Cancer Society, 2014). Despite this progress, cancer remains one of the leading causes of death worldwide with 8.2 million deaths reported in the year 2012 (International Agency for Research on Cancer and World Health Organization, 2014). As a major health concern for Africa, 715 000 new cancer cases and 54 000 cancer deaths occurred in 2008, with projections for the year 2030 predicting that these figures will in fact double (International Agency for Research on Cancer and Cancer Research UK, 2014). Due to the high mortality rate and the lack of fully operational treatments, it is imperative to study and develop novel treatment strategies with the purpose of alleviating the burden caused by cancer.

In this regard, it has been reported that gene therapy is a promising novel technique for the treatment of numerous incurable diseases such as cancer (Ibraheem *et al*., 2013). Gene therapy is defined as a method for the introduction of a functioning gene into cells to correct a cellular dysfunction or to offer a different cellular function in order to provide therapeutic benefit (Cotrim and Baum, 2016). There are several approaches to elicit the correction of a cellular dysfunction such as replacing the abnormal gene with a normal gene through the process of homologous recombination or returning the gene to its normal function by repairing the abnormal gene through selective reverse mutation and altering the regulation of a disease specific gene (Patil *et al*., 2012). Since the revolutionary experimentation by Malone *et al*. in 1989 involving the successful delivery of mRNA using cationic lipids, very few studies using mRNA have been reported (Bettinger *et al*., 2001) with plasmid DNA (pDNA) being used more widely in the field of gene therapy.

In comparison, mRNA based transfection provides many advantages over pDNA, for example there is no requirement for nuclear entry and the protein is expressed directly in cytoplasm, hence faster gene expression. Furthermore, there is no genomic integration. Protein expression is promoter-independent and it is suitable for hard-to-transfect cells (Matsui *et al*., 2015). To date, gene therapy has utilized two main vector systems viz., viral and non-viral as carriers for these therapeutic genes. However, the better choice of study points at non-viral vectors due to the fact that viral vectors are known to elicit immune responses. The size of genetic material that can be inserted is limited and they are difficult to prepare in large quantities and are highly expensive (Ibraheem *et al*., 2013). The challenge of gene therapy, currently, is in the development of safe and suitable carriers for efficient gene transfer. The carrier should meet the following criteria: protection of the gene from nucleases present in the cells, low or no cytotoxicity and effective transfer of the gene to the nucleus (Manjila *et al*., 2013).

Gold nanoparticles (AuNPs), in particular serve as excellent candidates for nucleic acid delivery applications (Ding *et al*., 2014). This is due to their many desirable properties such as its biocompatibility, safety and relatively inert core (Rana *et al*., 2011). Additionally, their relative ease of synthesis producing various shapes and sizes while controlling dispersity, high chemical stability, powerful surface plasmon resonance (SPR) and photothermal conversion rate have made AuNPs to be potentially good theranostic tools (Pedrosa *et al*., 2015). Above all, their high surface-to-volume ratio allows AuNPs to have a dense loading capacity in which they can be functionalised with many biological ligands and therapeutic molecules (Rana *et al*., 2011). It has been reported that more than 100 ligands can be conjugated to a 2 nm AuNP core (Hostetler *et al*., 1998). Carriers which incorporate cationic polymers are attractive due to their ease of synthesis and ability to integrate several functional groups within the same molecule without compromising nucleic acid binding ability (Zhou *et al*., 2008). Among these cationic polymers, chitosan has been chosen as an ideal candidate for functionalisation as it is non-toxic, biodegradable, biocompatible, able to interact and permeate the cell membrane making it an effective adjuvant (Boyles *et al*., 2015). Functionalisation with chitosan reduces AuNP precursors due to the polyelectrolyte behaviour provided by its protonated amine groups resulting in the stabilization of the AuNPs (Narayanan and Sivakumar, 2014).

In this study, we synthesized and characterized chitosan functionalised AuNPs using various chemical and physical techniques, assessed their ability to bind and protect luciferase-encoded mRNA (F*luc*-mRNA) and finally evaluated their cytotoxicity, transfection efficiency and apoptosis induction in three mammalian cell lines (HEK293, Caco-2 and MCF-7) with the aim of determining their effectiveness as gene therapy vectors for cancer treatment.

## 3.2 Materials and methods

For the preparation of all reagents and solutions, Ultrapure (18 M ohm) deionized water (Milli-Q Academic, Millipore, France) was utilized. All reagents and chemicals were commercially purchased and of analytical grade.

### 3.2.1 General materials and reagents

Gold (III) chloride trihydrate ($M_w$: 393.83 g/mol, HAuCl4.3H2O), chitosan ≥ 75% deacetylated, saccharose (Sucrose, $M_w$: 342.30 g/mol, $C_{12}H_{22}O_{11}$), 2, 2-dihydroxyindane-1, 3-dione (Ninhydrin, $M_w$: 178.14 g/mol, $C_9H_6O_4$) were supplied by Sigma-Aldrich Chemical Co., (St. Louis, USA). Sodium citrate tribasic dehydrate ($M_w$: 294.20 g/mol, $Na_3C_6H_5O_7.2H_2O$), 2-[4-(2-hydroxyethyl) piperazin-1-yl] ethanesulphonic acid (HEPES, $C_8H_{18}N_2O_4S$), tris (hydroxymethyl) aminomethane [Tris base, $M_w$: 121.14 g/mol, $H_2NC(CH_2OH)_3$], sodium dihydrogen orthophosphate dehydrate ($M_w$: 156.01 g/mol, $NaH_2PO_4.2H_2O$), ethylene diamine tetra acetic acid disodium salt ($M_w$: 372.24 g/mol, EDTA, $C_{10}H_{14}N_2Na_2O_8.2H_2O$), dodecyl sulphate sodium salt (SDS, $M_w$: 288.37 g/mol, $C_{12}H_2OSO_2Na$ ), bromophenol blue ($M_w$: 669.96 g/mol, $C_{19}H_{10}Br_4O_5S$) were supplied by Merck (Darmstadt, Germany). Glacial acetic acid ($M_w$: 60.05 g/mol, $CH_3COOH$) was supplied by BDH Chemicals Ltd. (Poole, England). UltraPure™ agarose, RNase free water (1 U/µl, supplied with $MnCl_2$) and UltraPure™ DEPC-treated water were supplied by Thermo Fischer Scientific Inc., (Waltham, Massachusetts, USA). Molecular grade ethidium bromide solution (10 mg/ml) [3, 8-Diamino-5-ethyl-6-phenylphenanthrinidium bromide, Homidium bromide, EtBr, ($M_w$: 394.31 g/mol, $C_{21}H_{20}BrN_3$) was supplied by Promega (Madison, Wisconsin, USA). Fetal Bovine Serum (FBS) was supplied by Hyclone GE Healthcare (Utah, USA). SYBR Green II RNA gel stain (10 000× concentrate in DMSO) was supplied by Cambrex Bio Science Rockland Inc., (Rockland, ME). The F*luc*-mRNA was provided by the

Laboratory of Molecular and Cellular Therapy, Department of Immunology-Physiology, Vrije University, Brussels, Belgium.

### 3.2.2 Experimental methods

#### 3.2.2.1 Colloidal AuNP synthesis by citrate reduction

An aqueous colloidal AuNP solution with a concentration of 0.45 x $10^{-3}$ M was prepared by the $HAuCl_4$ reduction method adapted from Turkevich *et al.*, 1951 (Figure 3.1). Approximately 25 ml of 18 M ohm water was heated to 90ºC and maintained at this temperature with constant mixing at a medium speed for the remaining steps using a MH-4 Analog heating magnetic stirrer (Fried Electric, Israel). Thereafter, 375 µl of a 3 x $10^{-2}$ M Gold (III) chloride trihydrate solution was added to the water, followed by the addition of 1 ml of a 1% (w/v) sodium citrate solution. The solution was then boiled for a further 15 minutes, taking note of the colour transitions during the boiling period as outlined in Figure 3.2. The colour changed within 2-3 minutes from pale yellow to dark blue, to black and after 10 minutes to ruby red, denoting the formation of the desired AuNPs. This solution was then boiled for a further 5 minutes and thereafter allowed to cool and stored at room temperature.

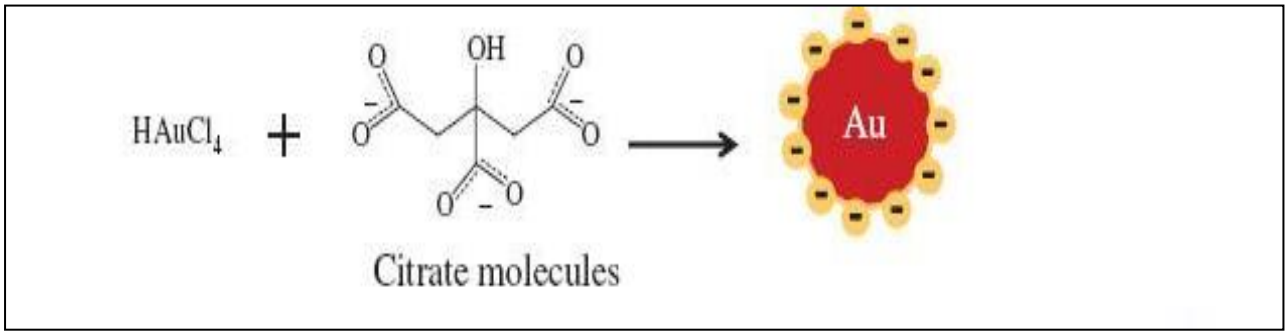


**Figure 3.1:** Diagram depicting the formation of a citrate reduced AuNP core resulting from the Turkevich method (Bahadur *et al*., 2013).

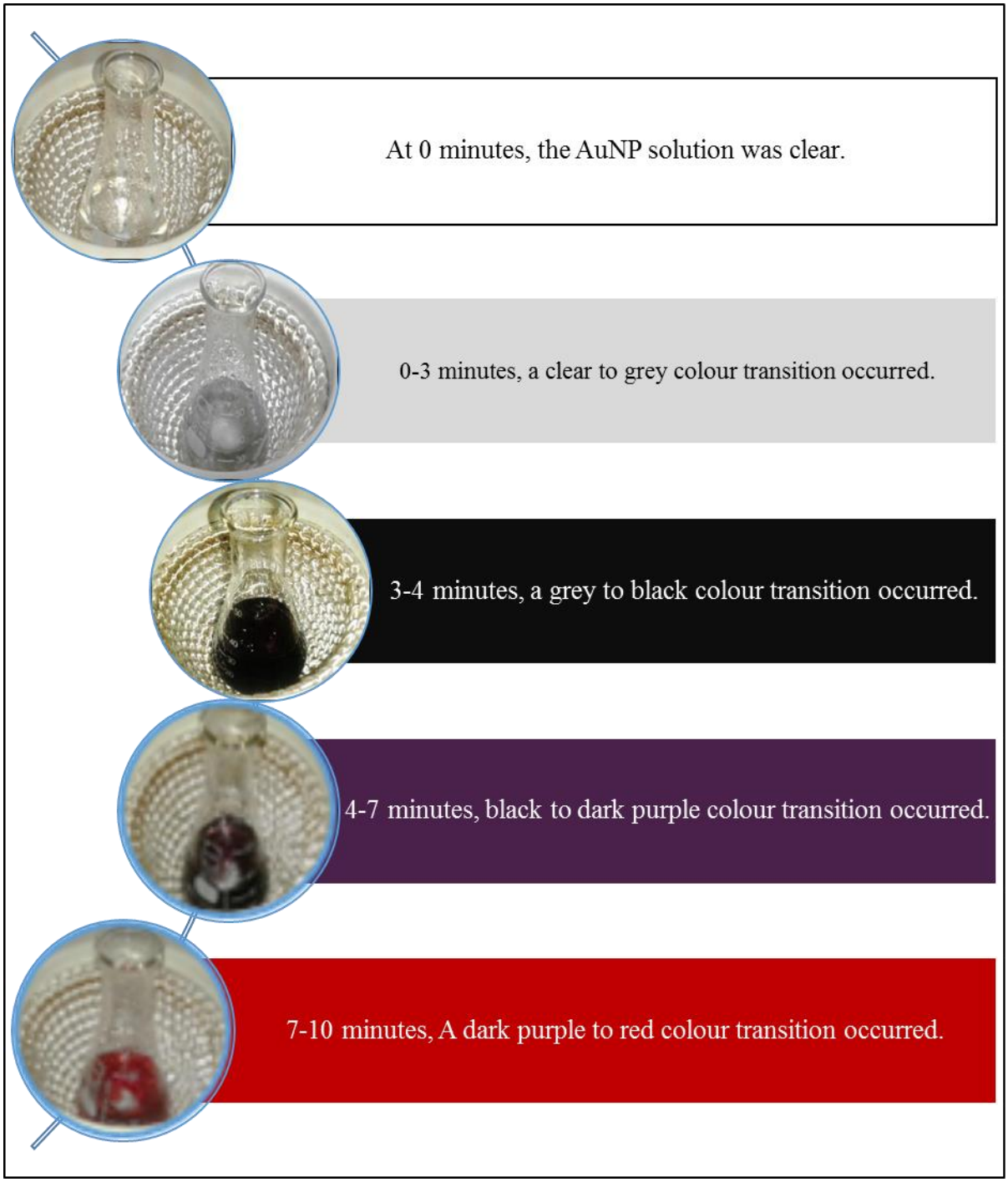


**Figure 3.2:** Schematic representation of the colour transitions observed during the synthesis of AuNPs.

### 3.2.2.2 Functionalisation of AuNPs with chitosan

A primary chitosan stock solution (1 mg/ml) was prepared by dissolving 50 mg of chitosan (CS) in 50 ml of 1% glacial acetic acid. For experimental use, a 0.025 µg/µl CS solution was prepared from the primary stock solution (1 mg/ml).

Functionalisation was carried out by the drop-wise addition of 1 ml of the AuNP solution to 1 ml of the CS primary stock solution (1 µg/µl) under constant moderate vortexing using a Genie 2 vortex (Scientific Industries, USA) producing CS functionalized gold nanoparticles (CS-AuNPs) with a AuNP:CS ratio of 1:1, (Figure 3.3). The final concentration of CS in solution was calculated to be 0.5 µg/µl as a result of dilution and was used in calculations for the subsequent protocols. A 0.025 µg/µl of CS-AuNP solution was prepared by dilution and all solutions then stored at room temperature.

**Figure 3.3:** Image of CS functionalised AuNP (CS-AuNP) solution.

Dialysis of the CS-AuNP solution was conducted to remove any unbound polymer from the solution and to determine the binding efficiency of the AuNPs to CS. The CS-AuNP solution was dialysed against 400 ml of 18 M Ohm water at room temperature for 2 hours using a cellulose dialysis membrane [(MWCO: 12-14000 Daltons, Sigma-Aldrich, USA].

### 3.2.2.3 Elemental verification of synthesized nanoparticle solutions

Prior to conducting any experimental analysis on the synthesized AuNP and CS-AuNP formulations, Inductively Coupled Plasma (ICP), Fourier Transformed Infrared Spectroscopy (FTIR) and the qualitative ninhydrin test were performed in order to verify the successful synthesis of these nanoparticle solutions based on their composition.

#### 3.2.2.3.1 Inductively Coupled Plasma (ICP) analysis

Elemental detection and quantification of the Au concentration in the AuNP solution was examined by inductively coupled plasma-optical emission spectroscopy (ICP-OES), performed on a Perkin Elmer Optima 5300 DV Optical Emission Spectrometer. A standard

calibration curve was set up between 1 and 20 ppm using a 100 ppm Au standard stock solution purchased from Fluka for the analysis.

#### 3.2.2.3.2 Fourier Transformed Infrared Spectroscopy (FTIR) analysis

FTIR analysis of the AuNPs was conducted in a Spectrum Perkin Elmer spectrophotometer, precisely equipped with a Universal ATR sampling accessory using a diamond crystal. Spectrum Analysis Software was used to obtain the respective IR spectra.

#### 3.2.2.3.3 Qualitative ninhydrin test for amino acids

A simple test to validate the successful functionalisation and verification of the presence of CS via its amine groups in the CS-AuNP solution was carried out using the qualitative ninhydrin reaction. Briefly, to 1 ml of the CS-AuNP solution was added 1 ml of a 0.1% ninhydrin solution and the mixture boiled for 3-5 minutes in a boiling water bath. Thereafter, the mixture was cooled and the presence or absence of a clear to blue/purple colour transition recorded was indicative of the presence of the amine functionality and hence successful functionalisation.

### 3.2.2.4 Formation of mRNA:NP complexes

Lyophilised F*luc*-mRNA (50 µg) was dissolved in 200 µl of RNase-free water and the stock solution stored at $4^0$C. The purity and concentration of the stock solution was verified and confirmed to be 0.25 µg/µl using a Nanospec 2000C spectrophotometer. The CS-AuNP solution (0.025 µg/µl) was sonicated for 1 minute in a Transsonic 460/H sonicator (Elma Schmidbauer GmbH, Germany) to evenly disperse the AuNPs in solution. The complexes were prepared by adding F*luc*-mRNA (0.25 µg/µl) to increasing amounts of the CS-AuNPs and CS, respectively, to create various CS-AuNP/CS:F*luc*-mRNA (w/w) mass ratios. CS on its own was included for comparison with CS-AuNP to verify if there are any enhanced properties due to functionalisation with AuNPs, over CS by itself. Thereafter, the complexes were made up to a final volume of 10 µl with HEPES buffered saline [HBS, (20 mM HEPES; 150 mM NaCl), pH 7.4]. The mixtures were then incubated at room temperature for 30 minutes to allow for the formation of CS-AuNP/CS:F*luc*-mRNA complexes.

### 3.2.2.5 Characterization of nanoparticle and nanocomplexes

#### 3.2.2.5.1 UV-Vis optical spectrophotometry analysis

The formation of nanoparticle solutions were monitored using UV spectrophotometry. The absorbance (Abs) readings of the AuNPs, CS-AuNPs and CS-AuNP:F*luc*-mRNA [Ratio 0.4:1 as prepared (3.2.2.4) and outlined in Table 3.1] solutions were measured over a wavelength range of 200 nm - 800 nm using a Biomate 3 spectrophotometer (Thermo Fischer Scientific Inc., Waltham, Massachusetts, USA) with 18 M ohm water as a blank. A UV spectrum was acquired and recorded as a plot of absorbance versus wavelength (nm) for each solution and compared to previous literature to confirm the expected SPR absorption of AuNPs in the range of 510 nm - 550 nm (Verma *et al*., 2014). UV spectrophotometry was also conducted on the dialysed CS-AuNP solution which provided an indication of the binding efficiency, using the formula: Unbound CS (%) = (Abs before dialysis – Abs after dialysis/Abs before dialysis) x 100% and thus bound CS (%) = 100% - unbound CS %.

#### 3.2.2.5.2 Transmission Electron Microscopy (TEM)

The shape, morphology, uniformity and distribution of all nanoparticle and nanocomplexes were evaluated using transmission electron microscopy. Approximately 1 µl of AuNP, CS-AuNP and CS-AuNP:F*luc*-mRNA (0.4:1 w/w) solutions were added to separate carbon coated Formvar grids and air-dried before viewing. Samples were viewed using a JEOL-JEM TEM1010 (Jeol, Tokyo, Japan) without warming above -150ºC at an acceleration voltage of 100 kV. Images were captured using the iTEM Soft Imaging Systems (SIS) Megaview III fitted with a side-mounted 3-megapixel digital camera.

#### 3.2.2.5.3 Nanoparticle Tracking Analysis (NTA)

The average size and concentration of nanoparticles in solution based on particle-particle analysis was determined using Nanoparticle Tracking Analysis (NTA) which also determines the zeta potential and, hence, colloidal stability of the nanoparticles.

The Nanosight NS500 Nanoparticle characterization system and NTA version 3.2 Software (Malvern Instruments Ltd., Worcestershire, UK) were used. The system was first primed and flushed with 18 M Ohm water, removing any trapped air bubbles and any residual mobile matter off the stage to ensure accurate readings. For this analysis, AuNP, CS-AuNP (1/500 dilution) and CS-AuNP:F*luc*-mRNA (1/100 dilution) solutions were examined.

#### 3.2.2.6 Assessment of CS and CS-AuNP binding to F*luc*-mRNA

##### 3.2.2.6.1 Gel retardation assay

The minimum concentration of CS-AuNP and CS required to fully bind 0.25 µg/µl of F*luc*-mRNA and the optimal ratio for complex formation was determined using the band shift or gel retardation assay.

A 2% (w/v) agarose gel containing 3 µl of ethidium bromide (10 mg/ml), 2 ml of 10 x Tris-phosphate-ethylenediamine tetra acetic acid (EDTA) [TPE] electrophoresis buffer fitted with an 8 well comb was prepared. The agarose gel was allowed to polymerise for approximately 1 hour on a flat surface, after which the comb was carefully removed and the casting tray placed into a Mini-Sub® electrophoresis tank (Bio-Rad Laboratories, Richmond, USA) filled with 1x TPE electrophoresis buffer (0.36 M Tris-HCl; 0.3 M $NaH_2PO_4$; 0.1 M EDTA, pH 7.5). The complexes for both CS-AuNP and CS were prepared as outlined in Table 3.1 in a total volume of 10 µl in HBS. A negative control containing F*luc*-mRNA (1 µl, 0.25 µg/µl) was also included. After the 30-minute hour incubation period and complex formation, 3 µl of 6x gel loading buffer [0.25% (w/v) bromophenol blue dye and 40% sucrose] was added to all samples. Thereafter, approximately 10 µl of each sample was loaded into separate wells. Electrophoresis was then conducted at 50 volts (V) for 30 minutes. The gels were then viewed under UV transillumination in a Vacutec Syngene G:Box gel documentation system and images were captured using the Syngene Gene-Snap programme (Syngene, Cambridge, UK) at an exposure time of 1-2 seconds.

**Table 3.1.** Preparation of complexes for the gel retardation assay.

| | Sample number | | | | | | | |
|---|---|---|---|---|---|---|---|---|
| **Composition of samples** | **1** | **2** | **3** | **4** | **5** | **6** | **7** | **8** |
| Ratio of F*luc*-mRNA to CS-AuNP/CS | 1:0 | 1:0.1 | 1:0.2 | 1:0.3 | 1:0.4 | 1:0.5 | 1:0.6 | 1:0.7 |
| CS-AuNP/CS (µg) | 0 | 0.025 | 0.05 | 0.075 | 0.1 | 0.125 | 0.15 | 0.175 |
| F*luc*-mRNA (µg/µl) | 0.25 | 0.25 | 0.25 | 0.25 | 0.25 | 0.25 | 0.25 | 0.25 |

#### 3.2.2.6.2 Dye displacement/Intercalation assays

##### 3.2.2.6.2.1 Ethidium bromide dye displacement

The fluorescent based Ethidium Bromide (EtBr) dye displacement assay was also used as confirmation of complex formation as well as to determine the extent of condensation of the nucleic acid by the respective NP. Fluorescence was measured at an excitation wavelength of 520 nm and emission wavelength of 600 nm using a Glomax® Multi-detection system (Promega Systems, Sunnyvale, USA). Approximately 100 µl of HBS was added to two separate wells on a 96 well FluorTrac flat-bottom black microplate. Subsequently, 2 µl of EtBr was added to each well, mixed thoroughly and fluorescence measured. This was taken as the 0% baseline relative fluorescence reading. Thereafter, 1 µl of F*luc*-mRNA (0.25 µg/µl) was added to each well and mixed, and fluorescence measured. This reading was taken as 100% relative fluorescence. Subsequently, 1 µl aliquots of the CS-AuNP solution (0.025 µg/µl) and the CS solution (0.025 µg/µl) were added separately to each well in a step-wise manner, and fluorescent measurements recorded after each addition until a point of inflection in fluorescence was achieved. Fluorescence measurements were calculated as relative fluorescence (Fr) and plotted using the equation $Fr\ (\%) = (F_i - F_0) / (F_{max} - F_0) \times 100$ where $F_0$ is the fluorescence intensity of EtBr/HBS mixtures, $F_i$ is the fluorescence intensity at each concentration of CS-AuNP or CS and $F_{max}$ is the fluorescence intensity of the EtBr/F*luc*-

mRNA mixture. Thereafter, relative fluorescence was plotted against the mass (µg) of CS-AuNP or CS.

#### 3.2.2.6.2.2 SYBR Green dye displacement

Further confirmation of complex formation was obtained using the SYBR Green RNA II gel stain (10 000× concentrated in DMSO) which is more sensitive and is selective for RNA molecules, unlike EtBr. The SYBR Green dye displacement technique employed the same protocol and calculations as described previously (3.2.2.6.2.1) with a few modifications. Fluorescence was measured at an excitation wavelength of 497 nm and an emission wavelength of 520 nm. Additionally, the baseline relative fluorescence reading of 0% was measured by adding 1 µl of the diluted SYBR Green dye to 100 µl of HBS.

### 3.2.2.7 Nuclease Protection assay

The level of protection offered by CS-AuNP and CS to the F*luc*-mRNA in an environment that mimics that of an *in vivo* system was assessed using the nuclease protection assay. Sub-optimum, optimum and supra-optimum ratios for CS-AuNP:F*luc*-mRNA and CS:F*luc*-mRNA were selected based on the results obtained from the gel retardation assay and prepared as outlined below (Table 3.2). The final volume of the complexes was made up to 10 µl with HBS. The mixtures were incubated at room temperature for 30 minutes to allow for the formation of CS-AuNP/CS:F*luc*-mRNA complexes. Thereafter, 1 µl of fetal bovine serum (FBS) was added to each complex to a final concentration of 10% FBS. The positive control contained F*luc*-mRNA (1 µl, 0.25 µg/µl) and the negative control contained F*luc*-mRNA (1 µl, 0.25 µg/µl) treated with FBS. Thereafter, all samples containing FBS were incubated at 37°C for 4 hours in a water bath (Model 130, Thermo Fischer Scientific Inc., Waltham, Massachusetts, USA) to facilitate the nuclease digestion reaction. After the 4-hour incubation period, EDTA was added to all samples to a final concentration of 10 mM EDTA, to terminate the FBS reaction, followed by the addition of SDS to a final concentration of 0.5% SDS and a further incubation at 55°C for 20 minutes. Thereafter, samples were subjected to agarose gel electrophoresis for 30 minutes, as described previously (3.2.2.6.1).

**Table 3.2.** Preparation of complexes for the nuclease digestion assay.

| **Sample title** | **Positive control** | **Negative control** | **CS-AuNP** | | | **CS** | | |
|---|---|---|---|---|---|---|---|---|
| **Sample number** | **1** | **2** | **3** | **4** | **5** | **6** | **7** | **8** |
| **Composition of samples** | | | | | | | | |
| Ratio of mRNA to CS-AuNP/CS | 1:0 | 1:0 | 1:0.3 | 1:0.4 | 1:0.5 | 1:0.3 | 1:0.4 | 1:0.5 |
| CS-AuNP/CS (µg) | 0 | 0 | 0.075 | 0.1 | 0.125 | 0.075 | 0.1 | 0.125 |
| F*luc*-mRNA (µg/µl) | 0.25 | 0.25 | 0.25 | 0.25 | 0.25 | 0.25 | 0.25 | 0.25 |

### 3.2.3 *In Vitro* cell culture studies

#### 3.2.3.1 Cell culture materials and reagents

Phosphate-buffered saline tablets [PBS, (140 mM NaCl, 10 mM phosphate buffer, 3 mM KCl)], 3-[(4, 5-dimethylthiazol-2-yl)-2, 5-diphenyl tetrazolium bromide] (MTT, $M_w$: 414.3 g/mol, $C_1H_1BrNS$) and Dimethyl Sulfoxide [DMSO, $M_w$: 78.13 g/mol, $(CH_3)_2SO$] were supplied by Merck (Darmstadt, Germany). Research Grade Fetal Bovine Serum (FBS) was supplied by Hyclone GE Healthcare (Utah, USA). Sterile Eagle's Minimum Essential Medium (EMEM) with L-glutamine (4.5 g/ml), Penicillin/Streptomycin/Amphotericin B (100×) antibiotic mixture [Amphotericin B (25 mcg/ml), NaCl (8.5 mg/l) Potassium penicillin (10 000 units/ml), Streptomycin sulphate (10 000 mcg/ml)] and Trypsin-versene-EDTA mixture [versene-EDTA (200 mg/l), Trypsin (170 000 U/l)] were supplied by Lonza Bio Whittaker (Verviers, Belgium). The luciferase assay kit consisting of the luciferase cell culture lysis reagent (5×) [25 mM Tris-phosphate, (pH 7.8), 2 mM dithriothreitol, 2 mM 1,2-diaminocyclohexane-N,N,N',N'-tetra-acetic acid, 10% (v/v) glycerol, 1% (v/v) triton X-100], luciferase assay reagent (20 mM tricine, 1.1 mM Magnesium carbonate hydroxide, pentahydrate, 2.7 mM Magnesium sulphate, 0.1 mM EDTA, 33.3 mM dithriothreitol, 270 µM coenzyme), Molecular grade ethidium bromide solution (10 mg/ml) ($M_w$: 394.31 g/mol,

$C_{21}H_{20}BrN_3$) were purchased from Promega (Madison, Wisconsin, USA). Acridine Orange hemi (zinc chloride) salt [3,6-Bis(dimethylamino)acridine hydrochloride zinc chloride double salt], bicinchoninic acid solution [1% 2,2'-Biquinoline-4,4-dicarboxylic acid disodium salt, 0.16% Sodium tartrate, 0.4% Sodium hydroxide, 2% $Na_2CO_3.H_2O$, 0.95% NaHCO3, (pH 11.25)], Copper (II) sulfate solution [4% (w/v)] and BSA protein standard (1 mg/ml in 0.15 M NaCl, 0.05% $NaN_3$) were purchased from Sigma-Aldrich Chemical Co. (St. Louis, USA). All routine sterile tissue culture plasticware were supplied by Corning Inc., (New York, USA). Human embryonic kidney cells (HEK293) were provided by the Anti-Viral Gene Therapy Unit, Medical School, University of Witwatersrand. Human epithelial colorectal adenocarcinoma cells (Caco-2) were purchased from Highveld Biologicals (Pty) Ltd, Kelvin, RSA and the MCF-7 (HTB-22™) breast cancer line was purchased from the American Type Culture Collection (ATCC®), Manassas, Virginia, USA.

#### 3.2.3.2 Reconstitution of frozen cells and routine cell culture maintenance

Aseptic techniques were followed for all processes and all cell culture work conducted in an Airvolution Class II Biohazard cabinet. All work surfaces were thoroughly wiped with 70% ethanol. Prior to use, all cell culture reagents were warmed to 37°C. Frozen cryogenic vials of each cell line were thawed in a 37°C water bath, followed by centrifugation at 3000 rpm for 1 minute in an Eppendorf centrifuge (Model 5415D, New York, USA). The DMSO-containing supernatant was then discarded and the cell pellet resuspended in 1 ml of fresh complete medium [EMEM, 10% (v/v) FBS and 1% (v/v) antibiotic mixture]. The cell suspension was then transferred to a cell culture flask containing 5 ml of complete medium and incubated at 37°C for 24 hours in a Steri-cult HEPA class 100 $CO_2$ incubator (Thermo-Electron Co., Waltham, Massachusetts, USA).

Thereafter, the medium in the cell culture flask was replaced with 5 ml of fresh complete medium to remove any remaining DMSO which is toxic to cells at a temperature greater than 4°C. The cells were then allowed to propagate by incubation at 37°C in a 5% $CO_2$ incubator and monitored visually on a daily basis using a Nikon TMS inverted light microscope (Nikon Co., Tokyo, Japan). The cells were routinely washed with 5 ml of PBS and medium replaced every 2-3 days until growth confluency was obtained. Cells were split as desired into flasks or multi-well plates for assays.

### 3.2.3.3 Trypsinization of cells and cell counts

Upon confluency, the spent medium was removed and discarded into a waste bottle. The cells were then washed with 5 ml PBS followed by the addition of 1 ml trypsin-versene. The cells were monitored under the inverted microscope to observe the action of the enzyme and the "rounding off" of the cells. Thereafter, 2 ml of complete medium was added to the flask to inhibit the enzyme reaction. The cell culture flask was then gently tapped against the palm of the hand to aid in completely dislodging the cells from the surface. Prior to any experiments, a cell count was conducted under the inverted microscope using a haemocytometer slide (Marienfield-Superior, Germany). The trypsinized cells were seeded into multi-well plates for the various cell culture experiments or flasks for routine maintenance or frozen for future studies.

### 3.2.3.4 Cryopreservation

Following trypsinization, the cells were centrifuged at 3000 rpm for 5 minutes, the supernatant discarded and the cell pellet resuspended in 0.9 ml complete medium and 0.1 ml of the cryoprotective storage medium (DMSO). The suspension was then mixed and 1 ml aliquots dispensed into respective cryogenic vials which were placed in a Nalgene™ "Mr Frosty" Cryo 1°C freezing container (Thermo Fischer Scientific Inc., Waltham, Massachusetts, USA) containing isopropanol and frozen at a rate of -1°C per minute to a temperature of -70°C in a biofreezer (Nuaire, Lasec laboratory and Scientific Equipment). Thereafter, the cryogenic vials were transferred to a cryobox and stored in a biofreezer at -80°C for short term storage or in liquid nitrogen for long term storage.

### 3.2.3.5 MTT cytotoxicity assay

Cells were trypsinized and seeded at a density of 7.8 x $10^4$ cells/well (HEK293), 9.6 x $10^4$ cells/well (Caco-2) and 2.1 x $10^5$ cells/well (MCF-7) in clear 48-well plates. To allow for attachment, cells were incubated at 37°C for 24 hours. Thereafter, all complexes were prepared in triplicate as described previously and outlined in table 3.2. Spent medium was removed from each well and replaced with fresh complete medium followed by the addition of the complexes to the respective wells. A positive control containing only cells (in triplicate) was included. The cells were then incubated at 37°C for 48 hours. Subsequently,

the spent medium was removed from each well and replaced with 200 µl of fresh complete medium together with 200 µl of MTT reagent (5 mg/ml in PBS) and cells incubated at 37°C for 4 hours. Thereafter, the MTT infused medium was removed and 200 µl of DMSO was added to solubilize the formazan crystals present (Figure 3.4).

The plate was then gently shaken and absorbance read at 570 nm in a Mindray MR-96A microplate reader (Vacutec, Hamburg, Germany) with DMSO as the blank. Results were calculated as cell viability (%) using the following equation: (Abs of treated – Abs of control/ Abs of control) x 100%; with the positive control being taken as 100% cell viability.

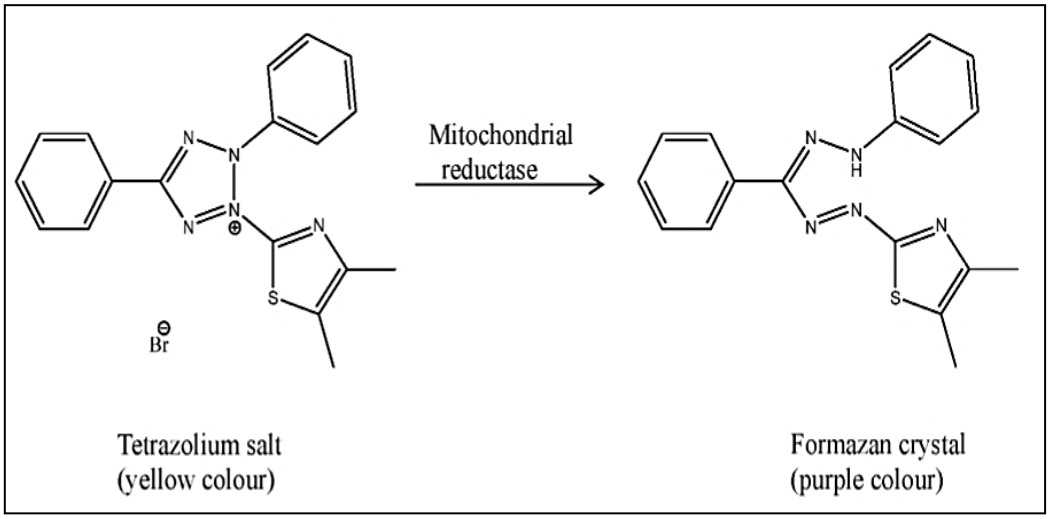


**Figure 3.4:** Mechanism depicting the reduction of MTT to formazan by mitochondrial reductase present in living cells (Barahuie *et al*., 2014).

### 3.2.3.6 Luciferase reporter gene assay

Transfection efficiency of the complexes was evaluated using the luciferase reporter gene assay that measures bioluminescence as a direct correlation of luciferase activity. The mechanism of action of the luciferase enzyme is depicted in figure 3.5.

Cells were seeded at a density of 7.8 x $10^4$ cells/well (HEK.293), 9.6 x $10^4$ cells/well (Caco-2) and 2.1 x $10^5$ cells/well (MCF-7) in a 48-well clear plate which was then incubated at $37^0$C for 24 hours. Thereafter, nanocomplexes (prepared as for cytotoxicity assay, table 3.2) in triplicate were added to respective wells that were replenished with fresh complete medium.

Two controls were set up in triplicate: one containing cells only and the other containing cells with naked Fl*uc*-mRNA (0.25 µg/µl). Cells were then incubated at 37°C for 48 hours, after

which the spent medium was removed and the cells were rinsed twice with 200 µl of PBS. Approximately 80 µl of 1× luciferase cell culture lysis reagent was then added and the plate shaken for 15 minutes at 30 rev/min on a STR6 platform shaker (Stuart Scientifc, Staffordshire, UK). Thereafter, the cells were scraped from the wells and the cell suspension centrifuged at 12000 x g to pellet the cell debris.

Approximately 20 µl of each cell free supernatant was transferred to individual wells on a 96-well FluorTrac flat-bottom white microplate (Promega Systems, Sunnyvale, USA), to which was added 50 µl of the luciferase assay reagent. This was thoroughly mixed and luminescence immediately read in a GloMax® Multi-detection system (Promega Biosystems, Sunnyvale, USA), operated by Instinct software and primed with the luciferase assay reagent and with the Photo Multiplier Tube (PMT) activated. Protein determination was performed on the cell free extracts using the bicinchoninic acid (BCA) assay and readings obtained using a Mindray MR-96A microplate reader at 562 nm. All luminescence readings were normalized against the protein content and expressed as relative light units per milligram protein (RLU/mg protein).

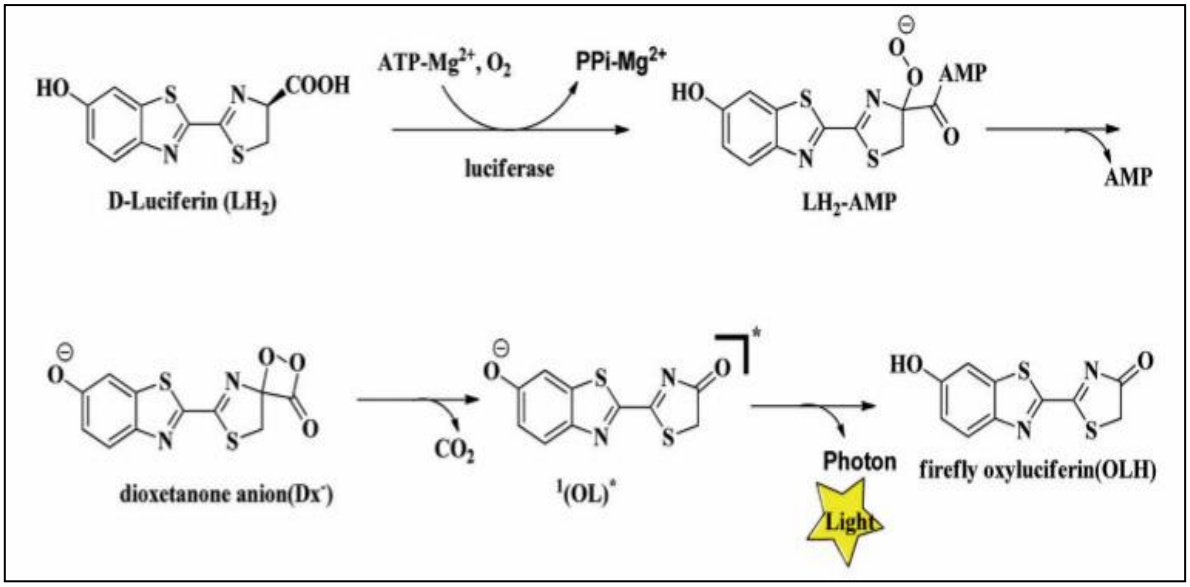


**Figure 3.5:** Mechanism of the bioluminescence exhibited upon oxidation of the substrate D-Luciferin by the luciferase enzyme present in transfected cells (Bai *et al*., 2015).

### 3.2.3.7 Acridine Orange/Ethidium Bromide (AO/EB) apoptosis assay

Cells were seeded at a density of 1.8 x $10^6$ cells/well (HEK293), 9.6 x $10^4$ cells/well (Caco-2) and 1.26 x $10^5$ cells/well (MCF-7) in a 48-well clear plate and incubated at 37°C for 24

hours. Thereafter, nanocomplexes were prepared, as previously described, in triplicate but were based on the optimal ratios obtained from the MTT cytotoxicity (3.2.3.5) and Luciferase reporter gene assays (3.2.3.6) as outlined in Table 3.3 below. After 24 hours, the spent medium in each well was replaced with fresh complete medium and the complexes added to individual wells. The positive control contained cells only. The cells were then incubated at 37°C for 24 hours, followed by removal of the spent medium and washing of the cells with 200 µl of PBS. Cells were then stained with 10 µl of the AO/EB dye (0.1 µg/µl acridine orange and 0.1 µg/µl Ethidium bromide in PBS) at room temperature for 5 minutes. The stain was then removed and the cells washed with 200 µl of PBS. The cells are then viewed for apoptotic-induced morphological changes against the control, using an Olympus inverted fluorescent microscope (200× magnification) fitted with a CC12 fluorescent camera, an excitation filter of 450-490 nm, a barrier filter of 520 nm and Soft Imaging System (SIS) software (Olympus Co., Tokyo, Japan). The apoptotic index for each sample was calculated using the following equation:

Apoptotic index = number of apoptotic cells / total number of cells

Acridine orange penetrates both the living and dead cells producing green fluorescence whereas ethidium bromide produces red fluorescence in cells with altered membranes indicating apoptosis. After visual analyses, the cells were scraped into 200 µl of PBS in a FluorTrac flat-bottom black microplate and fluorescence measured at an excitation wavelength of 520 nm and emission wavelength of 600 nm in the Glomax® Multi-detection system. The fluorescence readings were averaged over three replicates (n=3) and reported as fluorescent intensity (FI).

**Table 3.3.** Preparation of complexes for the AO/EB apoptosis assay.

| **Composition of samples** | **CS-AuNP** | **CS** |
|---|---|---|
| Ratio of F*luc*-mRNA to CS-AuNP/CS | 1:0.5 | 1:0.5 |
| CS-AuNP/CS (µg) | 0.125 | 0.125 |
| F*luc*-mRNA (µg/µl) | 0.25 | 0.25 |

#### 3.2.3.8 Statistical analysis

All data obtained was calculated as the mean ± standard deviation (±SD n=3) and plotted on graphs using Microsoft Excel 2010 (Microsoft, USA). Using the Graphpad Instat Prism 4.0.3 software, the one-way analysis of variance (ANOVA) test was conducted for multi-group comparisons of the calculated means. Thereafter, the Dunnett's *post hoc* test was carried out for the MTT cytotoxicity assay results and the Tukey-Kramer *post hoc* test was carried out for the Luciferase reporter gene assay results. Statistical significance (*P*) values determined to be less than 0.05 were regarded as significant and represent on the graph as *** $p < 0.001$, ** $p < 0.01$ and * $p < 0.05$.

## 3.3 Results and Discussion

### 3.3.1 Characterization of Nanoparticles and Nanocomplexes

#### 3.3.1.1 Chemical analysis

The ICP/OES system is one of the most dominant and standard analytical tools for the determination of trace elements in numerous types of samples such as agricultural, food, biological, clinical, geological, environmental, water, metals and organic materials (Hou *et al*., 2000). The concentration of the synthesized AuNP was confirmed by ICP against a standard Au sample by correlation of the electron signals emitted at each wavelength (Appendix A1).

The frequency of infrared radiation absorbed is characteristic to a molecule and thus may be used to identify and confirm the chemical composition of a given sample. FTIR spectroscopy confirmed the composition of the AuNP, CS and CS-AuNP solutions (Appendix A2). Citrate-capped AuNPs exhibited characteristic absorption peaks at 1635.63 cm−1 indicating the stretching of the C=O bond of the carboxylic carbonyl group and 3272.20 cm−1 indicating the stretching of O-H bonds as compared to previous literature (Chen *et al*., 2013). The spectrum of CS exhibited characteristic absorption peaks at 1028.14 $cm^{-1}$ and indicates the C-O stretch vibration, 1508.83 $cm^{-1}$ for the amide I band which indicates the C=O stretch vibration band and 3254.05 $cm^{-1}$ for the amide A band, indicating the N-H stretch vibration as compared to previous literature (Cardenas *et al*., 2002). In contrast to the AuNP FTIR spectrum, the characteristic peaks of the C=O and O-H stretches of the AuNPs increased to

1635.14 $cm^{-1}$ and decreased to 3270.35 $cm^{-1}$ after functionalisation with CS. These results indicate that the reducing ends of the citrate ions formed interactions with the amino groups of CS as reported in previous literature (Nivethaa *et al*., 2012).

### 3.3.1.2 UV-Vis optical spectrophotometry analysis and dialysis

Gold nanoparticles display the optical characteristic of surface plasmon resonance (SPR) and is defined as the collective oscillation of electrons in the conduction band of the nanoparticles in resonance with a specific wavelength of incident light (Doyen *et al*., 2013). The SPR of AuNPs generates a strong absorbance band in the visible region at 520 nm which is also accountable for the ruby red colour of the solution and can be measured by UV-Vis spectroscopy (Daniel and Didier, 2004).

UV-vis spectroscopy is a very valuable technique which allows approximation of gold nanoparticles size, concentration and aggregation level (Amendola and Meneghetti, 2009). The SPR phenomenon is influenced by factors such as size, shape, core charge, solvent, surface ligand and temperature (Yeh *et al*., 2012). The SPR of AuNPs enhances their absorption and scattering properties (Radwan and Azzazy, 2009).

The SPR absorbance of the synthesized AuNPs exhibited a distinct peak at 520 nm (Figure 3.6) correlating with literature and confirming the successful synthesis of citrate-capped AuNPs. Upon functionalisation with CS (Figure 3.6), the SPR absorbance experienced a red-shift to 530 nm, indicating a change in the nanoparticles causing an alteration of the normal local refractive index of the AuNPs. This red-shift has previously been reported for the functionalisation of AuNPs with CS (Mohd and Johan, 2014; Wu *et al*., 2009 and Bhumkar *et al*, 2009). In addition, this red-shift was also observed upon complex formation of CS-AuNP with F*luc*-mRNA, exhibiting an SPR absorbance at 540 nm (Figure 3.7). The absorbance of the CS-AuNP recorded after dialysis further indicated the successful removal of the unbound CS. The percentage of bound CS was determined to be 87%, indicating excellent binding efficiency of AuNP to CS which is imperative for transfection.

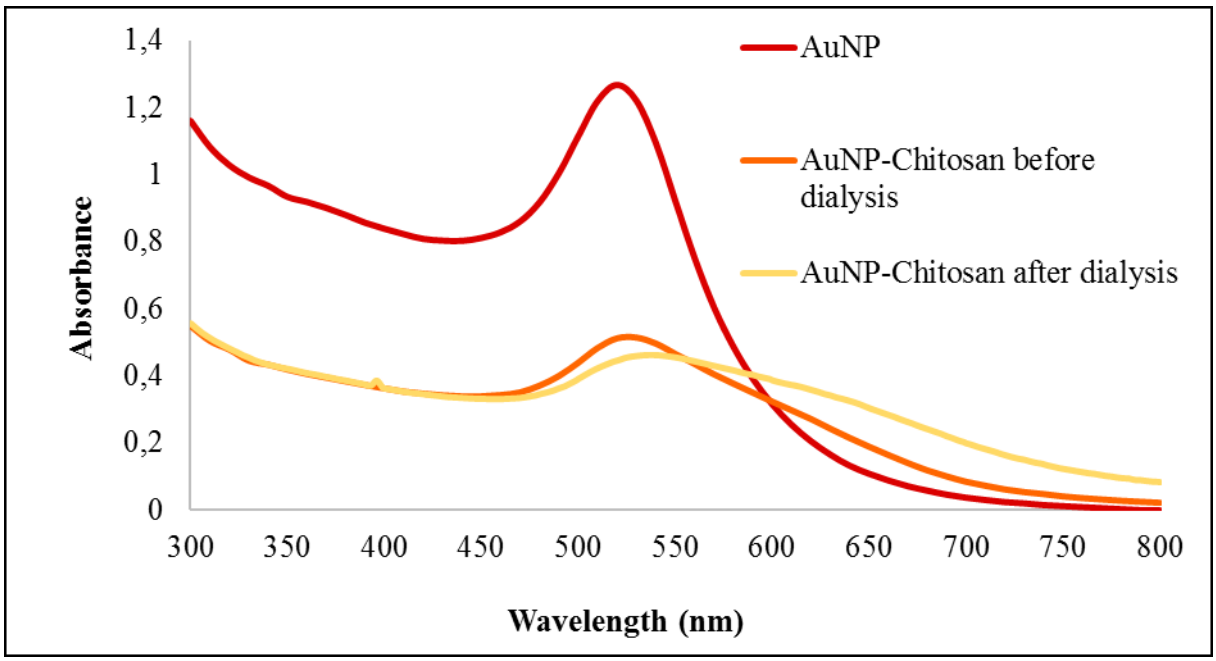


**Figure 3.6:** UV-Vis spectrum of AuNP, CS-AuNP before dialysis and CS-AuNP after dialysis indicating a shift in SPR absorbance after functionalization.

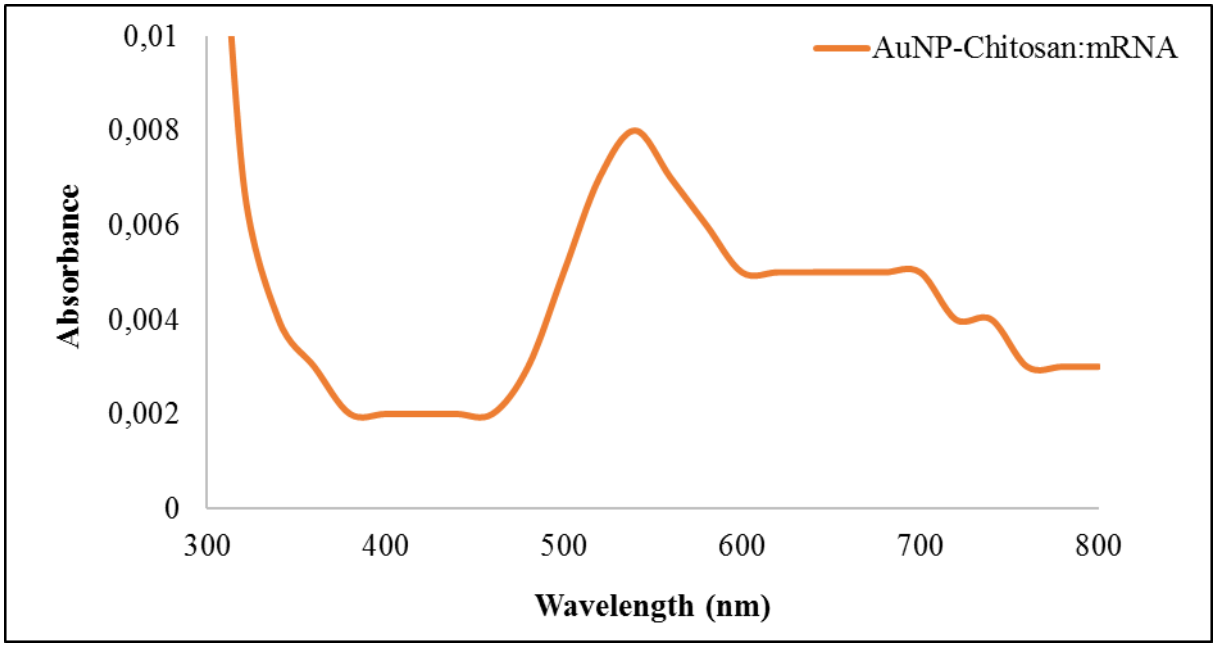


**Figure 3.7:** UV-Vis spectrum of the CS-AuNP:F*luc*-mRNA complex indicating an absorbance at 540 nm.

### 3.3.1.3 Qualitative Ninhydrin test for amine groups

The ninhydrin test has been well-established and extensively utilized for amino acid analysis over the years (Prochazkova *et al*., 1999). The principle of the ninhydrin reaction relies on the reaction of free primary amines with the ninhydrin reagent to produce a blue-purple coloured complex, a diketohydrindylidene-diketohydrindamine known as Ruhemann's purple and is indicative of a positive reaction. (Lago *et al*., 2011). In theory, based on the structure of CS which is a linear polymer of (1,4)-linked 2-amino-deoxy-*β*-D-glucan, the reaction with ninhydrin should yield a positive result, as obtained for the CS-AuNP (Figure 3.8) indicating the presence of CS and the successful functionalisation of AuNP with CS.

**Figure 3.8:** Image of the light purple CS-AuNP solution after the ninhydrin test indicating a positive reaction.

### 3.3.1.4 Transmission electron microscopy

Transmission electron microscopy (TEM) is a vital characterization technique to image the AuNPs which are presented as dark spheres (Figure 3.9). TEM is used to verify the morphology and size of the AuNPs and acts by transmitting a focussed beam of electrons through the sample, forming a high-resolution image (Lee, 2011). TEM micrographs displayed AuNPs, CS-AuNP and CS-AuNP:F*luc*-mRNA complexes as homogenous, spherical and smooth particles that were well-dispersed (Figure 3.9), similar to previously reported studies (Verma *et al*, 2014; Kumar *et al*., 2011; Philip, 2008 and Kimling *et al*., 2006). The AuNPs in each micrograph were displayed as dark spheres indicating that the $Au^{3+}$ ions were reduced to neutral gold atoms which nucleated and grew to produce dark, red spheres (Thanh *et al*., 2014).

The excellent dispersion of the AuNPs may be attributed to the electrostatic stabilization due to the citrate capping, repelling the AuNP atoms from each other (Polte, 2015). Upon functionalisation with CS (Figure 3.9 B), the nanospheres adopted chain-like structures which may have attributed to the red-shift observed in the UV-Vis spectroscopy analysis. It has been proposed that the morphology and size of CS functionalised AuNPs are dependent upon the varying chain length of CS and directly proportional to the amount of AuNPs absorbed along the chain (Narayanan and Sivakumar, 2014). In addition to electrostatic stabilization, CS provides steric stabilization to the AuNPs, preventing aggregation (Polte, 2015). Upon CS-AuNP and F*luc*-mRNA complexation (Figure 3.9 C), the formation of aggregates can be seen due to the condensation of F*luc*-mRNA and the overall interactions of the citrate-capped AuNPs, CS and F*luc*-mRNA.

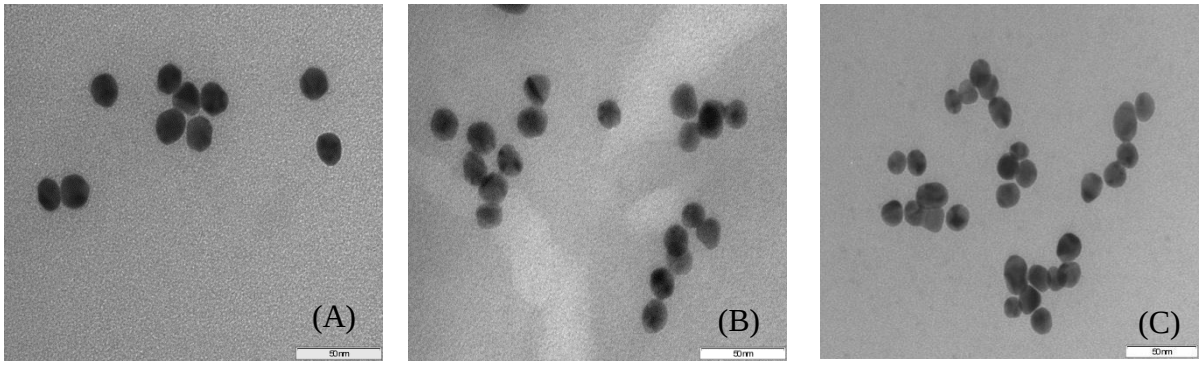


**Figure 3.9:** Transmission electron micrographs depicting the morphology of (A) AuNPs, (B) CS-AuNP and (C) CS-AuNP:F*luc*-mRNA at a magnification of 50 000×.

### 3.3.1.5 Nanoparticle tracking analysis (NTA)

Among the various properties of AuNPs which require complete characterisation, the size, quality and stability of their dispersion have a profound effect on their interactions with organisms and the environment (Hole *et al*., 2013). It has been reported that AuNP response to the surrounding environment is dependent on size (Jiang *et al*., 2008). This is attributed to their large surface area which interacts with the surrounding matrix and may influence their reactivity with targets in the cells (Lison and Huaux, 2011). Recently, Nanoparticle tracking analysis (NTA) has been utilized to determine the size, zeta potential, colloidal stability and distribution of AuNPs in liquids (Wagner *et al*., 2014).

NTA is based on the illumination of freely diffusing particles by use of an intense laser light analysis of monochrome images used to track the Brownian motion and size distribution of

the particles which is estimated by the Stokes-Einstein equation (Wagner *et al*., 2014). The NTA analysis (Table 3.4 and Appendix B) determined the average size of AuNPs in solution to be 65.9 +/- 9.8 nm over a concentration of 2.55e+008 +/- 1.69e+006 particles/ml. Upon functionalisation, the average size of CS-AuNPs increased to 69.6 +/- 15.2 nm over a concentration of 2.28e+008 +/- 5.38e+006 particles/ml, which may be due to the functionalization and the formation of chain-like structures as seen in the TEM micrographs.

Upon CS-AuNP and F*luc*-mRNA complexation, the size of CS-AuNP:F*luc*-mRNA particles increased to 95.0 +/- 9.9 nm over a concentration of 7.43e+008 +/- 1.99e+006 particles/ml, indicating the formation of aggregates due to the condensation of F*luc*-mRNA and the overall interactions of the AuNPs, CS and F*luc*-mRNA. All nanoparticle formulations displayed sizes below 100 nm, making them suitable for gene delivery purposes.

Apart from size, surface chemistry is predominantly important in inhibiting uncontrolled aggregation and is directly related to the transfection efficiency of nanoparticles (Son *et al*., 2000). Zeta potential analysis is a technique that involves the measurement of potential differences between the surface and the slipping plane of the stationary fluid layer of a nanoparticle (Arjmandi *et al*., 2012). This measurement is used to quantify surface charge in a buffer with a fixed composition, pH concentration and ionic strength.

In general, an excellent zeta potential (greater than 25 mV or -25 mV) indicates the formation of stable nanoparticles and as the zeta potential approaches the point of zero charge, the attraction between nanoparticles surpasses the repulsive forces between the nanoparticles causing aggregation (Ivanov, 2011). Thus, zeta potential analysis is important for determining nanoparticle surface chemistry and long-term stability.

From the zeta potential analysis (Table 3.4 and Appendix B) it was observed that the AuNPs by themselves did not have excellent colloidal stability as their surface charge was determined to be -7.3 +/- 1.6 mV. However, upon functionalisation with CS, the zeta potential increased to 55.5 +/- 1.2 mV which shows excellent colloidal stability of the nanoparticles. Similar measurements based on CS functionalisation of AuNPs have also been reported in previous studies (Boyles *et al*., 2015 and Bhumkar *et al*., 2007). This observation shows that CS with its high positive charge density improved the surface chemistry characteristics of the AuNPs, resulting in steric stabilization of the AuNPs preventing unwelcome aggregation. Upon CS-AuNP and F*luc*-mRNA complexation, the zeta ($\zeta$) potential decreased to 25.9 +/- 0.5 mV which also indicated a relatively stable nanocomplex.

This may be attributed to the electrostatic condensation of the negatively charged F*luc*-mRNA by the positively charged CS-AuNP particles. In addition, TEM micrographs indicated slight aggregation which will affect the zeta potential. Overall, the functionalized and complexed nanoparticles were proven to be stable and suitable for gene delivery studies.

**Table 3.4** Size, zeta potential and concentration of the nanoparticle solutions obtained from nanoparticle tracking and zeta potential analysis.

| Sample | Size (nm) (mean±SD) | Zeta Potenial (mV) (mean±SD) | Concentration (particles/ml) (mean±SD) |
|---|---|---|---|
| AuNP | 65.9 +/- 9.8 | -7.3 +/- 1.6 | 2.55e+008 +/- 1.69e+006 |
| CS-AuNP | 69.6 +/- 15.2 | 55.5 +/- 1.2 | 2.28e+008 +/- 5.38e+006 |
| CS-AuNP:F*luc*-mRNA | 95.0 +/- 9.9 | 25.9 +/- 0.5 | 7.43e+008 +/- 1.99e+006 |

### 3.3.2 Assessment of CS and CS-AuNP binding to F*luc*-mRNA

#### 3.3.2.1 Gel retardation assay

The gel retardation or band shift assay was conducted to determine the minimum concentration of CS-AuNP and CS required to fully bind 0.25 µg of F*luc*-mRNA (optimal binding ratio). Traditionally, agarose gel electrophoresis is used for the separation of biomolecules such as nucleic acids and proteins and has also recently been employed for the separation of metal nanoparticles such as AuNPs (Hasenoehrl *et al*., 2012). This assay has been extensively applied for the study of protein-nucleic acid interactions but may be adapted for the use of studying various nucleic acid conjugate interactions (Hellman and Fried, 2009). The principle of agarose gel electrophoresis separation and electrophoretic mobility is based on charge, size and shape of the migrating biomolecule (Laniel *et al*., 2001). However, in addition to separation, this assay allows for the study of the electrostatic binding ability of CS-AuNP and CS (positively charged) to entirely neutralize the F*luc*-mRNA (negatively charged), producing an electroneutral complex which will be restricted in electrophoretic mobility (Huang *et al*., 1998).

If F*luc*-mRNA present is not completely bound to the CS-AuNP/CS it will be free to migrate into the gel from the cathode to the anode based on general agarose gel electrophoresis principles. However, if F*luc*-mRNA is completely bound to the Cs-AuNP it will not able to

migrate into the gel due to the formation of an electroneutral complex. For transfection purposes, it is imperative to determine the concentration of CS-AuNP and CS required to fully bind the F*luc*-mRNA.

Both CS-AuNP (Figure 3.10 A) and CS (Figure 3.10 B) at varying concentrations, were assessed for their ability to electrostatically bind to the F*luc*-mRNA (0.25 µg/µl) in lanes 2-8 as outlined in Table 3.1. In both assessments, lane 1 served as a control containing 0.25 µg/µl of F*luc*-mRNA. The endpoint or optimal ratio for each assessment is indicated by a white arrow wherein electroneutrality was achieved. It was observed that the amount of CS-AuNP and CS complexes retained in the wells increased with increasing CS-AuNP and CS concentrations, respectively.

Electroneutrality and optimal binding ratios were achieved for CS-AuNP:F*luc*-mRNA (Figure 3.10 A) at a ratio of 0.4:1 (w/w) (lane 5) and for CS:F*luc*-mRNA (Figure 3.10 B) at a ratio of 0.4:1 (w/w) (lane 5). The efficient binding of F*luc*-mRNA by CS-AuNP and CS at low concentrations may be attributed to its high positive charge density.

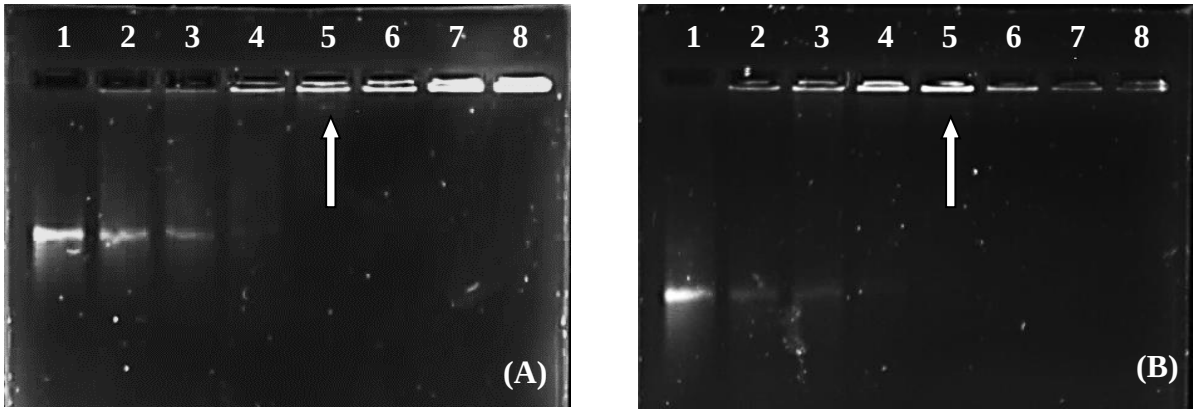


**Figure 3.10**: Gel retardation study of (A) CS-AuNP:F*luc*-mRNA and (B) CS:F*luc*-mRNA complexes. Incubation mixtures (10 µl) in 20 mM HEPES, 150 mM NaCl (pH 7.5) contained varying amounts of (A) CS-AuNP and, (B) CS in lanes 1–8 (0, 0.025, 0.05, 0.075, 0.1, 0.125, 0.15, 0.175 µg) and F*luc*-mRNA (0.25 µg).

#### 3.3.2.2 Dye Displacement/Intercalation assays

Fluorescent intercalation displacement assays have been used extensively to examine interactions and define the binding affinities of small ligands (Sau *et al*., 2012). These intercalation assays are based on the quenching of the fluorescence as a result of the displacement of mRNA-bound dye by mRNA-binding compounds such as CS-AuNP and CS as used in this study. In both assays (Figure 3.11 and 3.12), it was observed that both the CS-AuNP and CS solutions were able to successfully displace the dye from the F*luc*-mRNA.

It was observed that a lower concentration of CS was required to fully bind the F*luc*-mRNA in comparison to CS-AuNP which may be attributed to the lack of positive charges available on the surface of the AuNPs after binding to CS. The endpoints or points of inflection (indicated by arrows) specify the concentration of CS-AuNP or CS at which the F*luc*-mRNA was fully bound. In both methods (Figure 3.11-3.12), a step-wise decrease in fluorescence was observed as the NPs bound to the mRNA, displacing the bound dye.

The concentration required to fully bind the F*luc*-mRNA was 0.325 µg for CS-AuNP and 0.255 µg for CS which was higher than those obtained from the gel retardation assay. This may be due to the mechanism of action of EtBr as its tricyclic phenanthridine ring interacts with the base pairs of the hydrophobic interior of double-stranded DNA through Van der Waals forces to produce fluorescence (Banerjee *et al*., 2014). This technique has previously been reported on the study of AuNP-DNA conjugates and has proven successful (Jang *et al*., 2009). However, it has not been reported for the study of AuNP-mRNA conjugates. mRNA folds back on itself to produce local base pairing for intercalation with EtBr, hence the variation in results. Furthermore, it is possible that the EtBr method did not provide optimal parameters for this study while the SYBR Green method is regarded as having specificity towards intercalation of RNA (Siddiqui *et al*., 2013).

The concentration required to fully bind the F*luc*-mRNA was 0.15 µg for CS-AuNP and 0.125 µg for CS in the SYBR Green method. These values correlated with those obtained from the gel retardation assay, thus proving the accuracy of this technique and optimization of parameters for this study.

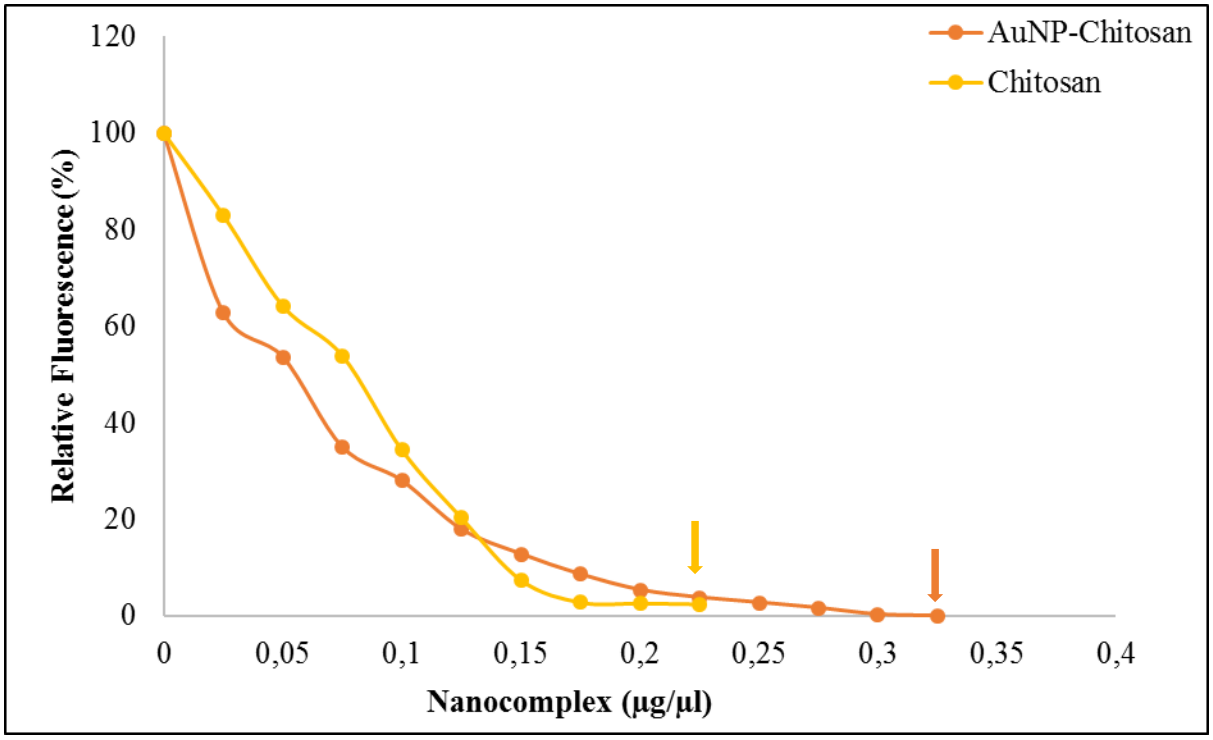


**Figure 3.11:** Comparison of relative fluorescence between the CS-AuNP and CS complexes using the Ethidium Bromide intercalation assay.

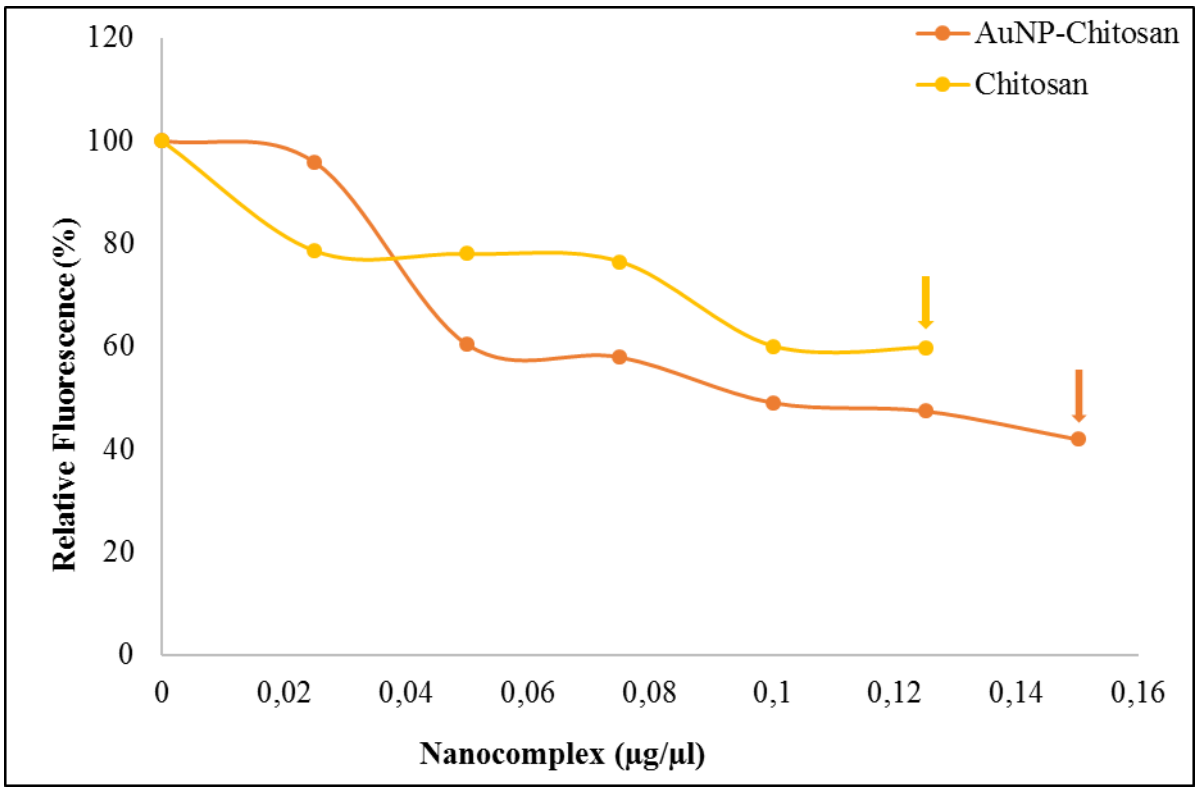


**Figure 3.12:** Comparison of the relative fluorescence between CS-AuNP and CS complexes using the SYBR Green intercalation assay.

### 3.3.3 Nuclease Protection assay

The efficient delivery of nucleic acids is dependent on factors associated with the vehicle of choice such as physiochemical properties, cellular interaction, target specificity and transfection efficiency. However, the physiological environment *in vivo* plays a crucial role in gene delivery and expression. Serum nucleases, present in biological fluids, are a great obstacle in gene delivery due to the risk of nucleic acid degradation. For effective expression, nucleic acids carried by the delivery vehicles must be protected against degradation by serum nucleases (Quong and Neufeld, 1998). Some studies have highlighted the instability of mRNA under physiological conditions, enforcing the need for an effective delivery system for safe mRNA delivery. AuNPs have shown potential to be effective delivery vectors (Kim *et al*., 2015) but the need for their optimization to suit these protective functions are yet to be fully recognised.

To examine the protection offered by our nanoparticles to the mRNA, a nuclease digestion study was conducted which mimics the physiological environment in biological fluids and involves the treatment of nanocomplexes with fetal bovine serum (FBS) containing nucleases. Using binding ratios obtained from the gel retardation assay, three ratios (sub-optimum, optimum and supra-optimum) were selected for assessment (Figure 3.13). The positive control (C1) contained undigested F*luc*-mRNA (0.25 µg) presented as a single distinctive bright band while the negative control (C2) containing FBS-digested F*luc*-mRNA (0.25 µg) showed degradation of the F*luc*-mRNA, indicating complete digestion. All complexes were treated with FBS to facilitate the digestion of any unprotected F*luc*-mRNA and thereafter the nuclease reaction was terminated by treatment with EDTA. Subsequently, the complexes were treated with SDS to facilitate the release of the F*luc*-mRNA from the nanocomplex. F*luc*-mRNA which has been digested by the FBS will migrate into the gel and appear as a smear after agarose gel electrophoresis similar to the negative control (C2) whereas undigested F*luc*-mRNA will appear as a distinct band similar to the positive control (C1).

Lanes 1-2 (Figure 3.13) showed partial digestion of the mRNA, indicating that the amount of CS-AuNP at the (sub-optimum and optimum) ratios provided some but not total protection of the F*luc*-mRNA. This may be attributed to the weak compaction, probably due to the lack of binding sites available on the surface of CS-AuNPs that are dependent on the electrostatic interactions between the AuNPs and CS.

However, at the supra-optimum ratio (lane 3) no digestion was observed, indicating complete protection of F*luc*-mRNA by CS-AuNPs at the ratio of 1:0.5. CS offered complete protection of F*luc*-mRNA at the sub-optimum (1:0.3) and optimum ratios (1:0.4) as no digestion of F*luc*-mRNA was observed (Lanes 4-5, Figure 3.13). However, at the supra-optimum ratio (1:0.5) partial digestion was observed and this may be due to looser binding of the F*luc*-mRNA at a higher ratio and possible aggregation of the CS particles. In comparison, CS exhibited enhanced protection ability over F*luc*-mRNA compared to CS-AuNP. Furthermore, the density of charges available on the surface of a particle plays a factor in binding and thus protection. Therefore, it can be assumed that the CS-AuNPs contained fewer binding sites for the mRNA than CS alone due to functionalisation. Hence, CS-AuNP seems to be most suitable at the supra-optimum ratio as seen from its good protection of F*luc*-mRNA against nucleases.

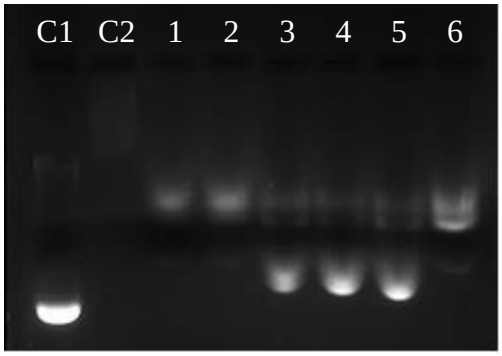


**Figure 3.13:** Nuclease digestion of CS-AuNP:F*luc*-mRNA and CS:F*luc*-mRNA complexes. Incubation mixtures (10 µl) in 20 mM HEPES, 150 mM NaCl (pH 7.5) contained a constant amount of F*luc*-mRNA (0.25 µg) in all lanes and varying amounts of CS-AuNP, lanes 1-3 (0.075, 0.1, 0.125 µg) and CS, lanes 4-6 (0.075, 0.1, 0.125 µg). C1 contained undigested F*luc*-mRNA and C2 contained FBS-digested F*luc*-mRNA.

### 3.3.4 *In Vitro* cell culture studies

#### 3.3.4.1 Reconstitution and cell culture maintenance

All cell lines were successfully propagated in complete medium (EMEM, 10% FBS and 1% antibiotic). All cells were monitored with an inverted microscope and images captured under phase contrast microscopy.

HEK293 cells (Figure 3.14 A) showed an epithelial fibroblast morphology, Caco-2 cells (Figure 3.14 B) exhibited a polarized epithelial morphology and MCF-7 cells exhibited a dome-like morphology (Figure 3.14 C).

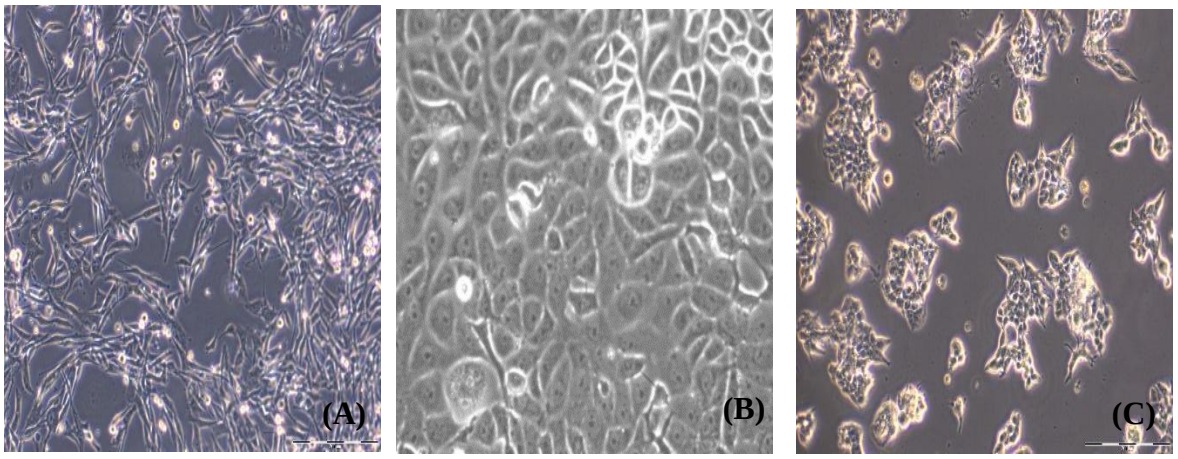


**Figure 3.14:** Images of confluent cell lines (A) HEK293, (B) Caco-2 and (C) MCF-7 using phase contrast microscopy at a 10 000× magnification.

### 3.3.4.2 MTT cytotoxicity assay

The wide applications of AuNPs have raised concerns on its impact on health due to long term exposure. Hence, it is important to evaluate its toxicological implications first *in vitro* (Chueh *et al*., 2014). The MTT cytotoxicity assay has been termed the ‘‘gold standard’’ colorimetric assay for cytotoxicity and is based on the measurement of mitochondrial enzymatic activity (Alkilany and Murphy, 2010). This assay is based on the principle that viable cells possess an active metabolism which will convert MTT into formazan, an insoluble purple coloured product (Marquis *et al*., 2009) while dead cells are incapable of making this conversion. Hence, this method serves as a useful indicator of the cytotoxic effects inferred by complexes. For all cell lines, a control consisted of cells only (without treatment to the complexes) and was taken as 100% cell viability. For the HEK293 cell line (Figure 3.15 A), a general trend was seen wherein the cell viability (%) increased as the ratio of CS and CS-AuNP to F*luc*-mRNA increased. Maximum cell viability of 70% and 60% was observed at the supra-optimal ratio (ratio 3) for both CS and CS-AuNP, respectively.

A similar observation was reported in a study by Ramezani *et al*., 2014 where scanning electron microscopy (SEM) further indicated that the surface of CS-AuNPs was moderately

rough and porous and therefore can be assumed to interact well with the cell membrane due to similar surface characteristics. For the Caco-2 cell line (Figure 3.15 B), the cell viability increased as the ratio of CS to F*luc*-mRNA increased but the opposite occurred when the ratio of CS-AuNP to F*luc*-mRNA increased. Cell viability of 96% and 81% was observed at the supra-optimal ratio (ratio 3) for CS and the sub-optimal ratio (ratio 1) for CS-AuNP, respectively. In the MCF-7 cell line (Figure 3.15 C), the cell viability (%) decreased as the ratio of CS to F*luc*-mRNA increased but increased as the CS-AuNP to F*luc*-mRNA ratio increased. Maximum cell viability of 97% and 81% was observed at the sub-optimal ratio (ratio 1) for CS and the optimal ratio for CS-AuNPs (ratio 2), respectively. Researchers have shown that in the MCF-7 cells an increase of AuNP concentration resulted in a decrease of cell viability (Selim and Hendi, 2012). In general, the cell viability results show that treatment with these complexes are concentration or dose dependent and cell type specific. Overall, both nanocomplexes performed similarly in all cell lines with cell viability over 50% at all ratios.

Cationic nanoparticles possess the ability to interact with the cellular membrane which is negatively charged and therefore resulting in membrane disruption (Goodman *et al*., 2004). Further studies have shown that cationic AuNPs can alter the mitochondrial membrane potential resulting in oxidative stress (Yah, 2013). Their interaction may be attributed to the zeta potential of the nanoparticle surface. For the CS-AuNP:F*luc*-mRNA complex, the zeta potential was 25.9 +/- 0.5 mV and may have resulted in strong electrostatic binding with the cell membrane, resulting in membrane destruction and cytotoxicity. It has also been reported that cytotoxicity is size-dependent. Larger nanoparticles have a high surface area to volume ratio which provides platforms for an increase in surface particle activity (Van Doren and Temmerman, 2011). Although the size of the CS-AuNP:F*luc*-mRNA complex was 95.0 +/- 9.9 nm which is not very large, they may still be susceptible to various surface particle activities. In addition, the size range of nanoparticles was similar to that of proteins and small viruses which would trigger the immune system resulting in induced immunotoxicity (Dobrovolskaia and McNeil, 2007). *In vitro* studies require the use of growth media which contain serum proteins, essential amino acids, vitamins, electrolytes, antibiotics and trace metals which could interact with the nanoparticles, altering their physiochemical properties such as size, surface charge, surface chemistry and aggregation state (Alkilany and Murphy, 2010). The high ionic strength and the presence of electrolytes in the growth media can result

in nanoparticle aggregation leading to disruption of the cell (Vesaratchano *et al*., 2007). Aggregation was noted for the CS-AuNP:mRNA in the TEM analysis (Figure 3.9 C).

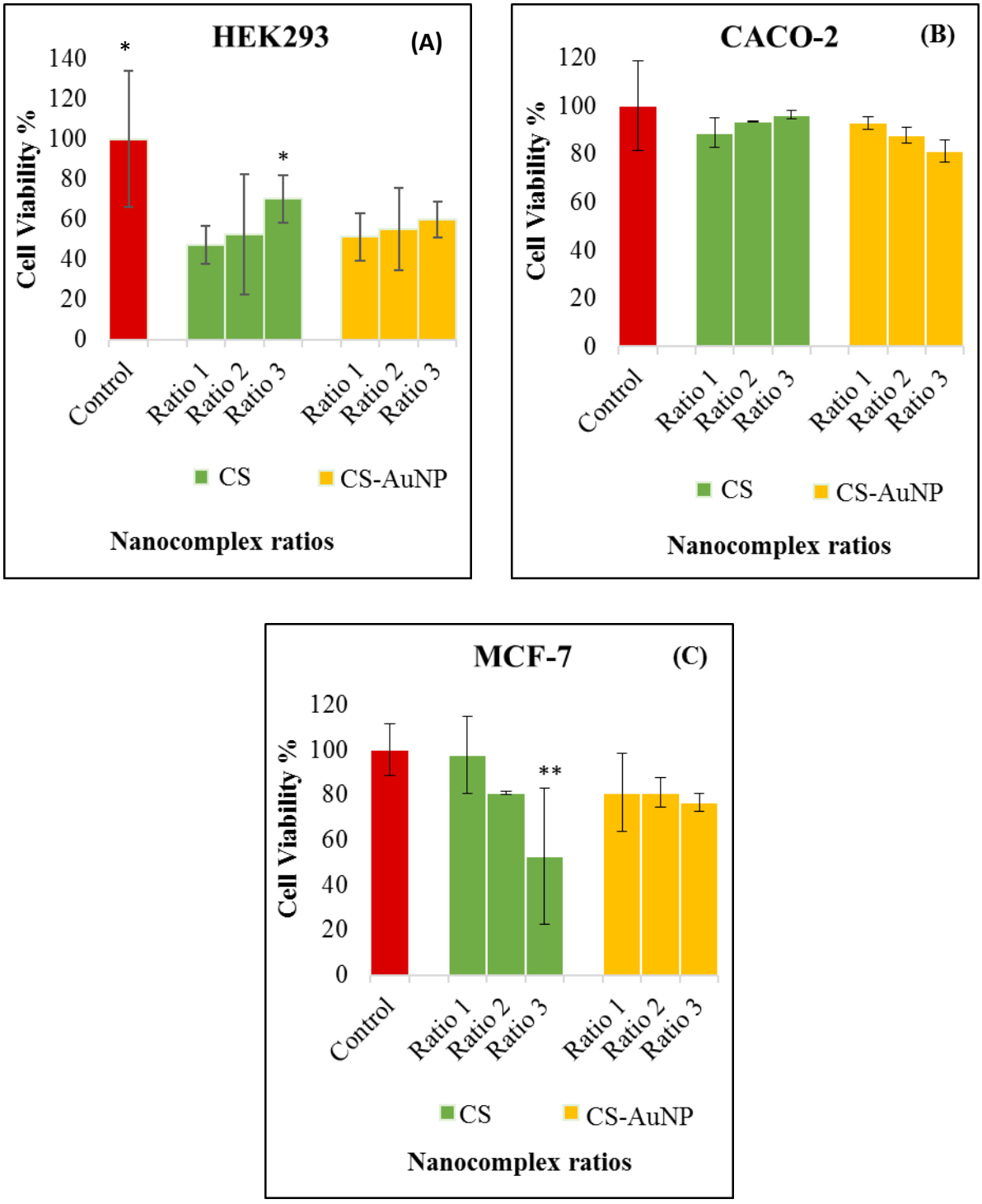


**Figure 3.15:** MTT cytotoxicity assay of complexes in cell lines: (A) HEK293, (B) Caco-2 and (C) MCF-7. Data represented as means ± SD (n=3), * $p<0.05$, **$p<0.01$ and **$p<0.001$ were considered statistically significant as determined by the Dunnet test.

### 3.3.4.3 Luciferase reporter gene assay

AuNPs are emerging as attractive synthetic vehicles for nucleic acid delivery due to their ease of control in terms of size and surface functionality, allowing modulation of cytotoxicity and bio-distribution (Ding *et al*., 2014). In the hope of developing a highly efficient gene carrier, we have functionalised AuNPs with CS and evaluated their transfection efficiency using the luciferase reporter gene assay. Gene expression is commonly studied in cell biology using genetic reporter assays (Allard and Kopish, 2008). The firefly (*Photinus pyralis*) luciferase of 16 kDa, a monomeric enzyme, is an extensively utilized reporter (Fan and Wood, 2006). The luciferase reporter gene expression assay is a highly sensitive and rapid assay which allows immediate measurement of reporter activity after translation as the resulting protein does not require post-translational processing (Allard and Kopish, 2008). The reaction is ATP-dependent in which the luciferase enzyme catalyses the conversion of beetle luciferin (substrate) to an enzyme-bound intermediate, luciferyl-AMP.

This intermediate then reacts with oxygen to generate the final product oxyluciferin in a high-energy state. A yellow-green light is produced by the subsequent energy transition to the ground state and this bioluminescence is measured as relative light units (RLU) at 560 nm. The RLU measurements are usually normalized against its corresponding soluble protein content in the cell lysates which we determined using the BCA assay. Following the incubation of complexes with the cells, the transfection efficiency of the complexes containing the luciferase encoded mRNA (F*luc*-mRNA) was evaluated by directly correlating the luciferase activity (RLU/mg protein) produced by each complex in each cell line.

For all cell lines, two controls, cells only and cells treated with naked F*luc*-mRNA (0.25 µg/µl) were used. In all cell lines the best transgene activity was observed at the sub-optimal ratios (ratio 1) for both the CS and CS-AuNP:mRNA complexes ( Figures 3.16 A-C). Maximum luciferase activity for the CS and CS-AuNP:mRNA complexes were $3.3 \times 10^5$ and $3.8 \times 10^5$ RLU/mg protein in the HEK293 cell line (Figure 3.16 A), $4.6 \times 10^5$ and $5.3 \times 10^5$ RLU/mg protein in the Caco-2 cell line (Figure 3.16 B), and $4.2 \times 10^3$ and $6.6 \times 10^3$ RLU/mg protein in the MCF-7 cell line (Figure 3.16 C). In all cell lines, a general trend was seen wherein the luciferase activity decreased as the ratio of CS and CS-AuNP to F*luc*-mRNA increased, indicating that transfection efficiency was concentration dependent.

This observation may be attributed to the high compaction and restricted release of F*luc*-mRNA which is due to the high binding efficiency of CS and CS-AuNP, as established by the band shift, dye displacement assays and TEM micrographs which further indicated the formation of nano-aggregates. As expected, luciferase activity in comparison to the controls was significant, highlighting the importance of the nanovector system. Overall, CS-AuNP:F*luc*-mRNA complexes displayed higher trangene activity than CS:F*luc*-mRNA complexes, indicating that the transfection efficiency of CS was improved by its combination with the AuNPs. The transfection and binding efficiency of CS with nucleic acids are linearly correlated with its molecular mass which may result in inferior transfection efficiency (Zhou *et al*., 2008).

AuNPs have been reported to be taken up voluntarily by cells with their intracellular uptake and distribution being dependent on characteristics such as zeta potential, surface modification, shape and size (Huefner *et al*., 2014). Experimental procedures and their parameters such as concentration and exposure time also influence their uptake and distribution (Mironava *et al*., 2010). Furthermore, the differences in cell types greatly influence the functioning and processing of AuNPs (Doane and Burda, 2012). The synthesized CS-AuNP properties such as excellent zeta potential, ability to protect the F*luc*-mRNA and inherent low cytotoxicity all contributed in enhancing the transfection efficiency of the complex.

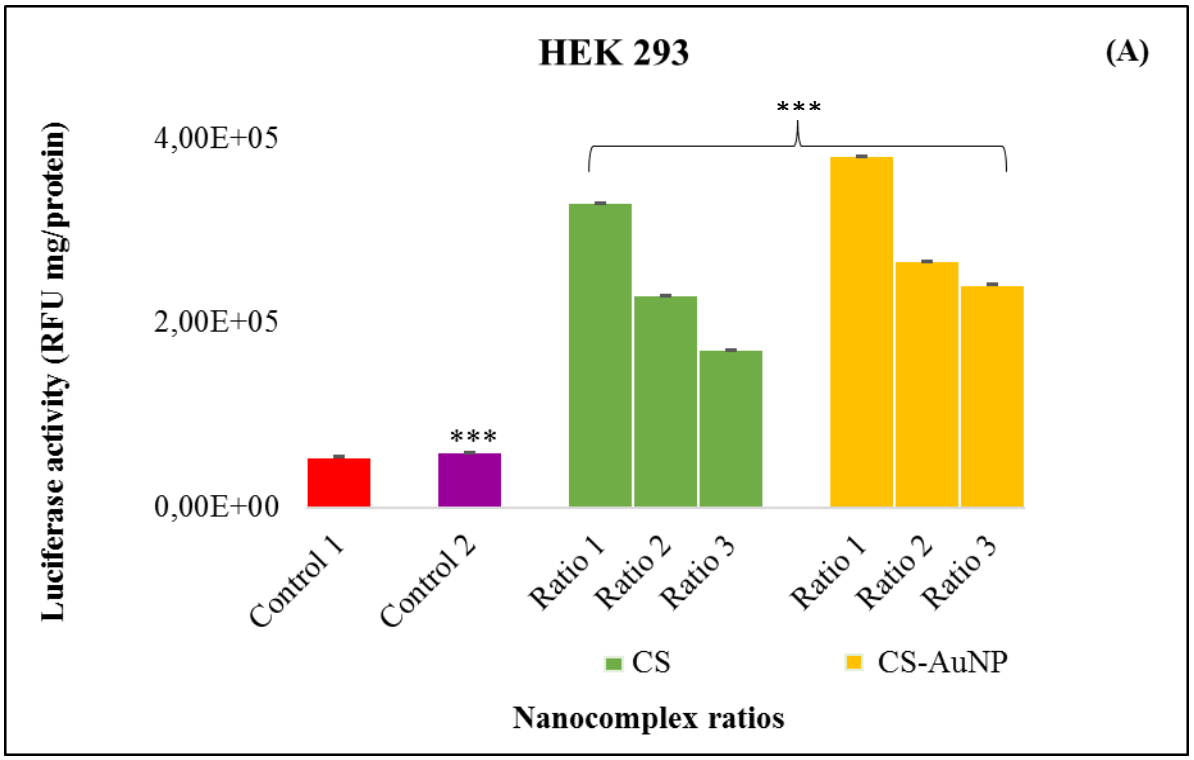

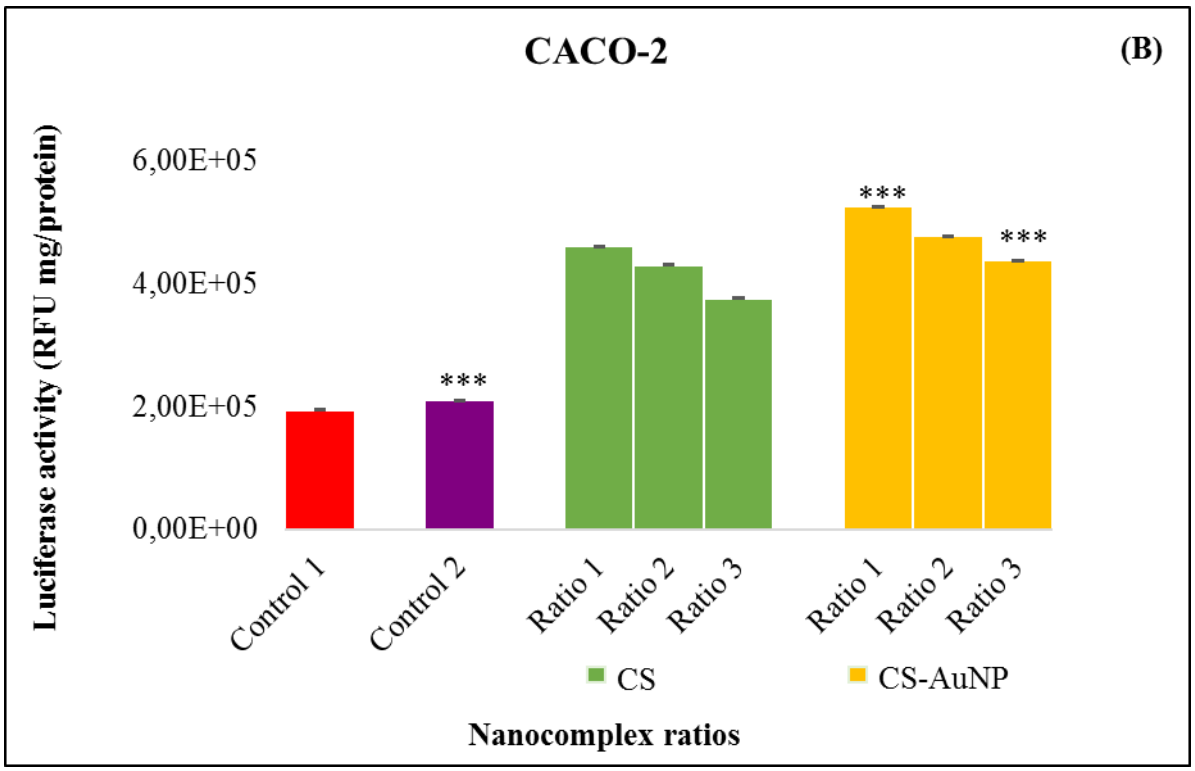


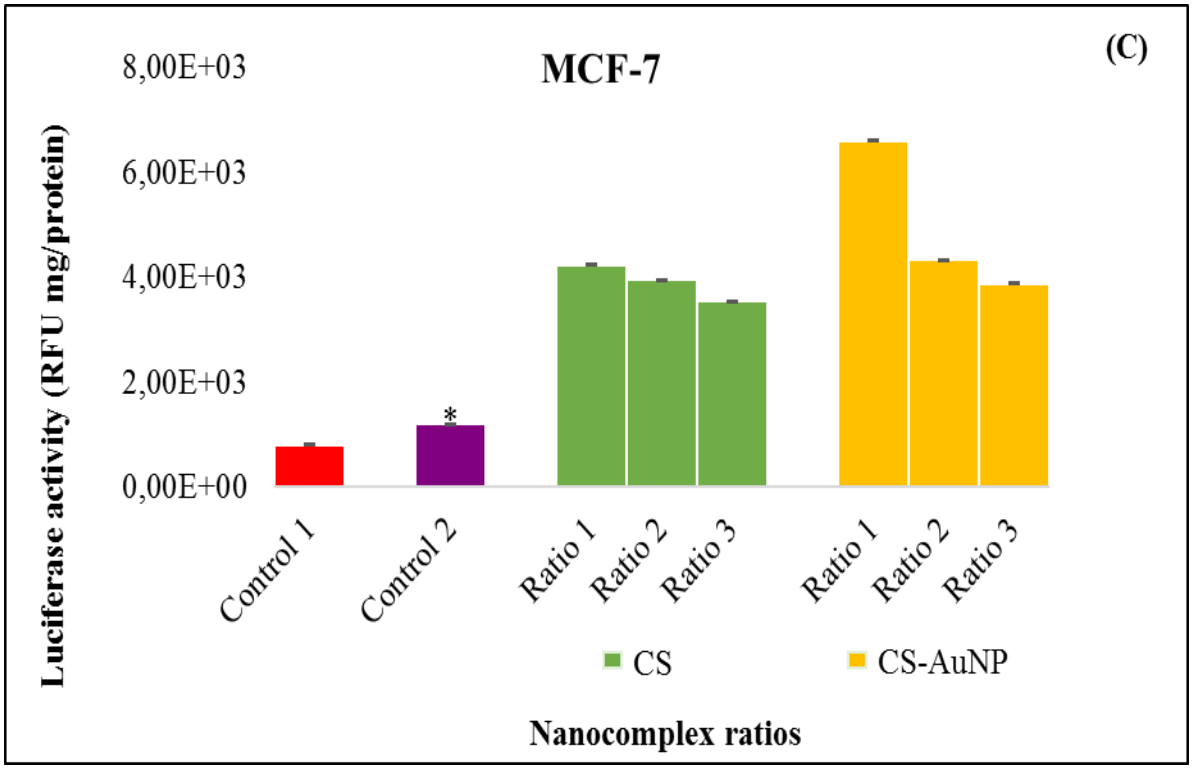


**Figure 3.16:** Luciferase gene expression activity of complexes measured in RLU/mg protein assayed in cell lines: (A) HEK293, (B) Caco-2 and (C) MCF-7. Data represented as mean ± SD (n=3), * $p<0.05$, ** $p<0.01$ and *** $p<0.001$ were considered statistically significant as determined by the Tukey-Kramer test.

### 3.3.4.4 Acridine Orange/Ethidium Bromide (AO/EB) apoptosis assay

Nanoparticles can elicit adverse effects such as organelle or DNA damage, oxidative stress and apoptosis at the cellular level by interacting with vital cell components such as the membrane, mitochondria or nucleus (Mironava *et al*., 2010). Apoptosis is a type of programmed cell death that is genetically regulated to control the development of tissues and multi-cellular organisms by eliminating physiologically defective, damaged and abnormal cells (Liu *et al*., 2015), hence an effective defence mechanism of the body to kill tumour cells. However, cancer is known to inhibit normal cellular processes causing a defect of this mechanism. Chemotherapeutics acts by destroying tumour cells and restraining their proliferation mainly by promoting apoptosis (Yamamoto *et al*., 1999). In contrast, the efficacy of gene therapy is measured by the vectors' ability to detect cancer cells and selectively repairing damaged genes triggering apoptosis.

Apoptosis is morphologically characterized by a change in the refractive index of the cell, cytoplasmic shrinkage, nuclear condensation and lack of preserving phospholipid asymmetry (Pan *et al*., 2012). The cell membrane forms protrusions which eventually separate from the cells to form apoptotic bodies. In addition, the mitochondrial outer membrane forms pores which results in a loss of its electrochemical gradient, allowing the leaking of substances into the cytoplasm without evoking inflammatory responses. The dying cells and apoptotic bodies are then phagocytosed by adjacent cells or macrophages. In contrast, necrosis is morphologically characterized by the swelling of the cytoplasm and mitochondria in the cell leading to lysis, affecting the adjacent cells and evoking inflammatory responses (Pan *et al*., 2012). The remains of the necrotic cells are then phagocytosed by macrophages.

To determine the mechanism of cell death due to exposure to the formulated nanocomplexes, the apoptosis assay using the AO/EB dual staining method and phase-contrast microscopy was employed. The fluorescence intensity of AO/EB in cells was further measured for each complex in each cell line. The amount of fluorescence generated is proportional to the number of apoptotic cells present. The acridine orange/ethidium bromide (AO/EB) dual fluorescence staining coupled with visualization with a fluorescence microscope is a useful technique to identify apoptosis-associated changes in cells and accurately distinguish cells at different stages of apoptosis (Gherghi *et al*., 2003).

Acridine orange acts by permeating the cell and causes the cells to fluoresce green. Thereafter, cells which have lost their cytoplasmic membrane integrity selectively take up the

ethidium bromide stain and cause the nucleus to fluoresce red (Liu *et al*., 2015). The nucleus of live cells fluoresces green, apoptotic cells have fragmented chromatin fluoresce red and necrotic cells orange (Ribble *et al*., 2005). All control cells fluoresced green, indicating the absence of apoptosis and necrosis (Figure 3.17). The number of apoptotic cells after treatment with the CS-AuNP:F*luc*-mRNA complex was far greater than that of the CS:F*luc*-mRNA complex, indicating the ability of the CS-AuNP:F*luc*-mRNA to induce apoptosis. The distinct morphological characteristics of red apoptotic cells were seen and included cellular shrinking and blebbing (labelled as 'A' in figure 3.17) and orange necrotic cells which showed swelling (labelled as 'N' in figure 3.17).

The apoptotic index (Table 3.5) for the CS:F*luc*-mRNA complex was 0.05, 0.24 and 0.14, while the CS-AuNP:F*luc*-mRNA complex apoptotic index (Table 3.4) was 0.06, 0.39 and 0.20 in the HEK293, Caco-2 and MCF-7 cell lines, respectively. These values directly correlated to the fluorescent intensity (Figure 3.18) measurements. The greater apoptotic index for the CS-AuNP:F*luc*-mRNA complex indicates that the normal cellular apoptosis defence mechanism was restored upon treatment with this complex and may be correlated with their excellent transfection efficiency and level of cytotoxicity.

It has previously been reported that an increase in size, concentration and exposure time of cells to AuNPs results in a higher percentage of cells undergoing apoptosis (Mironava *et al*., 2010). Additionally, AuNPs show cell-type specificity for induction of apoptosis as seen between the HEK293, Caco-2 and MCF-7 cell lines with the highest apoptotic index values seen in the Caco-2 cell line. Previous studies have reported apoptosis induction in melanoma, fibroblast and macrophage cell lines (Pan *et al*., 2007 and Patra *et al*., 2007).

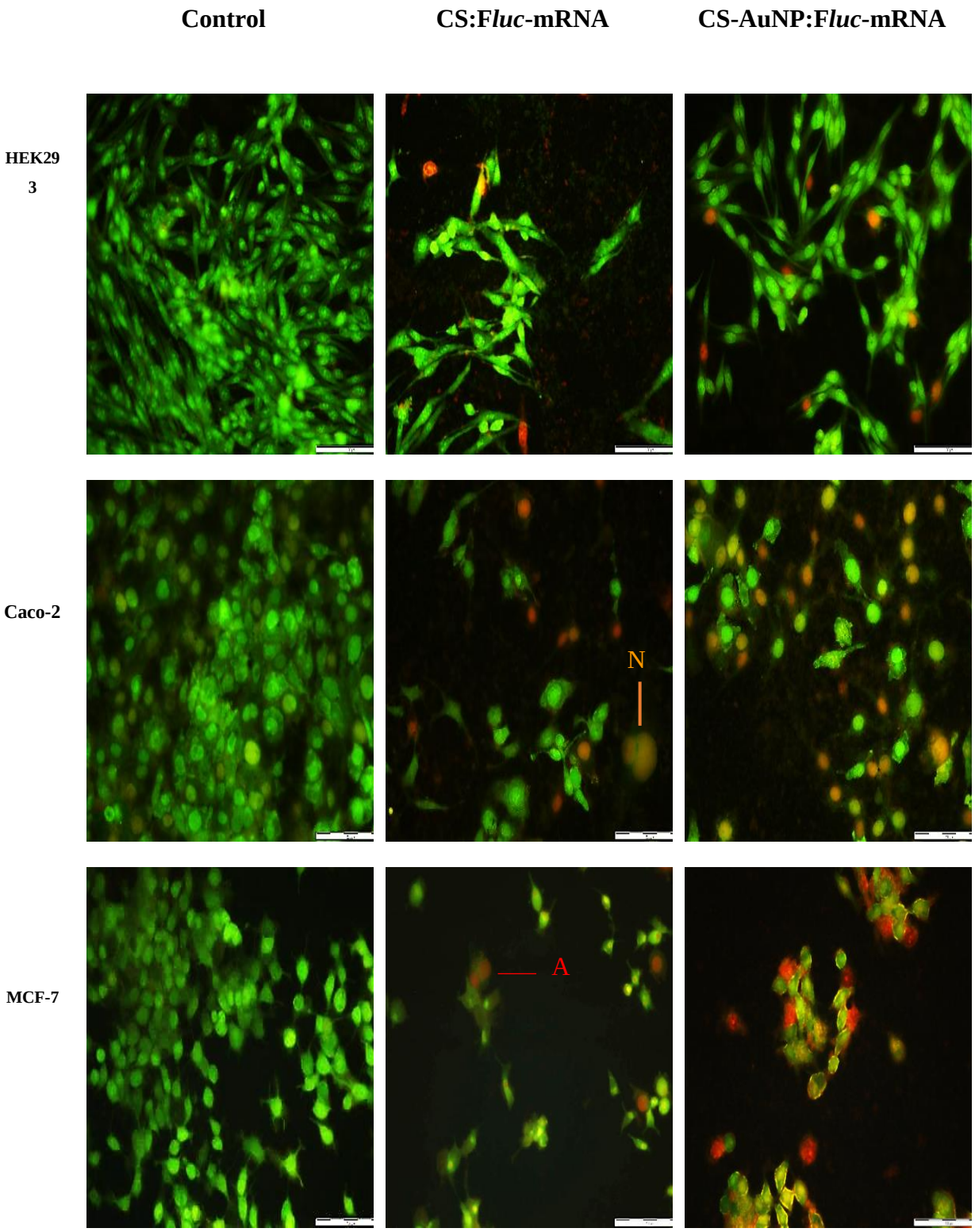


**Figure 3.17:** Fluorescence images obtained from the AO/EB apoptosis assay on HEK293, Caco-2 and MCF-7 cell lines at 20× magnification. A= apoptotic cells, N= necrotic.

**Table 3.5.** Apoptotic index values for each complex on each cell line.

| Cell line | Sample | Number of apoptotic cells | Total number of cells | Apoptotic index |
|---|---|---|---|---|
| **HEK293** | 1.CS:F*luc*-mRNA | 3 | 56 | 0.05 |
| | 2. CS-AuNP:F*luc*-mRNA | 9 | 149 | 0.06 |
| **Caco-2** | 1. CS:F*luc*-mRNA | 10 | 42 | 0.24 |
| | 2. CS-AuNP:F*luc*-mRNA | 24 | 61 | 0.39 |
| **MCF-7** | 1. CS:F*luc*-mRNA | 5 | 37 | 0.14 |
| | 2. CS-AuNP:F*luc*-mRNA | 10 | 49 | 0.20 |

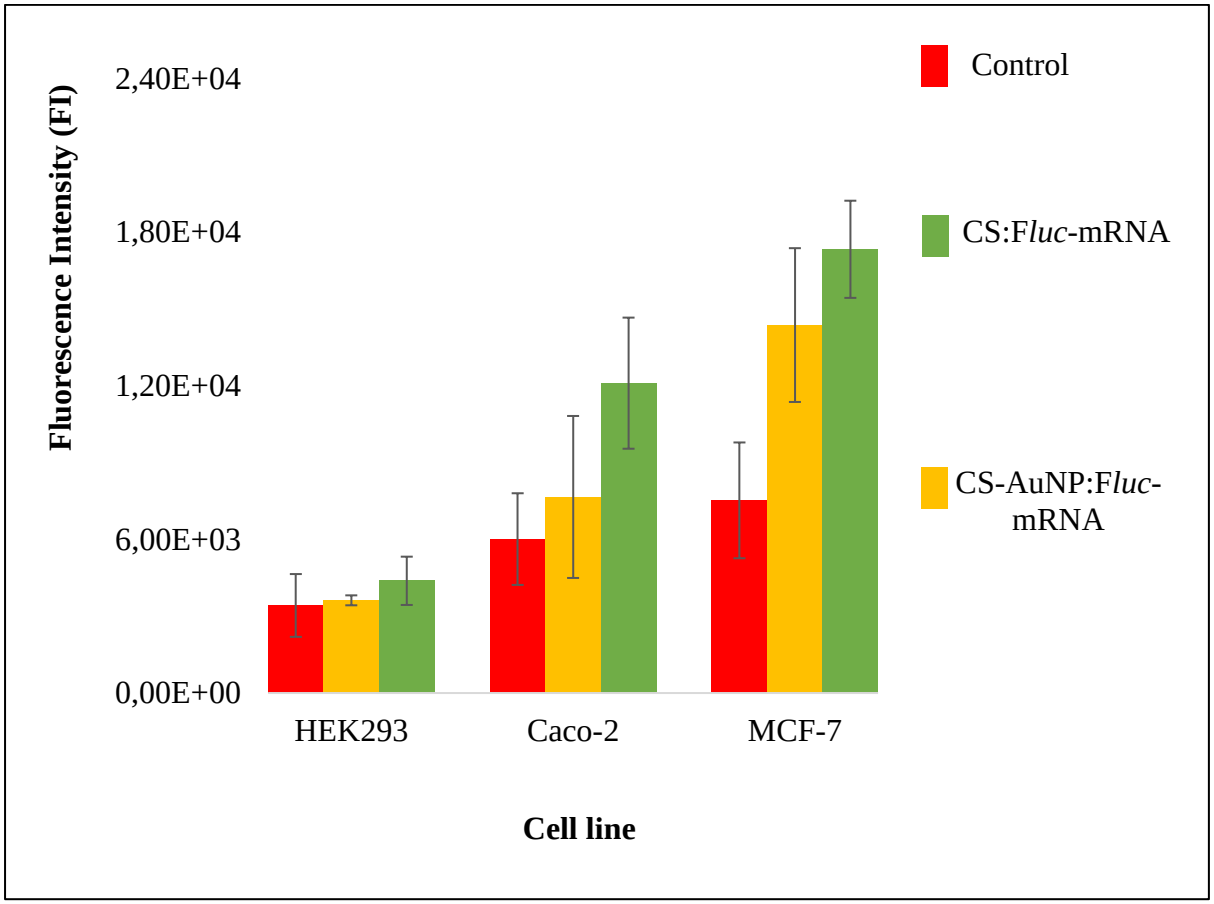


**Figure 3.18:** Fluorescence intensity (FI) of cell lines HEK293, Caco-2 and MCF-7 with and without treatment of the complexes. Data represented as mean ± SD (n=3).

## 3.4 Conclusion

The design and successful synthesis of CS functionalised AuNP-based gene carriers has been shown to significantly influence transgene expression in the three cell lines tested. These nanocomplexes were able to bind and compact F*luc*-mRNA at low concentrations as evidenced from the gel retardation and florescence-based dye displacement assays. Their favourable SPR absorption, spherical morphology, small size for cellular uptake, colloidal stability, low cytotoxicity and significant reporter gene expression augur well for future *in vivo* studies. Furthermore, these nanocomplexes afforded protection to the mRNA against nucleases, facilitating safe delivery of the cargo and were able to induce apoptosis, more so in the cancer cell lines (Caco-2 and MCF-7) than in the normal HEK293 cell line. Preliminary results indicate that these CS-AuNPs have the potential to be effective gene delivery vectors, especially for cancer treatment.

Since cytotoxicity, transfection efficiency and apoptosis induction are highly dependent on the formulation characteristics of the nanoparticles, the physiological environment and the type of cells, future studies will have to take this into consideration. It is recommended that formulations of the CS-AuNPs of various concentrations, sizes, shapes and surface charge be prepared with the addition of the steric stabilizing polymer, polyethyleneycol (PEG) and suitable targeting ligands. Furthermore, studies of different environmental parameters such as exposure time and pH levels for the optimization of protocols could be critical.

## REFERENCES


Alkilany, A. M., and Murphy, C. J. (2010). Toxicity and cellular uptake of gold nanoparticles: what we have learned so far? *Journal of Nanoparticle Research, 12*(7), 2313-2333.

Allard, S., and Kopish, K. (2008). Luciferase reporter assays: Powerful, adaptable tools for cell biology research. *Cell Notes, 21*, 23-26.

Amendola, V., and Meneghetti, M. (2009). Laser ablation synthesis in solution and size manipulation of noble metal nanoparticles. *Physical chemistry chemical physics, 11*(20), 3805-3821.

American Cancer Society. (2014). The history of cancer.

Arjmandi, N., Van Roy, W., Lagae, L., and Borghs, G. (2012). Measuring the electric charge and zeta potential of nanometer-sized objects using pyramidal-shaped nanopores. *Analytical chemistry, 84*(20), 8490-8496.

Bahadur, K., Thapa, B., and Bhattarai, N. (2014). Gold nanoparticle-based gene delivery: promises and challenges. *Nanotechnology Reviews, 3*(3), 269-280.

Bai, H., Zhu, P., Wu, W., Li, J., Ma, Z., Zhang, W., and Li, M. (2015). Synthesis and biological evaluation of a series of aryl triazoles as firefly luciferase inhibitors. *MedChemComm, 6*(3), 418-424.

Balasubramanian, S. K., Yang, L., Yung, L.-Y. L., Ong, C.-N., Ong, W.-Y., and Liya, E. Y. (2010). Characterization, purification, and stability of gold nanoparticles. *Biomaterials, 31*(34), 9023-9030.

Banerjee, A., Majumder, P., Sanyal, S., Singh, J., Jana, K., Das, C., and Dasgupta, D. (2014). The DNA intercalators ethidium bromide and propidium iodide also bind to core histones. *FEBS open bio, 4*(1), 251-259.

Barahuie, F., Hussein, M. Z., Fakurazi, S., and Zainal, Z. (2014). Development of drug delivery systems based on layered hydroxides for nanomedicine. *International journal of molecular sciences, 15*(5), 7750-7786.

Bettinger, T., Carlisle, R. C., Read, M. L., Ogris, M., and Seymour, L. W. (2001). Peptide-mediated RNA delivery: a novel approach for enhanced transfection of primary and post-mitotic cells. *Nucleic acids research, 29*(18), 3882-3891.

Bhumkar, D. R., Joshi, H. M., Sastry, M., and Pokharkar, V. B. (2007). Chitosan reduced gold nanoparticles as novel carriers for transmucosal delivery of insulin. *Pharmaceutical research, 24*(8), 1415-1426.

Boyles, M. S., Kristl, T., Andosch, A., Zimmermann, M., Tran, N., Casals, E., and Lütz-Meindl, U. (2015). Chitosan functionalisation of gold nanoparticles encourages particle uptake and induces cytotoxicity and pro-inflammatory conditions in phagocytic cells, as well as enhancing particle interactions with serum components. *Journal of nanobiotechnology, 13*(1), 1.

Cancer Association of South Africa. (2016). Fact Sheet on a Health Profile of South Africa and Related Information.

Cardenas, T. G., Sanzana, L. J., Mei, I., and Lucia, H. (2002). Synthesis and Characterization of Chitosan-PHB Blends. *Boletín de la Sociedad Chilena de Química, 47*(4), 529-535.

Chen, Y.-C., Lee, I.-L., Sung, Y.-M., and Wu, S.-P. (2013). Triazole functionalized gold nanoparticles for colorimetric Cr 3+ sensing. *Sensors and Actuators B: Chemical, 188*, 354-359.

Chueh, P. J., Liang, R.-Y., Lee, Y.-H., Zeng, Z.-M., and Chuang, S.-M. (2014). Differential cytotoxic effects of gold nanoparticles in different mammalian cell lines. *Journal of hazardous materials, 264*, 303-312.

Cotrim, A. P., and Baum, B. J. (2008). Gene therapy: some history, applications, problems, and prospects. *Toxicologic pathology, 36*(1), 97-103.

Daniel, M.-C., and Astruc, D. (2004). Gold nanoparticles: assembly, supramolecular chemistry, quantum-size-related properties, and applications toward biology, catalysis, and nanotechnology. *Chemical reviews, 104*(1), 293-346.

Ding, Y., Jiang, Z., Saha, K., Kim, C. S., Kim, S. T., Landis, R. F., and Rotello, V. M. (2014). Gold nanoparticles for nucleic acid delivery. *Molecular Therapy, 22*(6), 1075.

Doane, T. L., and Burda, C. (2012). The unique role of nanoparticles in nanomedicine: imaging, drug delivery and therapy. *Chemical Society Reviews, 41*(7), 2885-2911.

Dobrovolskaia, M. A., and McNeil, S. E. (2007). Immunological properties of engineered nanomaterials. *Nature nanotechnology, 2*(8), 469-478.

Does, A., Thiel, T., and Johnson, N. (2003). Rediscovering biology: molecular to global perspectives. *Annenberg Learner, Washington*.

Doyen, M., Bartik, K., and Bruylants, G. (2013). UV–Vis and NMR study of the formation of gold nanoparticles by citrate reduction: observation of gold–citrate aggregates. *Journal of colloid and interface science, 399*, 1-5.

Fan, F., and Wood, K. V. (2007). Bioluminescent assays for high-throughput screening. *Assay and drug development technologies, 5*(1), 127-136.

Gherghi, I. C., Girousi, S. T., Voulgaropoulos, A., and Tzimou-Tsitouridou, R. (2003). Study of interactions between DNA-ethidium bromide (EB) and DNA-acridine orange (AO), in solution, using hanging mercury drop electrode (HMDE). *Talanta, 61*(2), 103-112.

Goodman, C. M., McCusker, C. D., Yilmaz, T., and Rotello, V. M. (2004). Toxicity of gold nanoparticles functionalized with cationic and anionic side chains. *Bioconjugate chemistry, 15*(4), 897-900.

Hasenoehrl, C., Alexander, C. M., Azzarelli, N. N., and Dabrowiak, J. C. (2012). Enhanced detection of gold nanoparticles in agarose gel electrophoresis. *Electrophoresis, 33*(8), 1251-1254.

Hellman, L. M., and Fried, M. G. (2007). Electrophoretic mobility shift assay (EMSA) for detecting protein–nucleic acid interactions. *Nature protocols, 2*(8), 1849-1861.

Hole, P., Sillence, K., Hannell, C., Maguire, C. M., Roesslein, M., Suarez, G., and Dybowska, A. (2013). Interlaboratory comparison of size measurements on nanoparticles using nanoparticle tracking analysis (NTA). *Journal of Nanoparticle Research, 15*(12), 1-12.

Hostetler, M. J., Wingate, J. E., Zhong, C.-J., Harris, J. E., Vachet, R. W., Clark, M. R., and Wignall, G. D. (1998). Alkanethiolate gold cluster molecules with core diameters from 1.5 to 5.2 nm: core and monolayer properties as a function of core size. *Langmuir, 14*(1), 17-30.

Hou, X., Amais, R. S., Jones, B. T., and Donati, G. L. (2000). Inductively coupled plasma optical emission spectrometry. *Encyclopedia of analytical chemistry*.

Huang, X., Jain, P. K., El-Sayed, I. H., and El-Sayed, M. A. (2007). Gold nanoparticles: interesting optical properties and recent applications in cancer diagnostics and therapy.

Huefner, A., Septiadi, D., Wilts, B. D., Patel, I. I., Kuan, W.-L., Fragniere, A., and Mahajan, S. (2014). Gold nanoparticles explore cells: Cellular uptake and their use as intracellular probes. *Methods, 68*(2), 354-363.

Ibraheem, D., Elaissari, A., and Fessi, H. (2014). Gene therapy and DNA delivery systems. *International journal of pharmaceutics, 459*(1), 70-83.

International Agency for Research on Cancer and Cancer Research UK. (2014). World Cancer Fact sheet. London: Cancer Research UK.

International Agency for Research on Cancer and World Health Organization. (2014). World Cancer.

Ivanov, M. R. (2011). Covalently functionalized gold nanoparticles: synthesis, characterization, and integration into capillary electrophoresis.

Jang, K. J., Lee, H., Jin, H. L., Park, Y., and Nam, J. M. (2009). Restriction-Enzyme-Coded Gold-Nanoparticle Probes for Multiplexed DNA Detection. *Small, 5*(23), 2665-2668.

Jiang, W., Kim, B. Y., Rutka, J. T., and Chan, W. C. (2008). Nanoparticle-mediated cellular response is size-dependent. *Nature nanotechnology, 3*(3), 145-150.

Kim, H., Park, Y., and Lee, J. B. (2015). Self-assembled messenger RNA nanoparticles (mRNA-NPs) for efficient gene expression. *Scientific reports, 5*.

Kimling, J., Maier, M., Okenve, B., Kotaidis, V., Ballot, H., and Plech, A. (2006). Turkevich method for gold nanoparticle synthesis revisited. *The Journal of Physical Chemistry B, 110*(32), 15700-15707.

Kumar, S. V., and Ganesan, S. (2011). Preparation and characterization of gold nanoparticles with different capping agents. *International Journal of Green Nanotechnology, 3*(1), 47-55.

Lago, M., Rodríguez Bernaldo de Quirós, A., Sendón, R., Sanches-Silva, A., Costa, H., Sánchez-Machado, D., and Angulo, I. (2011). Compilation of analytical methods to characterize and determine chitosan, and main applications of the polymer in food active packaging Recopilación de métodos analíticos para la caracterización y determinación del quitosano y las principales aplicaciones del polímero en los envases activos alimentarios. *CyTA-Journal of Food, 9*(4), 319-328.

Laniel, M.-A., Béliveau, A., and Guérin, S. L. (2001). Electrophoretic mobility shift assays for the analysis of DNA-protein interactions. *DNA-Protein Interactions: Principles and Protocols*, 13-30.

Lee, A. V., Oesterreich, S., and Davidson, N. E. (2015). MCF-7 cells—changing the course of breast cancer research and care for 45 years. *Journal of the National Cancer Institute, 107*(7), djv073.

Lison, D., and Huaux, F. (2011). *In vitro* studies: ups and downs of cellular uptake. *Nature nanotechnology, 6*, 332-333.

Liu, K., Liu, P.-c., Liu, R., and Wu, X. (2015). Dual AO/EB staining to detect apoptosis in osteosarcoma cells compared with flow cytometry. *Medical science monitor basic research, 21*, 15.

Malone, R. W., Felgner, P. L., and Verma, I. M. (1989). Cationic liposome-mediated RNA transfection. *Proceedings of the National Academy of Sciences, 86*(16), 6077-6081.

Manjila, S. B., Baby, J. N., Bijin, E. N., Constantine, I., Pramod, K., and Valsalakumari, J. (2013). Novel gene delivery systems. *International journal of pharmaceutical investigation, 3*(1), 1.

Marquis, B. J., Love, S. A., Braun, K. L., and Haynes, C. L. (2009). Analytical methods to assess nanoparticle toxicity. *Analyst, 134*(3), 425-439.

Matsui, A., Uchida, S., Ishii, T., Itaka, K., and Kataoka, K. (2015). Messenger RNA-based therapeutics for the treatment of apoptosis-associated diseases. *Scientific reports, 5*.

Mironava, T., Hadjiargyrou, M., Simon, M., Jurukovski, V., and Rafailovich, M. H. (2010). Gold nanoparticles cellular toxicity and recovery: effect of size, concentration and exposure time. *Nanotoxicology, 4*(1), 120-137.

Mohd, S. N., and Johan, M. R. (2014). Synthesis and Ultraviolet Visible Spectroscopy Studies of Chitosan Capped Gold Nanoparticles and Their Reactions with Analytes. *The Scientific World Journal, 2014*.

Narayanan, R., and Sivakumar, M. (2014). *Preparation and Characterization of Gold Nanoparticles in Chitosan Suspension by One-Pot Chemical Reduction Method.* Paper presented at the Nano Hybrids.

Nivethaa, E., Dhanavel, S., Narayanan, V., Vasu, C. A., and Stephen, A. (2015). An *in vitro* cytotoxicity study of 5-fluorouracil encapsulated chitosan/gold nanocomposites towards MCF-7 cells. *RSC Advances, 5*(2), 1024-1032.

Pan, Y., Guo, M., Nie, Z., Huang, Y., Peng, Y., Liu, A., and Yao, S. (2012). Colorimetric detection of apoptosis based on caspase-3 activity assay using unmodified gold nanoparticles. *Chemical Communications, 48*(7), 997-999.

Pan, Y., Neuss, S., Leifert, A., Fischler, M., Wen, F., Simon, U., and Jahnen-Dechent, W. (2007). Size-dependent cytotoxicity of gold nanoparticles. *Small, 3*(11), 1941-1949.

Patil, P., Chaudhari, P., Sahu, M., and Duragkar, N. (2012). Review article on gene therapy. *International Journal of Genetics, 4*(1), 74.

Patra, H. K., Banerjee, S., Chaudhuri, U., Lahiri, P., and Dasgupta, A. K. (2007). Cell selective response to gold nanoparticles. *Nanomedicine: Nanotechnology, Biology and Medicine, 3*(2), 111-119.

Pedrosa, P., Vinhas, R., Fernandes, A., and Baptista, P. V. (2015). Gold nanotheranostics: proof-of-concept or clinical tool? *Nanomaterials, 5*(4), 1853-1879.

Philip, D. (2008). Synthesis and spectroscopic characterization of gold nanoparticles. *Spectrochimica Acta Part A: Molecular and Biomolecular Spectroscopy*, *71*(1), 80-85.

Polte, J. (2015). Fundamental growth principles of colloidal metal nanoparticles–a new perspective. *CrystEngComm, 17*(36), 6809-6830.

Prochazkova, S., Vårum, K. M., and Ostgaard, K. (1999). Quantitative determination of chitosans by ninhydrin. *Carbohydrate polymers, 38*(2), 115-122.

Quong, D., and Neufeld, R. (1998). DNA protection from extracapsular nucleases, within chitosan-or poly-L-lysine-coated alginate beads. *Biotechnology and bioengineering, 60*(1), 124-134.

Radwan, S. H., and Azzazy, H. M. (2009). Gold nanoparticles for molecular diagnostics. *Expert review of molecular diagnostics, 9*(5), 511-524.

Ramezani, M. R., Naderi-Manesh, H., Pour, R., and Ali, H. (2014). Cytotoxity Assessment of Gold Nanoparticle-Chitosan Hydrogel Nanocomposite as an Efficient Support for Cell Immobilization: toward Sensing Application. *Environmental Studies of Persian Gulf, 1*(2), 126-134.

Rana, S., Bajaj, A., Mout, R., and Rotello, V. M. (2012). Monolayer coated gold nanoparticles for delivery applications. *Advanced drug delivery reviews, 64*(2), 200-216.

Ribble, D., Goldstein, N. B., Norris, D. A., and Shellman, Y. G. (2005). A simple technique for quantifying apoptosis in 96-well plates. *BMC biotechnology, 5*(1), 12.

Sau, S. P., Kumar, P., Sharma, P. K., and Hrdlicka, P. J. (2012). Fluorescent intercalator displacement replacement (FIDR) assay: determination of relative thermodynamic and kinetic parameters in triplex formation—a case study using triplex-forming LNAs. *Nucleic acids research, 40*(21), e162-e162.

Selim, M. E., and Hendi, A. A. (2012). Gold nanoparticles induce apoptosis in MCF-7 human breast cancer cells. *Asian Pacific Journal of Cancer Prevention, 13*(4), 1617-1620.

Siddiqui, S., Khan, I., Zarina, S., and Ali, S. (2013). Use of the SYBR Green dye for measuring helicase activity. *Enzyme and microbial technology, 52*(3), 196-198.

Son, K. K., Patel, D. H., Tkach, D., and Park, A. (2000). Cationic liposome and plasmid DNA complexes formed in serum-free medium under optimum transfection condition are negatively charged. *Biochimica et Biophysica Acta (BBA)-Biomembranes, 1466*(1), 11-15.

Thanh, N. T., Maclean, N., and Mahiddine, S. (2014). Mechanisms of nucleation and growth of nanoparticles in solution. *Chemical reviews, 114*(15), 7610-7630.

Turkevich, J., Stevenson, P. C., and Hillier, J. (1951). A study of the nucleation and growth processes in the synthesis of colloidal gold. *Discussions of the Faraday Society, 11*, 55-75.

Van Doren, E. A., De Temmerman, P.-J. R., Francisco, M. A. D., and Mast, J. (2011). Determination of the volume-specific surface area by using transmission electron tomography for characterization and definition of nanomaterials. *Journal of nanobiotechnology, 9*(1), 1.

Verma, H. N., Singh, P., and Chavan, R. (2014). Gold nanoparticle: synthesis and characterization. *Veterinary world, 7*(2), 72-77.

Vesaratchanon, S., Nikolov, A., and Wasan, D. T. (2007). Sedimentation in nano-colloidal dispersions: effects of collective interactions and particle charge. *Advances in colloid and interface science, 134*, 268-278.

Wagner, T., Lipinski, H.-G., and Wiemann, M. (2014). Dark field nanoparticle tracking analysis for size characterization of plasmonic and non-plasmonic particles. *Journal of Nanoparticle Research, 16*(5), 1-10.

Wu, Y., Hussain, M., and Fassihi, R. (2005). Development of a simple analytical methodology for determination of glucosamine release from modified release matrix tablets. *Journal of pharmaceutical and biomedical analysis, 38*(2), 263-269.

Yah, C. S. (2013). The toxicity of gold nanoparticles in relation to their physiochemical properties. *Biomed Res, 24*(3), 400-413.

Yamamoto, A., Kormann, M., Rosenecker, J., and Rudolph, C. (2009). Current prospects for mRNA gene delivery. *European journal of pharmaceutics and biopharmaceutics, 71*(3), 484-489.

Yeh, Y.-C., Creran, B., and Rotello, V. M. (2012). Gold nanoparticles: preparation, properties, and applications in bionanotechnology. *Nanoscale, 4*(6), 1871-1880.

Zhou, X., Zhang, X., Yu, X., Zha, X., Fu, Q., Liu, B., and Shan, Y. (2008). The effect of conjugation to gold nanoparticles on the ability of low molecular weight chitosan to transfer DNA vaccine. *Biomaterials, 29*(1), 111-117.

# CHAPTER FOUR

# POLY-L-LYSINE FUNCTIONALISED GOLD NANOPARTICLE MEDIATED DELIVERY OF F*luc*-mRNA *IN VITRO*: SYNTHESIS, CHARACTERIZATION, CYTOTOXICITY AND TRANSFECTION EFFICIENCY

**S. Pillay[1] and M. Singh[1*]**

[1]Non-Viral Gene Delivery Laboratory, Discipline of Biochemistry, School of Life Sciences, University of Kwa-Zulu Natal, Private Bag X54001, Durban, South Africa

[*]Corresponding author: Moganavelli Singh, email: Singhm1@ukzn.ac.za

**Abstract**

Gold nanoparticles (AuNPs) have entrenched themselves in nanomedicine, providing a multi-platform scaffold for biomedical applications such as the delivery of a variety of biomolecules due to their unique physical, chemical and optical properties. In addition, AuNPs are low in toxicity, biocompatible and are easily manipulated to control size, shape, stability, dispersity, surface composition and charge. AuNPs have shown proven applicability as gene therapy vehicles for the treatment of heterogenous diseases such as cancer. For many years, plasmid DNA (pDNA) has been the nucleic acid of choice for gene therapy studies. However, its use is associated with many limitations such as inefficient intracellular trafficking and nuclear entry of genes. As an attractive alternative are mRNA molecules that possess the ability to overcome most of these barriers. In this study, we exploit the above mentioned desirable properties of mRNA using poly-l-lysine (PLL) functionalised AuNPs (PLL-AuNPs) as delivery vehicles for mRNA and assess the level of transgene expression in three human cell lines: embryonic kidney (HEK293), colorectal adenocarcinoma (Caco-2), and breast adenocarcinoma (MCF-7). AuNPs were synthesized using established protocols and functionalised with PLL. All nanoparticles (AuNPs and PLL-AuNPs) and the nanocomplexes (PLL-AuNP:F*luc*-mRNA) were characterized using UV-Vis spectrophotometry, Transmission Electron Microscopy (TEM) and Nanoparticle Tracking Analysis (NTA). PLL-AuNP:F*luc*-mRNA binding, compaction and stability were evaluated using the gel retardation, dye displacement and nuclease protection assays, respectively. The levels of cytotoxicity and gene expression *in vitro* were determined using the MTT and luciferase reporter gene assays, respectively. The mechanism for the cytotoxicity was ascertained using the AO/EB dual apoptosis assay. PLL:F*luc*-mRNA and PLL-AuNP:F*luc*-mRNA nanocomplexes were assayed for comparative analysis. Results indicate that PLL-AuNPs and their nanocomplexes display appropriate and desirable properties such as small size (PLL-AuNP: 90.4 nm, nanocomplexes: 89.4 nm), colloidal stability (zeta potential: PLL-AuNP: -5.3 mV, nanocomplexes: -97.1 mV), excellent binding, low cytotoxicity (<40%), and significant transgene expression. In addition, PLL-AuNPs proved to be more efficient than the PLL polymer itself, indicating that AuNPs improve PLL's biological activity. Overall, these results favour the use of PLL-AuNPs as potential vehicles for the delivery of mRNA in gene therapy studies.

Keywords: biomedical, cancer, cytotoxicity, F*luc*-mRNA, gene expression, gold nanoparticles, immunotherapy, poly-l-lysine

## 4.1 Introduction

Cancer is one of the most difficult diseases to treat and this global burden has resulted in increased efforts towards determining the underlying genetic processes contributing to the development of malignancies and tumorigenesis. Many of these genetic processes have been altered by various risk factors such as exposure to certain physical and chemical agents, radiation, improper diet and exercise, infection, inadequate hormone levels and inherited genetic defects (Cancer Association of South Africa, 2016). The past decade has seen an explosion in information on tumor biology leading to a variety of therapeutic methods. In this regard, prevention and treatment strategies such as chemotherapy, surgery and radiation have since been developed and implemented. However, these interventions are employed to kill off malignant cells and generally just lead to prolonged survival times. In addition, these treatments suffer from a lack of target cell specificity, development of multi-drug resistance, poor drug penetration of cancer cells and unbearable side-effects for the patients (Sivaramakrishnan *et al*., 2014).

Recently, new molecular therapeutic strategies encompassing gene therapy have been developed to selectively target tumour cells and correct, supplement or inhibit cancer promoting genes which are defective in normal cellular function. In contrast to the commonly utilized pDNA in gene expression studies, the use of mRNA holds promise in efficient gene expression and overcoming the cellular barriers limiting the use of pDNA and is therefore investigated in this study. The advantages of mRNA based therapy include no requirement for nuclear entry, rapid promoter-independent protein expression directly in the cytoplasm, no genomic integration and it is suitable for hard-to-transfect cells (Matsui *et al*., 2015). Non-viral gene delivery vectors have recently gained much attention due to their superiority over viral vectors in terms of simplicity, safety and large loading capacity (Shan *et al*., 2012). However, the development of highly efficient non-viral vectors remains a challenge for delivery due to cellular trafficking barriers such cellular uptake, protection, release and passage across the nuclear membrane of the genetic cargo (Manjila *et al*., 2013).

The application of gold nanoparticles (AuNPs) in nanomedicine and diagnostics is a rapidly emerging field due to their facile synthesis, manipulation of parameters such as size, shape, stability and dispersity, biocompatibility and unique optical properties such as surface plasmon resonance.

The high surface-volume-ratio of AuNPs allows for easy functionalisation with biomolecules to anchor therapeutic modalities and control reactivity, stability, charge, cellular uptake, tissue biocompatibility and toxicity (Sivaramakrishnan *et al*., 2014). In addition, their inert nature, low-toxicity, favourable interaction with cells and ability to stabilize and protect nucleic acids has encouraged the use of AuNPs as gene delivery vectors (De Long *et al*., 2010). Nanoparticles that have been functionalised with cationic polymers greatly favour solubility, biodegradability, bioavailability and circulation half-life (Pedrosa *et a*l., 2015). In addition, cationic polymers aid in effective condensation of nucleic acids *via* electrostatic interactions without compromising functionality, cellular internalisation *via* endocytosis, protection against nuclease degradation and release via the "proton sponge effect" (Nayerossadat *et al*. , 2012).

Poly-l-lysine (PLL) has been one of the first cationic polymer vectors used in gene therapy (Jin *et al*., 2014). Poly-l-lysine is derived from polymerisation of the N-carboxy-anhydride component of lysine and is therefore biodegradable, a characteristic suitable for gene delivery (Gascón *et al*., 2013). In addition, PLL has been reported to cause stress-induced apoptosis and hence applied as an anti-tumour agent (Symonds *et al*., 2005). These characteristics are hence exploited when conjugated to AuNP carriers. PLL forms electrostatic interactions and hydrogen bonds with citrate stabilized AuNPs resulting in a condensed structure which is efficient for binding and protecting nucleic acids. Furthermore, PLL-AuNPs have been used in a variety of applications such as biorecognition systems developed for DNA and antibody-antigen interactions, bactericidal and viricidal vaccines, as scaffolds in tissue repair and as stem cell carriers (Stobiecka and Hepel, 2011). However, reports on their use as gene delivery vectors are limited with those only stating the efficient electrostatic binding of nucleic acid fragments, penetration of eukaryotic membranes and low cytotoxicity. In this study, we synthesized and characterized PLL functionalised AuNPs using various chemical and physical techniques, assessed their ability to bind and protect luciferase-encoded mRNA (F*luc*-mRNA), evaluated their cytotoxicity and apoptosis induction and finally their transfection efficiency in the HEK293, Caco-2 and MCF-7 cell lines with the aim of determining their effectiveness as gene therapy vectors for cancer treatment.

## 4.2 Materials and methods

Ultrapure (18 M ohm) deionized water (Milli-Q Academic, Millipore, France) was utilized throughout and all reagents and chemicals were of analytical grade.

### 4.2.1 Materials

Gold (III) chloride trihydrate ($M_w$: 393.83 g/mol, HAuCl4.3H2O), poly-l-lysine hydrobromide ($M_w$: 1000-5000, PLL), 2, 2-dihydroxyindane-1, 3-dione (Ninhydrin, $M_w$: 178.14 g/mol, $C_9H_6O_4$) were supplied by Sigma-Aldrich Chemical Co., (St. Louis, USA). Sodium citrate tribasic dehydrate ($M_w$: 294.20 g/mol, $Na_3C_6H_5O_7.2H_2O$), 2-[4-(2-hydroxyethyl) piperazin-1-yl] ethanesulphonic acid (HEPES, $C_8H_{18}N_2O_4S$), tris (hydroxymethyl) aminomethane [Tris base, $M_w$: 121.14 g/mol, $H_2NC(CH_2OH)_3$], sodium dihydrogen orthophosphate dehydrate ($M_w$: 156.01 g/mol, $NaH_2PO_4.2H_2O$), ethylene diamine tetra acetic acid disodium salt ($M_w$: 372.24 g/mol, EDTA, $C_{10}H_{14}N_2Na_2O_8.2H_2O$), Dodecyl sulphate sodium salt (SDS, $M_w$: 288.37 g/mol, $C_{12}H_2OSO_2Na$ ), bromophenol blue ($M_w$: 669.96 g/mol, $C_{19}H_{10}Br_4O_5S$) were supplied by Merck (Darmstadt, Germany). UltraPure™ agarose, RNase free water (1 U/µl, supplied with $MnCl_2$) and UltraPure™ DEPC-treated water were supplied by Thermo Fischer Scientific Inc., (Waltham, Massachusetts, USA). Molecular grade ethidium bromide solution (10 mg/ml) was supplied by Promega (Madison, Wisconsin, USA). Fetal Bovine Serum (FBS) was supplied by Hyclone GE Healthcare (Utah, USA). SYBR Green II RNA gel stain (10 000× concentrate in DMSO) was supplied by Cambrex Bio Science Rockland Inc., (Rockland, ME, USA). The F*luc*-mRNA was provided by the Laboratory of Molecular and Cellular Therapy, Department of Immunology-Physiology, Vrije University, Brussels, Belgium.

## 4.3. Synthesis, Characterisation and Nanocomplex Evaluation

### 4.3.1 Synthesis of citrate reduced colloidal AuNP solution

The citrate reduction of Gold (III) chloride trihydrate ($HAuCl_4$), adapted from the method of Turkevich *et al.*, 1951, was used to synthesize a 0.45 x $10^{-3}$ M colloidal AuNP solution. Approximately 25 ml of 18 M ohm water was heated to 90°C with moderate stirring using a MH-4 Analog heating magnetic stirrer (Fried Electric, Israel). Thereafter, 375 µl of a $HAuCl_4$

solution (3 x $10^{-2}$ M) was rapidly introduced into the vortex of the solution, followed by the immediate addition of 1 ml of a 1% (w/v) sodium citrate solution. Subsequently, the solution was boiled for 15 minutes until the formation of a ruby red solution containing the desired AuNPs was formed. Boiling time was extended for 5 minutes and the resultant AuNP solution was cooled and stored at room temperature.

### 4.3.2 Functionalisation of AuNPs with poly-l-lysine (PLL)

Functionalisation was carried out by the drop-wise addition of 1 ml of the AuNP solution to 1 ml of a PLL (1 mg/ml in 18 M ohm water) solution with moderate stirring, producing PLL functionalized gold nanoparticles (PLL-AuNPs) in a AuNP:PLL ratio of 1:1. The final concentration of PLL in solution was calculated to be 0.5 µg/µl which was diluted to 0.025 µg/µl for experimental use. Dialysis of the PLL-AuNP solutions against 18M Ohm water at room temperature for 2 hours (MWCO: 12-14000 Daltons, Sigma-Aldrich, USA) was conducted to remove unbound PLL from the solution and to determine the binding efficiency of the AuNPs to PLL.

### 4.3.3 Inductively Coupled Plasma (ICP) analysis

Inductively coupled plasma-optical emission spectroscopy (ICP-OES) was used for the elemental detection and quantification of the Au concentration in the AuNP solution. Analysis was performed on a Perkin Elmer Optima 5300 DV Optical Emission Spectrometer. For the analysis, a standard calibration curve was set up with a range of 1-20 ppm using a 100 ppm Au standard stock solution purchased from Fluka.

### 4.3.4 Fourier Transformed Infrared Spectroscopy (FTIR) analysis

FTIR analysis of the AuNPs was conducted in a Spectrum Perkin Elmer spectrophotometer, precisely equipped with a Universal ATR sampling accessory using a diamond crystal. Spectrum Analysis Software was used to obtain the respective IR spectra.

### 4.3.5 Qualitative ninhydrin test for amino groups

The ninhydrin reaction was used as a simple qualitative test to confirm the successful functionalisation and the presence of PLL *via* its amine groups in the PLL-AuNP solution.

Briefly, a mixture of PLL-AuNP stock solution and 0.1% ninhydrin solution (1 ml each) was boiled for 3-5 minutes with a colour transition from clear to blue/purple colour, indicating a positive reaction for the presence of the amine functionalities.

### 4.3.6 Formation of mRNA:PLL-AuNP complexes

The nanocomplexes were prepared with various PLL-AuNP/PLL:F*luc*-mRNA (w/w) mass ratios by adding F*luc*-mRNA (0.25 µg/µl in RNase-free water) to increasing amounts of the PLL-AuNPs and free PLL for comparative purposes. The nanocomplexes were made up to a constant volume of 10 µl with HEPES buffered saline [HBS, (20 mM HEPES; 150 mM NaCl), pH 7.4] and incubated at room temperature for 30 minutes to facilitate the formation of PLL-AuNP/PLL:F*luc*-mRNA nanocomplexes.

### 4.3.7 UV-Visible spectrophotometry analysis

Nanoparticle formation was characterized by their optical properties using UV spectrophotometry. The absorbance (Abs) readings of the AuNPs, PLL-AuNPs and PLL-AuNP:F*luc*-mRNA [Ratio 0.7:1; Table 4.1] solutions were scanned over a wavelength range of 200 nm - 800 nm using a Biomate 3 spectrophotometer (Thermo Fischer Scientific Inc., Waltham, Massachusetts, USA) with 18 M ohm water as the blank. The spectrum generated for each solution was compared to previous literature to confirm the expected SPR absorption of AuNPs in the range of 510 nm - 550 nm (Verma *et al*., 2014). The dialysed PLL-AuNP solution was also measured by UV spectrophotometry to provide an indication of their binding efficiency using the following formula:

*unbound PLL (%) = (Abs before dialysis – Abs after dialysis/ Abs before dialysis) x 100%:*
*Total bound PLL (%) = 100% - unbound PLL %*

### 4.3.8 Transmission electron microscopy (TEM)

The ultrastructural morphology, shape, distribution and uniformity of all nanoparticle and nanocomplex solutions were assessed using transmission electron microscopy (TEM). Briefly, 1 µl of the AuNP, PLL-AuNP and PLL-AuNP:F*luc*-mRNA (0.7:1 w/w) solutions were spotted onto separate carbon coated Formvar grids and air-dried. Samples were viewed using a JEOL-JEM TEM1010 (Jeol, Tokyo, Japan) without warming above -150ºC at an

acceleration voltage of 100 kV. The iTEM Soft Imaging Systems (SIS) Megaview III fitted with a side-mounted 3-megapixel digital camera was used to capture images of each sample.

### 4.3.9 Nanoparticle Tracking Analysis (NTA)

The average individual size and concentration of the nanoparticles and nanocomplexes was determined using Nanoparticle Tracking Analysis (NTA), a laser based system providing a particle-particle analysis. NTA also determines zeta potential which was used to assess colloidal stability of the nanoparticles and nanocomplexes.

NTA and zeta potential analysis were investigated at 25°C using a Nanosight NS500 Nanoparticle characterization system equipped with NTA version 3.2 Software (Malvern Instruments Ltd., Worcestershire, UK). The AuNP, PLL-AuNP (1/500 dilution) and PLL-AuNP:F*luc*-mRNA (1/100 dilution) solutions were prepared and examined in compliance with NTA system requirements.

### 4.3.10 Gel retardation assay

The minimum concentration and optimal ratio of PLL-AuNPs and PLL required to completely bind and complex F*luc*-mRNA (0.25 µg/µl) and was determined using the gel retardation assay or band shift assay. An agarose gel (2% w/v) fitted with an 8 well comb and containing 3 µl of ethidium bromide (10 mg/ml) was prepared. The nanocomplexes for both PLL-AuNP and PLL were prepared as in Table 4.1. Naked F*luc*-mRNA (0.25 µg/µl) was used as a control. Following the 30-minute incubation period for complex formation, 3 µl of gel loading buffer [0.25% (w/v) bromophenol blue dye and 40% sucrose] was added to all samples and 10 µl of each sample was loaded into separate wells on the agarose gel. Electrophoresis was carried out at 50 volts (V) for 30 minutes in a Mini-Sub® electrophoresis tank (Bio-Rad Laboratories, Richmond, USA) containing 1x TPE electrophoresis buffer (0.36 M Tris-HCl; 0.3 M $NaH_2PO_4$; 0.1 M EDTA, pH 7.5).

Thereafter, the gels were viewed under UV transillumination in a Vacutec Syngene G:Box gel documentation system and images captured at an exposure time of 1-2 seconds using the Syngene Gene-Snap programme (Syngene, Cambridge, UK).

**Table 4.1.** Nanocomplex preparations for gel retardation assay.

| Composition of samples | Sample number 1 | 2 | 3 | 4 | 5 | 6 | 7 | 8 |
|---|---|---|---|---|---|---|---|---|
| Ratio of F*luc*-mRNA to PLL-AuNP/PLL | 1:0 | 1:0.1 | 1:0.2 | 1:0.3 | 1:0.4 | 1:0.5 | 1:0.6 | 1:0.7 |
| PLL-AuNP/PLL (µg) | 0 | 0.025 | 0.05 | 0.075 | 0.1 | 0.125 | 0.15 | 0.175 |
| F*luc*-mRNA (µg/µl) | 0.25 | 0.25 | 0.25 | 0.25 | 0.25 | 0.25 | 0.25 | 0.25 |

### 4.3.11 Dye displacement/Intercalation assays

Fluorescence based assays entailing dye displacement were also used to verify complex formation and the degree of F*luc*-mRNA condensation by PLL-AuNPs and PLL.

#### 4.3.11.1 Ethidium bromide dye displacement

Fluorescence quenching due to displacement of ethidium bromide (EtBr) was measured at an excitation wavelength of 520 nm and emission wavelength of 600 nm using the Glomax® Multi-detection system (Promega Systems, Sunnyvale, USA). Approximately 100 µl of HBS and 2 µl of EtBr (100 µg/ml) were added to two separate wells on a 96 well FluorTrac flat-bottom black microplate and mixed thoroughly. Fluorescence was measured and taken as the 0% baseline relative fluorescence. The fluorescence measurement after addition of 1 µl of F*luc*-mRNA (0.25 µg/µl) to each well was taken as 100% relative fluorescence. Thereafter, 1 µl aliquots of the PLL-AuNP solution (0.025 µg/µl) and the PLL solution (0.025 µg/µl) were added and fluorescence measurements recorded after each addition until a point of inflection in fluorescence was attained. Fluorescence measurements were calculated as relative fluorescence (Fr) using the equation: $Fr\ (\%) = (F_i - F_0)/ (F_{max} - F_0) \times 100\%$, where $F_0$ is the fluorescence intensity of EtBr/HBS mixtures, $F_i$ is the fluorescence intensity at each concentration of PLL-AuNP or PLL and $F_{max}$ is the fluorescence intensity of the EtBr/F*luc*-mRNA mixture. The relative fluorescence was then plotted against the mass (µg) of PLL-AuNP or PLL.

#### 4.3.11.2 SYBR Green dye displacement

The SYBR Green RNA II gel stain (10 000× concentrated in DMSO) was additionally utilised for displacement studies since this dye is more sensitive and selective for RNA molecules than EtBr. This assay was performed as described in 4.3.11.1 above by using the SYBR Green dye and measuring fluorescence at an excitation and emission wavelength of 497 nm and 520 nm, respectively.

### 4.3.12 Nuclease Protection assay

The extent of protection offered by the PLL-AuNP and PLL to the F*luc*-mRNA in an environment that imitates that of an *in vivo* system was assessed using the nuclease protection assay. Based on the results obtained from the gel retardation assay, sub-optimum, optimum and supra-optimum ratios for PLL-AuNP:F*luc*-mRNA and PLL:F*luc*-mRNA complexes were selected and prepared as outlined below (Table 4.2). The final volume of the complexes was made up to 10 µl with HBS and the mixtures incubated at room temperature for 30 minutes to allow for complex formation. Thereafter, FBS was added to each complex to a final concentration of 10%. Naked F*luc*-mRNA (0.25 µg/µl) was used as a positive control and naked F*luc*-mRNA (0.25 µg/µl) containing FBS was used as a negative control. To facilitate nuclease digestion, all samples containing FBS were incubated at 37°C for 4 hours. The reaction was terminated by the addition of EDTA to a final concentration of 10 mM EDTA. Subsequently, 5% SDS was added to all samples to a final concentration of 0.5% and the samples incubated at 55°C for 20 minutes. The samples were then subjected to agarose gel electrophoresis for 30 minutes as previously described (4.3.10).

**Table 4.2.** Preparation of complexes for the nuclease protection assay.

| **Sample title** | **Positive control** | **Negative control** | **PLL-AuNP** | | | **PLL** | | |
|---|---|---|---|---|---|---|---|---|
| **Sample number** | **1** | **2** | **3** | **4** | **5** | **6** | **7** | **8** |
| **Composition of samples** | | | | | | | | |
| Ratio of mRNA to PLL-AuNP /PLL | 1:0 | 1:0 | 1:0.7 | 1:0.8 | 1:0.9 | 1:0.6 | 1:0.7 | 1:0.8 |
| PLL-AuNP/PLL (µg) | 0 | 0 | 0.15 | 0.175 | 0.2 | 0.125 | 0.15 | 0.175 |
| mRNA (µg/µl) | 0.25 | 0.25 | 0.25 | 0.25 | 0.25 | 0.25 | 0.25 | 0.25 |

## 4.4 *In Vitro* cell culture studies

### 4.4.1 Cell culture materials and reagents

Phosphate-buffered saline tablets [PBS, (140mM NaCl, 10mM phosphate buffer, 3mM KCl)], 3-[(4, 5-dimethylthiazol-2-yl)-2, 5-diphenyl tetrazolium bromide] (MTT, $M_w$: 414.3 g/mol, $C_1H_1BrNS$) and Dimethyl Sulfoxide [DMSO, $M_w$: 78.13 g/mol, $(CH_3)_2SO$] were supplied by Merck (Darmstadt, Germany). Research Grade Fetal Bovine Serum was supplied by Hyclone GE Healthcare (Utah, USA). Sterile filtered Eagle's Minimum Essential Medium (EMEM) with L-glutamine (4.5 g/ml), Penicillin/ Streptomycin/ Amphotericin B (100×) antibiotic mixture [Amphotericin B (25 mcg/ml), NaCl (8.5 mg/l) Potassium penicillin (10 000 units/ml), Streptomycin sulphate (10 000 mcg/ml)] and Trypsin-versene-EDTA mixture [versene-EDTA (200 mg/l), Trypsin (170 000 U/l)] were supplied by Lonza Bio Whittaker (Verviers, Belgium). The luciferase assay kit consisting of the luciferase cell culture lysis reagent (5×) [25 mM Tris-phosphate, (pH 7.8), 2 mM dithriothreitol, 2 mM 1,2-diaminocyclohexane-N,N,N',N'-tetra-acetic acid, 10% (v/v) glycerol, 1% (v/v) triton X-100], luciferase assay reagent (20 mM tricine, 1.1 mM Magnesium carbonate hydroxide, pentahydrate, 2.7 mM Magnesium sulphate, 0.1 mM EDTA, 33.3 mM dithriothreitol, 270 µM coenzyme), Molecular grade ethidium bromide solution (10 mg/ml) [3,8-Diamino-5-ethyl-6-phenylphenanthrinidium bromide and EtBr, ($M_w$: 394.31 g/mol, $C_{21}H_{20}BrN_3$) were purchased from Promega (Madison, Wisconsin, USA). Acridine Orange hemi (zinc chloride) salt [3,6-Bis(dimethylamino)acridine hydrochloride zinc chloride double salt], bicinchoninic acid solution [1% 2,2'-Biquinoline-4,4-dicarboxylic acid disodium salt, 0.16% Sodium tartrate, 0.4% Sodium hydroxide, 2% $Na_2CO_3.H_2O$, 0.95% NaHCO3, (pH 11.25)], Copper (II) sulfate solution [4% (w/v) prepared from copper (II) sulfate pentahydrate] and protein standard (1ml/amp, 1mg BSA/ml in 0.15 M NaCl, 0.05% $NaN_3$) were purchased from Sigma-Aldrich Chemical Co. (St. Louis, USA). All sterile tissue culture plasticware were supplied by Corning Inc., (New York, USA). Human embryonic kidney cells (HEK293) was provided by the Anti-Viral Gene Therapy Unit, Medical School, University of Witwatersrand, human epithelial colorectal adenocarcinoma cells (Caco2) was purchased from Highveld Biologicals (Pty) Ltd, Kelvin, RSA and the MCF-7 (HTB-22™) breast cancer line was purchased from the American Type Culture Collection (ATCC®), Manassas, Virginia, USA.

### 4.4.2 Cell culture maintenance

All techniques were aseptically performed with cell culture work conducted in an Airvolution Class II Biohazard cabinet. Cryogenically frozen cells were thawed in a 37°C water bath and cells then pelleted at 3000 rpm for 1 minute in an Eppendorf centrifuge (Model 5415D, New York, USA). The pelleted cells were suspended in 1 ml of fresh complete medium [EMEM, 10% (v/v) FBS and 1% (v/v) antibiotic mixture] and transferred to a cell culture flask containing 5 ml of complete medium. The cells were then incubated at 37°C in a Steri-cult HEPA class 100 $CO_2$ incubator (Thermo-Electron Co., Waltham, Massachusetts, USA) and growth was routinely monitored under a Nikon TMS inverted light microscope (Nikon Co., Tokyo, Japan). Medium was changed when necessary and cells sub-cultivated as desired upon confluency.

For sub-cultivation or trypsinisation, the spent medium was removed and cells were washed with 5 ml PBS, followed by the addition of 1 ml trypsin-versene. To monitor the action of trypsin and the effect of "rounding off", the cells were viewed under the inverted microscope. The trypsinization reaction was terminated by the addition of 2 ml complete medium to the cells which were then dislodged from the flask surface by gently tapping the flask against the palm of the hand. Prior to cell culture experiments, a cell count was conducted under the inverted microscope using a haemocytometer slide (Marienfield-Superior, Germany). The cells were then sub-divided into cell-culture flasks for routine maintenance and seeded into multi-well plates for the various cell culture assays or cryopreserved for future studies.

For cryopreservation, trypsinized cells were pelleted at 3000 rpm for 5 minutes and then suspended in 0.9 ml complete medium and 0.1 ml of DMSO cryoprotective storage medium. This suspension was then mixed and dispensed into individual cryogenic vials which were placed into a Nalgene™ "Mr Frosty" Cryo 1°C freezing container (Thermo Fischer Scientific Inc., Waltham, Massachusetts, USA), filled with isopropanol. Freezing was achieved at a rate of -1°C per minute to a temperature of -70°C in a biofreezer (Nuaire, Lasec laboratory and Scientific Equipment). Thereafter, the cryogenic vials were transferred to a cryobox and stored in a biofreezer at -80°C for short term storage or in liquid nitrogen for long term storage.

### 4.4.3 MTT cytotoxicity assay

HEK293, Caco-2 and MCF-7 cells were separately trypsinized and seeded into clear 48-well plates at a density of 7.8 x $10^4$, 9.6 x $10^4$ cells/well and 2.1 x $10^5$ cells/well, respectively. Cells were incubated at 37°C for 24 hours to facilitate attachment and growth. Thereafter, the medium was replenished with fresh complete medium and the prepared complexes (in triplicate) (Table 4.2) were added to the respective wells. A positive control (100% viability) containing cells only was set up. The cells were then incubated at 37°C for 48 hours after which the spent medium was replenished with 200 µl of fresh complete medium and 200 µl of MTT reagent (5 mg/ml in PBS) and the cells incubated at 37°C for 4 hours. Thereafter, the MTT containing medium was discarded and the resultant formazan crystals were solubilized with gentle shaking in DMSO (200 µl). Absorbance at 570 nm was then measured in a Mindray MR-96A microplate reader (Vacutec, Hamburg, Germany) against a DMSO blank. Results were calculated as cell viability (%) using the following equation:
Abs (Test)/ Abs (control) x 100 %.

### 4.4.4 Luciferase reporter gene assay

The luciferase reporter gene assay was conducted to determine the transfection efficiency of the complexes and is based on the measurement of bioluminescence as a direct correlation of luciferase activity. Cells were seeded and complexes prepared in triplicate and added as in 4.4.3. Two controls, one containing cells only and one containing naked Fl*uc*-mRNA (0.25 µg/µl) were included.

The cells were then incubated at 37°C for 48 hours, followed by removal of the spent medium and rinsing of the cells with 200 µl of PBS. Thereafter, 80 µl of 1x luciferase cell culture lysis reagent was added to the cells which were then shaken for 15 minutes at 30 rev/min on a STR6 platform shaker (Stuart Scientifc, Staffordshire, UK). The lysed cells were then harvested and the cell lysates pelleted at 12000 x g using an Eppendorf centrifuge. Approximately 20 µl of each cell free supernatant was transferred to individual wells on a 96-well FluorTrac flat-bottom white microplate to which 50 µl of the luciferase assay reagent was added. The samples were immediately mixed and luminescence read using a GloMax® Multi-detection system (Promega Biosystems, Sunnyvale, USA), operated by Instinct software, primed with luciferase assay reagent and the Photo Multiplier Tube (PMT) activated prior to measurements.

The protein content of each cell free extract was determined using the bicinchoninic acid (BCA) assay and absorbance was measured at 562 nm in a microplate reader. All luminescence readings were normalized against the protein content and expressed as relative light units per milligram protein (RLU/mg protein).

### 4.4.5 Acridine Orange/Ethidium Bromide (AO/EB) apoptosis assay

Cells were seeded, incubated and complexes added as in 4.4.3. However, complex preparation was based on the optimal ratios obtained from the MTT cytotoxicity and luciferase reporter gene assays as outlined in Table 4.3 below. The positive control used was cells not exposed to the complexes. After a 24-hour incubation at 37°C, the spent medium was removed, cells washed with 200 µl of PBS and stained with 10 µl of the AO/EB dye (0.1 µg/µl acridine orange and 0.1 µg/µl EtBR in PBS) at room temperature for 5 minutes. The stain was then removed and the cells washed with 200 µl of PBS. Apoptotic-induced morphological changes of the treated cells were compared against the control using an Olympus inverted fluorescence microscope (200× magnification) fitted with a CC12 fluorescent camera, an excitation filter of 450-490 nm, a barrier filter of 520 nm and Soft Imaging System (SIS) software (Olympus Co., Tokyo, Japan). The apoptotic index for each sample was calculated using the following equation:

Apoptotic index = number of apoptotic cells / total number of cells

Apoptosis was detected based on the selectivity of the two dyes, acridine orange which penetrates both the living and dead cells producing green fluorescence, whereas EtBr produces red fluorescence when cells have altered membranes. After visual analyses, the cells were harvested into 200 µl of PBS and transferred to individual wells on a FluorTrac flat-bottom black microplate. Fluorescence was measured at an excitation wavelength of 520 nm and emission wavelength of 600 nm in the Glomax® Multi-detection system. The fluorescence readings were averaged over three replicates (n=3) and reported as fluorescent intensity (FI).

**Table 4.3.** Composition of complexes used in the AO/EB apoptosis assay.

| Composition of samples | PLL-AuNP | PLL |
|---|---|---|
| Ratio of F*luc*-mRNA to PLL-AuNP /PLL | 1:0.9 | 1:0.8 |
| PLL-AuNP/PLL (µg) | 0.2 | 0.175 |
| F*luc*-mRNA (µg/µl) | 0.25 | 0.25 |

### 4.4.6 Statistical analysis

All data obtained was calculated as the mean ± standard deviation (±SD n=3) and plotted on graphs using Microsoft Excel 2010 (Microsoft, USA). Using the Graphpad Instat Prism 4.0.3 software, the one-way analysis of variance (ANOVA) test was conducted for multi-group comparisons of the calculated means. Thereafter, the Dunnett's *post hoc* test was carried out for the MTT cytotoxicity assay results and the Tukey-Kramer *post hoc* test was carried out for the luciferase reporter gene assay results. Statistical significance (*P*) values determined to be less than 0.05 were regarded as significant and represented on the graph as *** $p < 0.001$, ** $p < 0.01$ and * $p < 0.05$.

## 4.5 Results and Discussion

### 4.5.1 Characterization of nanoparticles and complexes

#### 4.5.1.1 Chemical analysis

ICP analysis has been proven as an efficient technique for elemental determination (Szpunar, 2005). The concentration of the synthesized AuNP was confirmed by ICP against a standard Au sample by correlation of the electron signals emitted at each wavelength (Appendix A1).

FTIR spectroscopy is a useful tool for identifying chemical bonds of inorganic and organic molecules generating an infrared absorption spectrum which serves as a "molecular fingerprint" that is characteristic to a certain molecule. FTIR spectroscopy confirmed the composition of the AuNP, PLL and PLL-AuNP solutions (Appendix A2). Citrate-capped AuNPs exhibited characteristic absorption peaks at 1635.63 $cm^{-1}$, indicating the stretching of

the C=O bond of the carboxylic carbonyl group and 3272.20 $cm^{-1}$ indicating the stretching of O-H bonds as compared to previous literature (Chen *et al*., 2013). The spectrum of PLL exhibited characteristic absorption peaks at 1637.91 $cm^{-1}$ for the amide I band which indicates the C=O stretch vibration band, 2020.63 $cm^{-1}$ indicating the C-N stretch, 2184.69 $cm^{-1}$ indicating the C-H stretch and 3269.95 $cm^{-1}$ for the amide A band indicating the N-H stretch vibration as compared to previous literature (Bathrinarayanan *et al*., 2013; Rozenberg and Shoham, 2007; Zhuang *et al*., 2015). These absorption peaks are characteristic for the random coil formation at pH 7 which was utilized in this assay.

In contrast to the AuNP FTIR spectrum, the PLL-AuNP spectrum exhibits two additional absorption peaks at 2020.63 $cm^{-1}$ and 2184.69 $cm^{-1}$, indicating the C-N and C-H stretch of PLL, respectively. In addition, the characteristic peaks of the C=O and O-H stretches of the AuNPs increased to 1636.56 $cm^{-1}$ and decreased to 3270.93 $cm^{-1}$ after functionalisation with PLL. These results indicate that the reducing ends of the citrate ions formed interactions with the amino groups of PLL, as reported in previous literature (Shen *et al*., 2012).

#### 4.5.1.2 UV-Vis optical spectrophotometry analysis

AuNPs exhibit surface plasmon resonance (SPR) which occurs when the electron cloud oscillates on the AuNP surface, resulting in electromagnetic radiation absorption at a particular energy (Philip, 2008) and enhances the absorption and scattering properties of AuNPs (Radwan and Azzazy, 2009). The ruby red colour of a AuNP solution arises from their strong SPR absorption in the visible region at 520 nm (Jain *et al*. 2006), as confirmed in this study (Figure 4.1). UV-vis spectroscopy provides valuable information such as approximation of size, concentration and aggregation level of AuNPs (Amendola and Meneghetti, 2009). Functionalisation with PLL (Figure 4.1) resulted in a red-shift of SPR absorbance to 600 nm which was also visually confirmed by the colour transition in solution from ruby red to black upon functionalisation of the AuNPs with PLL. Factors such as size, shape, surface composition and charge, solvent, temperature and aggregation of AuNPs have been reported to induce a red-shift coupled with broadening of the absorbance peak and decrease in intensity as seen in Figure 4.1 (Yeh *et al*., 2012). This occurrence of a red-shift has previously been reported for the functionalisation of AuNPs with PLL (Stobiecka and Hepel, 2011). A red-shift was also observed upon complex formation of PLL-AuNP with F*luc*-mRNA and with a SPR absorbance at 620 nm (Figure 4.2). The absorbance of the PLL-

AuNP recorded after dialysis further indicated the successful removal of unbound PLL by dialysis. The percentage of bound PLL was determined to be 31%.

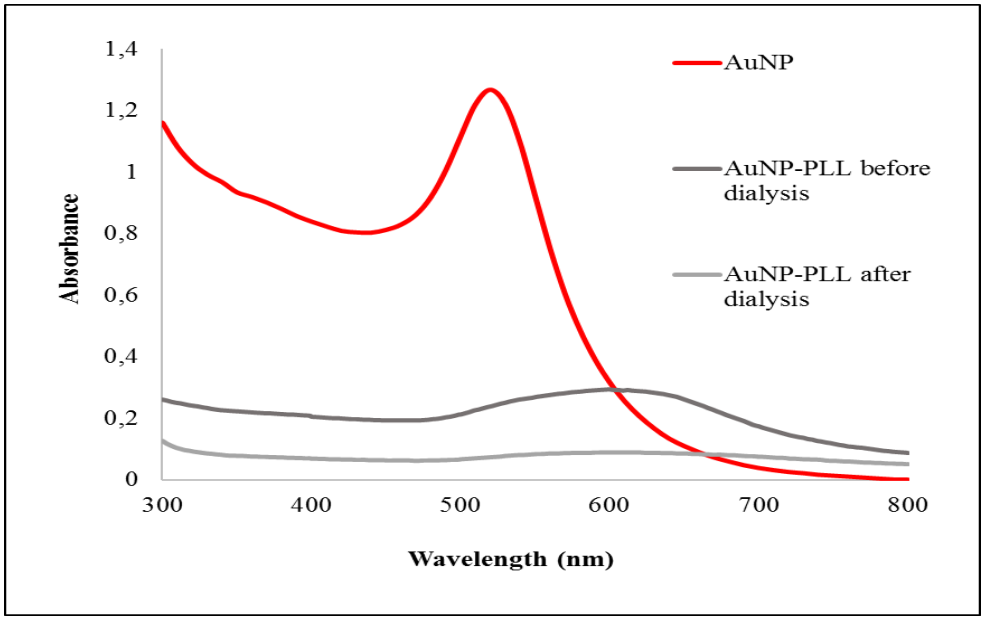


**Figure 4.1:** UV-Vis spectrum of AuNPs, PLL-AuNPs before and after dialysis indicating the shift in SPR absorbance after functionalization.

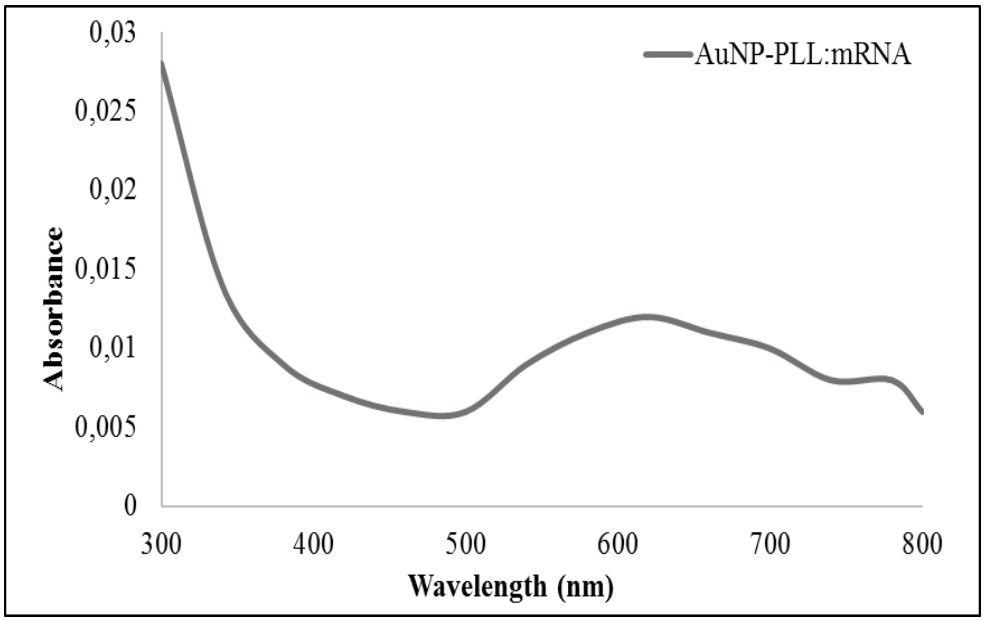


**Figure 4.2:** UV-Vis spectrum of the PLL-AuNP:F*luc*-mRNA nanocomplex indicating a red shift to 620 nm.

#### 4.5.1.3 Qualitative ninhydrin test for amine groups

The ninhydrin test was used as a simple qualitative test to confirm the presence of $–NH_2$ groups and hence the functionalisation of AuNPs with PLL. The ninhydrin reagent reacts with a variety of primary and secondary amines present in the structure of PLL. Heating results in the hydrolysis of the amines to produce a blue-purple colour complex commonly known as Ruhemann's purple (Wu *et al*., 2005) as evidenced in this study (Figure 4.3).

**Figure 4.3:** The positive dark purple PLL-AuNP reaction produced in the ninhydrin test.

#### 4.5.1.4 Transmission electron microscopy (TEM)

TEM involves the use of passing a beam of electrons through a nanoparticle sample to produce a high-resolution image providing information such as size, shape, self-organisation and core to core spacing of the AuNPs in solution (Zhou *et al*., 2009). Both AuNPs and PLL-AuNPs (Figure 4.4 A-B) displayed as homogenous, spherical and smooth particles with monodisperse distribution with AuNPs appearing more dense, similar to previously reported studies (Stobiecka and Hepel, 2011; Verma *et al*., 2014).

The excellent dispersion of the AuNPs are a result of electrostatic stabilization induced by the sodium citrate capping, causing the AuNP atoms to repel each other (Polte, 2015). PLL functionalisation (Figure 4.4 B) resulted in agglomerate and chain-like structures due to electrostatic interactions between the citrate-capped AuNPs and PLL. The PLL-AuNP:F*luc*-mRNA nanocomplexes (Figure 4.4 C) are assumed "flower-like" branched structures due to the condensation of F*luc*-mRNA. This occurrence of "flower-like" structures has previously been reported for AuNP–protein conjugation (Das *et al*., 2012).

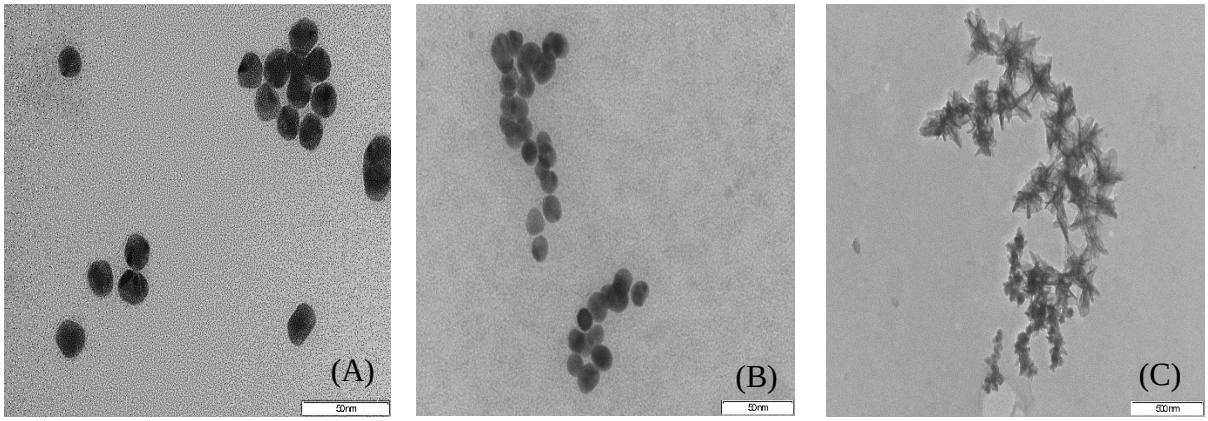


**Figure 4.4:** Transmission electron micrographs of (A) AuNPs, (B) PLL-AuNPs at 50 000 ×, and (C) PLL-AuNP:F*luc*-mRNA at a magnification of 500 000 ×. Bar = 50 nm.

#### 4.5.1.5 Nanoparticle tracking analysis (NTA)

The size of nanoparticles plays a vital role in cellular interaction. Nanoparticles up to 200 nm are suitable for cellular uptake by receptor-mediated endocytosis. The use of NTA served to determine the size, zeta potential, colloidal stability and distribution of the synthesized AuNPs. NTA is a pioneering technology based on a particle-by-particle methodology for determining the average size, size distribution and concentration of nanoparticles in a population (Carr and Wright, 2008).

The NTA software identifies and tracks individual nanoparticles moving under Brownian motion, allowing for the diffusion coefficient to be calculated. Particle size is related to the movement of the nanoparticle and calculated according to the Stokes-Einstein equation (Filipe *et al*., 2010).

Table 4.4 and Appendix B show the average sizes, zeta potentials and concentrations for the AuNP, PLL-AuNP and the nanocomplex. The average size of the AuNPs was 65.9 +/- 9.8 nm which increases to 90.4 +/- 15.0 nm for the PLL-AuNP, possibly due to the functionalization and the formation of agglomerates and chain-like structures as seen under TEM. Upon F*luc*-mRNA binding, the size of PLL-AuNP:F*luc*-mRNA nanocomplex decreased to 89.4 nm due to condensation of the mRNA, correlating to the "flower-like" condensed structures seen under TEM. All formulations displayed sizes below 100 nm, making them suitable for gene delivery purposes.

Apart from size, the surface charge of nanocomplexes influence their colloidal stability, intracellular uptake, cytotoxicity and release of the therapeutic cargo (Pedrosa *et al*., 2015).

Furthermore, the colloidal stability of AuNPs is an important parameter in preventing aggregation when introduced into an *in vivo* system.

**Table 4.4.** Size, zeta potential and concentration of the nanoparticle solutions obtained from nanoparticle tracking and zeta potential analysis.

| Sample | Size (nm) (mean±SD) | Zeta Potential (mV) (mean±SD) | Concentration (particles/ml) (mean±SD) |
|---|---|---|---|
| AuNP | 65.9 +/- 9.8 | -7.3 +/- 1.6 | 2.55e+008 +/- 1.69e+006 |
| PLL-AuNP | 90.4 +/- 15.0 | -5.3 +/- 0.2 | 2.94e+008 +/- 5.93e+006 |
| PLL-AuNP:F*luc*-mRNA | 89.4 +/- 0.0 | -97.1 +/- 102.4 | 7.25e+007 +/- 6.86e+007 |

Zeta potential is the sum of potential differences between the surface and the slipping plane of the stationary fluid layer of a nanoparticle (Arjmandi *et al*., 2012). Zeta potential measurements detect the magnitude of repulsion between particles and their tendency to aggregate which can be used to confirm stabilization by functional ligands (De Long *et al*., 2010).

In general, an excellent zeta potential (greater than 25 mV or -25 mV) indicates the formation of stable nanoparticles and as the zeta potential approaches the point of zero the attraction between nanoparticles surpasses the repulsive forces between the nanoparticles causing aggregation (Ivanov, 2011). Thus, zeta potential analysis is important for determining nanoparticle surface chemistry and long-term stability.

From the zeta potential analysis (Table 4.4), it was observed that the AuNPs (-7.3 +/- 1.6 mV) and PLL-AuNPs (-5.3 +/- 0.2 mV) did not have excellent colloidal stability. This can be correlated to the formation of agglomerates and chain-like structures as seen under TEM. PLL is a positively-charged polymer and therefore should confer a positive charge to the AuNPs upon functionalisation. The PLL-AuNP:F*luc*-mRNA nanocomplexes produced a zeta ($\zeta$) potential increase to -97.1 +/- 102.4 mV, indicative of excellent colloidal stability which could be attributed to the high condensation of the mRNA. Overall, the functionalized AuNPs and their nanocomplexes were proven to be relatively stable and suitable for gene delivery studies.

### 4.5.2 Assessment of PLL and PLL-AuNP binding to F*luc*-mRNA

#### 4.5.2.5 Gel retardation assay

The gel retardation or band shift assay was conducted to determine the ability of PLL-AuNPs and PLL to bind and complex the mRNA. This assay determined the point of saturation beyond which further loading of the PLL-AuNPs or PLL caused no further migration of the mRNA into the gel due to complete binding of mRNA by the nanoparticle, causing it to remain in the well as an electroneutral complex. Hence, partial binding of the F*luc*-mRNA will result in free migration of the negatively-charged molecule from the cathode to the anode. Figure 4.5 A-B shows the binding of the F*luc*-mRNA to varying concentrations of PLL-AuNP and PLL, respectively. F*luc*-mRNA (0.25 µg/µl) served as a control. The endpoint or optimal ratio for each assessment is indicated by a white arrow wherein electroneutrality was achieved.

It was observed that the amount of PLL-AuNP and PLL complexes retained in the wells increased with increasing PLL-AuNP and PLL concentrations, respectively. Electroneutrality and optimal binding ratios were achieved for PLL-AuNP:Fluc-mRNA (Figure 4.5 A) at a ratio of 0.7:1 (w/w) (lane 8) and for PLL:F*luc*-mRNA (Figure 4.5 B) at a ratio of 0.6:1 (w/w) (lane 7). The differences between the binding ratios can be attributed to the greater availability of positive charges of PLL particles to effectively bind the F*luc*-mRNA than PLL-AuNPs as many of the latter's positive-charges are involved in other interactions. Both PLL-AuNP and PLL have shown to efficiently bind F*luc*-mRNA low concentrations.

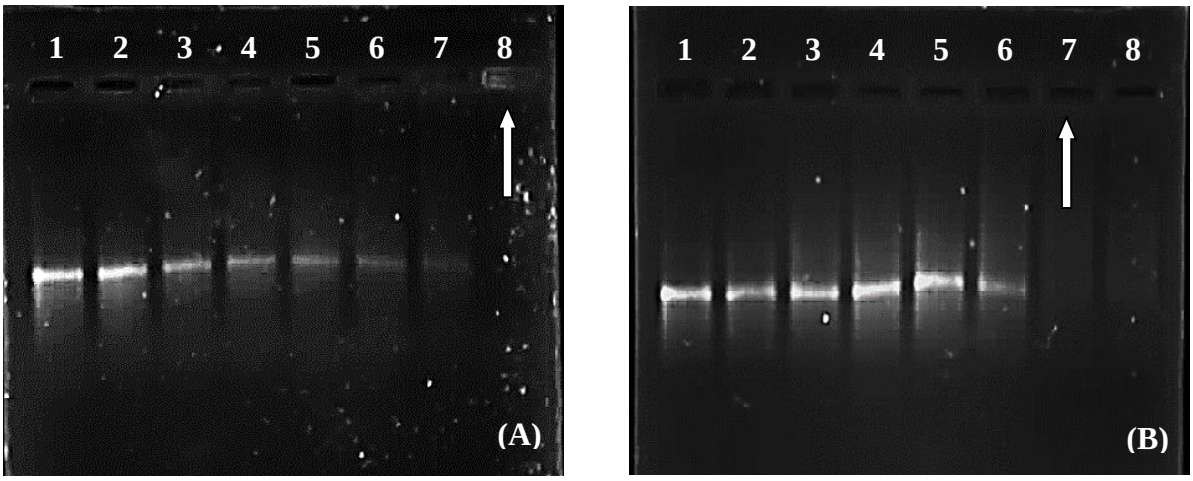


**Figure 4.5**: Gel retardation study of (A) PLL-AuNP:F*luc*-mRNA and (B) PLL:F*luc*-mRNA complexes. Incubation mixtures (10 µl) in 20 mM HEPES, 150 mM NaCl (pH 7.5) contained varying amounts of (A) PLL-AuNP and (B) PLL in lanes 1–8 (0, 0.025, 0.05, 0.075, 0.1, 0.125, 0.15, 0.175 µg) and F*luc*-mRNA (0.25 µg).

#### 4.3.2.2 Dye displacement/Intercalation assays

Fluorescent intercalation displacement assays have been widely used as diagnostic tools to confirm the interactions and binding affinities of small ligands to therapeutic molecules (Sau *et al*., 2012). These intercalation assays are based on the displacement of mRNA-intercalated dye by PLL-AuNPs and PLL used in this study, resulting in a quenching of fluorescence. As the dye is displaced, a point of inflection in fluorescence is reached, correlating to the optimum concentration of the PLL-AuNPs or PLL required to fully bind the mRNA. From Figures 4.6 and 4.7, it can be observed that both the PLL-AuNP and PLL solutions were able to successfully displace the dye from the F*luc*-mRNA. As with the gel retardation study, it was observed that a lower concentration of PLL was required to fully bind the F*luc*-mRNA in comparison to PLL-AuNPs.

In both methods (Figure 4.6 and 4.7), fluorescence decreased in a step-wise manner as a result of the mRNA-intercalated dye being displaced upon the binding of the nanoparticles to mRNA. In the EtBr assay, the concentration required to fully condense the F*luc*-mRNA was 0.325 µg for PLL-AuNP and 0.275 µg for PLL which were higher than those obtained from the gel retardation assay. This observation may be due to the intercalating mechanism of EtBr being more specific for interaction with the base pairs of the hydrophobic interior of double-stranded DNA through Van der Waal's forces (Banerjee *et al*., 2014). In contrast, mRNA folds back on itself to produce local base pairing for intercalation with EtBr, hence the variation in results. This technique has previously been reported successful for the study of AuNP-DNA conjugates (Jang *et al*., 2009). However, it has not been reported for the evaluation of AuNP-mRNA conjugates.

Hence, the additional use of the SYBR green assay has a higher affinity for RNA and has a greater sensitivity limit (Lonza Rockland Inc., 2007). In this assay (Figure 4.7), the concentration required to fully bind the F*luc*-mRNA was 0.125 µg for PLL-AuNP and 0.175 µg for PLL. These values correlated with those obtained from the gel retardation assay, thus confirming the sensitivity of this technique.

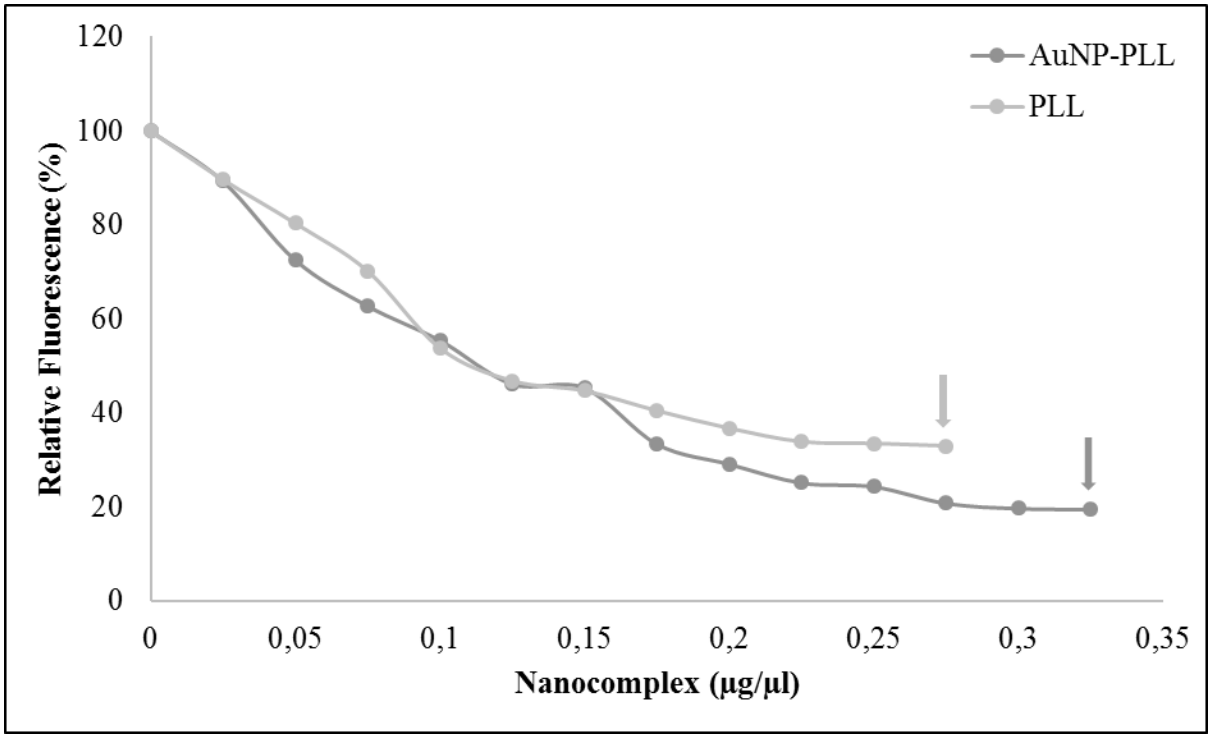


**Figure 4.6:** Comparison of the relative fluorescence between the PLL-AuNP and PLL complexes using the EtBr intercalation assay. Arrows indicate the point of inflection.

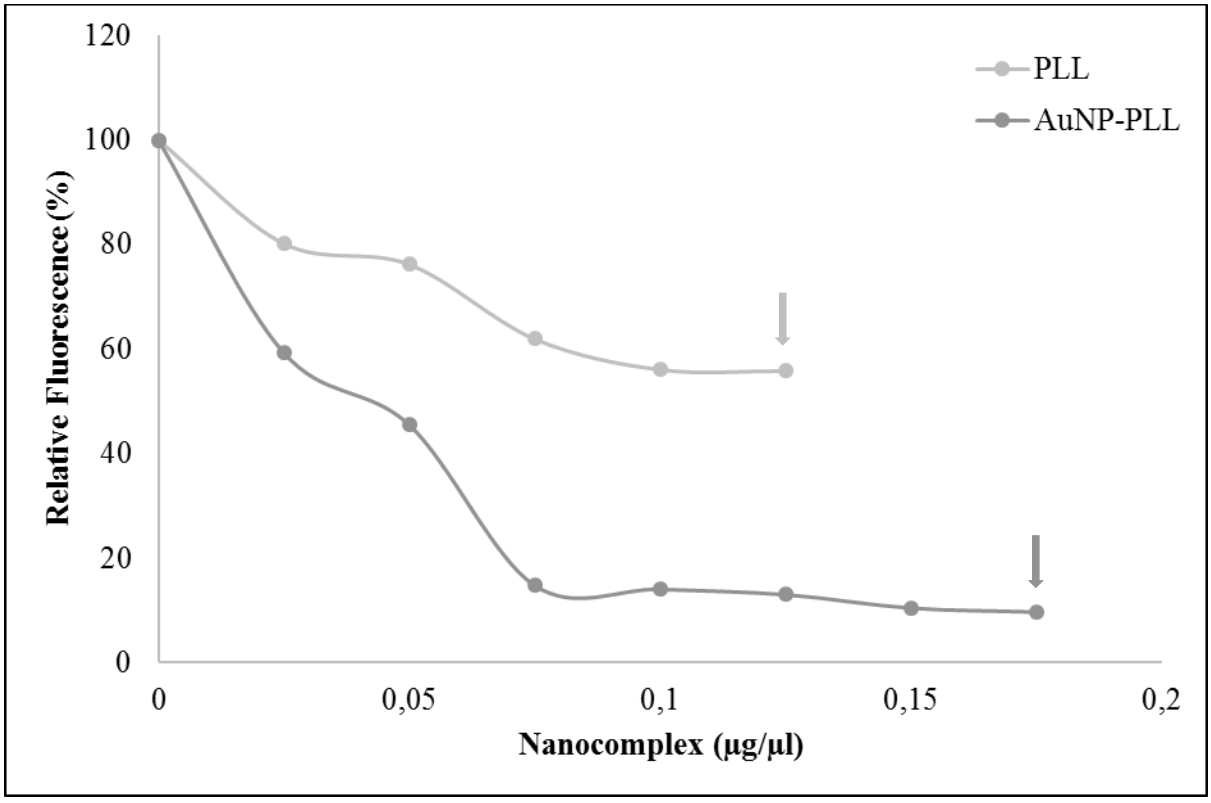


**Figure 4.7:** Comparison of the relative fluorescence between PLL-AuNP and PLL complexes using the SYBR Green intercalation assay. Arrows indicate the point of inflection.

### 4.5.3 Nuclease protection assay

The presence of serum nucleases in culture in *vitro* and biological fluids *in vivo* poses a challenge in safe gene delivery applications due to risk of nucleic acid degradation. Hence, the choice of the delivery vehicle is crucial. Molecular RNA are reported to have short half-lives and are less stable than RNA conjugated to AuNPs due to direct degradation by RNases, reducing their efficacy (Giljohann *et al*., 2009).

The sub-optimum, optimum and supra-optimum binding ratios from the gel retardation studies were used. Naked undigested F*luc*-mRNA, the positive control (C1, Figure 4.8), presented a single distinctive bright band whereas FBS-digested F*luc*-mRNA, the negative control (C2, Figure 4.8), showed complete digestion. The addition of SDS to the complexes after FBS treatment served to facilitate the release of the F*luc*-mRNA from the nanocomplexes. Digested F*luc*-mRNA will appear as a smear on the gel similar to the negative control (C2) whereas undigested F*luc*-mRNA will appear as a distinct band as exhibited by the positive control (C1).

Lane 1 (Figure 4.8) showed minimal digestion of the mRNA, indicating that the amount of PLL-AuNP at the sub-optimum ratio provided some but not total protection of the F*luc*-mRNA. However, at the supra-optimum and optimum ratios (lane 2 and 3) no digestion was observed, indicating complete protection of F*luc*-mRNA by PLL-AuNP at the weight ratios of 1:08 and 1:0.9. PLL also offered complete protection to F*luc*-mRNA at all ratios as no digestion of F*luc*-mRNA was observed (Lanes 4-6, Figure 4.8) which could be due to the more compact binding offered by the PLL as a result of its density of amine groups that are adumbrated upon functionalization with the AuNPs.

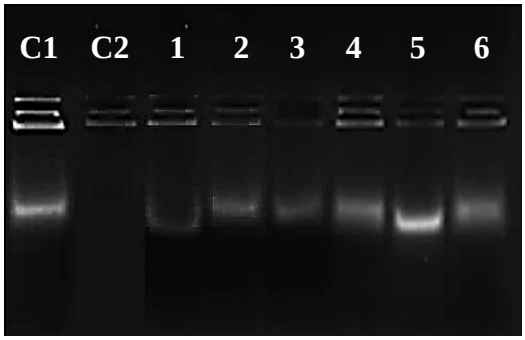


**Figure 4.8:** Nuclease digestion of PLL-AuNP:F*luc*-mRNA and PLL:F*luc*-mRNA complexes. Incubation mixtures (10 µl) in 20 mM HEPES, 150 mM NaCl (pH 7.5) contained a constant amount of F*luc*-mRNA (0.25 µg) in all lanes and varying amounts of PLL-AuNP, lanes 1-3 (0.15, 0.175, 0.2 µg) and PLL, lanes 4-6 (0.125, 0.15, 0.175µg). C1 contained undigested F*luc*-mRNA and C2 contained FBS-digested F*luc*-mRNA.

### 4.5.4 *In Vitro* cell culture studies

#### 4.5.4.1 Cell culture maintenance

All cell lines (Figure 4.9 A-C) were successfully propagated in complete medium (EMEM, 10% FBS and 1% antibiotic) with HEK293 cells (Figure 4.9 A) showing an epithelial fibroblast morphology, Caco-2 cells (Figure 4.9 B) a polarized epithelial morphology and MCF-7 cells exhibited a dome-like morphology (Figure 4.9 C).

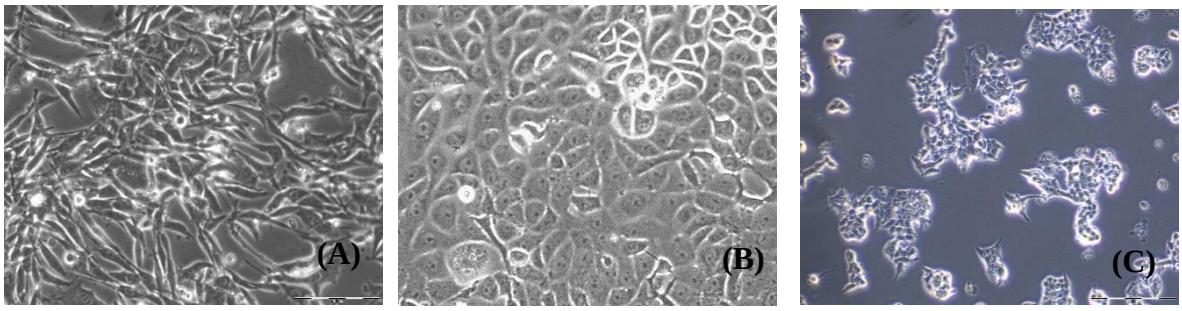


**Figure 4.9:** Images of cell lines (A) HEK293, (B) Caco-2 and (C) MCF-7 using phase contrast microscopy at a 10 000× magnification.

#### 4.5.4.2 MTT cytotoxicity assay

Understanding the extent and mechanisms of cytotoxicity associated with exposure to cationic polymer-based nanoparticles is imperative as their toxicological profiles *in vitro* can be used as an indication for future *in vivo* applications.

The MTT is a simple colorimetric assay which is based on the mitochondrial enzymatic activity in cells. Metabolically active cells possess mitochondrial succinate dehydrogenases that reduce MTT, a yellow-brown solution, to a water-insoluble blue-purple formazan product which can be solubilized and absorbance measured as an indicator of the cytotoxicity.

In the HEK293 cell line (Figure 4.10 A), a general trend was seen wherein the cell viability decreased as the ratio of PLL and PLL-AuNP to F*luc*-mRNA increased. Maximum cell viability of 116% and 82% was observed at the sub-optimal ratio (ratio 1) for both PLL and PLL-AuNP, respectively. For the Caco-2 cell line (Figure 4.10 B), the cell viability increased as the ratio of PLL and PLL-AuNP to F*luc*-mRNA increased. Maximum cell viability of 78% and 100% was observed at the supra-optimal ratios (ratio 3) for PLL and PLL-AuNP, respectively. In the MCF-7 cell line (Figure 4.10 C), the cell viability decreased as the ratio

of PLL to F*luc*-mRNA increased but increased as the PLL-AuNP to F*luc*-mRNA ratio increased. Maximum cell viability of 62% and 99% was observed at the sub-optimal ratio (ratio 1) for PLL and the supra-optimal ratio for PLL-AuNPs (ratio 3), respectively.

Overall, PLL nanocomplexes were less tolerated by all cell lines compared to the PLL-AuNP nanocomplexes. This is more evident in the MCF-7 cells with a maximum cell death of 50% being recorded at the supra-optimal ratio.

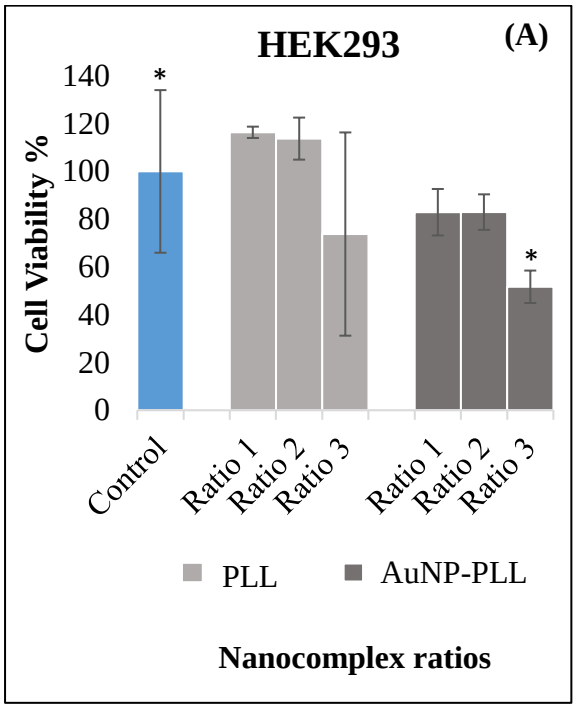


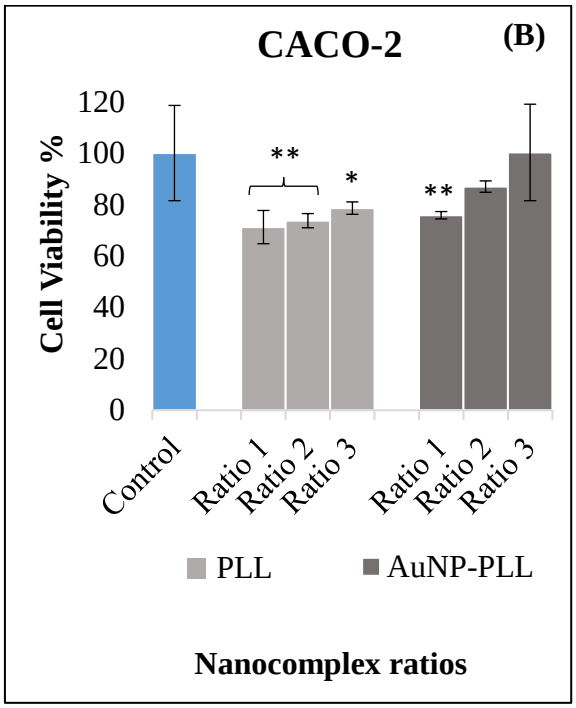

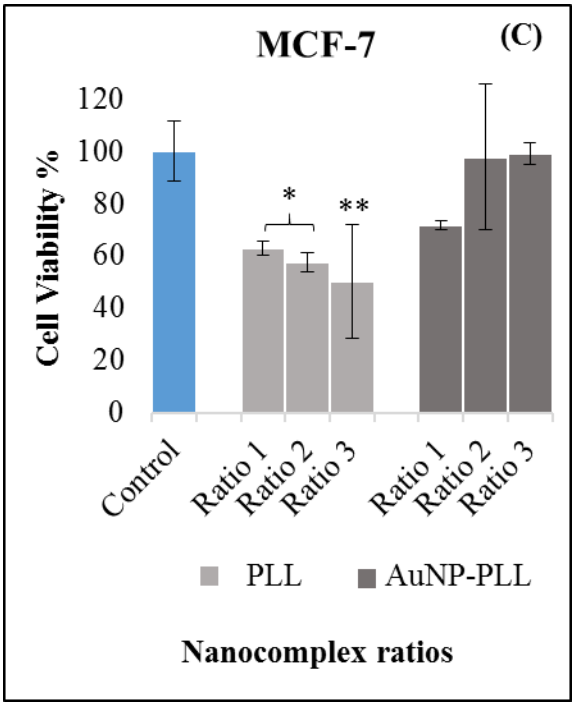


**Figure 4.10:** MTT cytotoxicity assay of complexes in cell lines: (A) HEK293, (B) Caco-2 and (C) MCF-7. Data represented as means ± SD (n=3), * $p<0.05$, **$p<0.01$ and **$p<0.001$ were considered statistically significant as determined by the Dunnet test.

PLL exhibited growth stimulation effects at lower ratios in the HEK293 cell line and at higher concentrations in the Caco-2 cell line when compared to their respective controls. This may attributed to the normal cellular function of PLL in the stimulation of immunoglobulin production such as interferon-β. Increased cellular proliferation in astrocytes was also observed (Stobiecka and Hepel, 2011). Other studies have reported the excessive cytoplasmic accumulation of PLL in cells leading to the disruption of homeostasis mechanisms which tightly regulate intracellular polyamine concentration, thus inducing mitochondrial permeabilization (Stefanneli *et al*., 2000) which may have played a role on the cytotoxic effects seen in the MCF-7 cell line. The toxicity of AuNPs are influenced by several factors such as their synthesis method, size, hydrodynamic diameter, shape, surface composition, charge, density, hydrophobicity, dose, administration route and incubation time. It has also been reported that larger nanoparticles have a high surface area to volume ratio which provides platforms for an increase in surface particle activity (Van Doren *et al*., 2011). The size of the PLL-AuNP:F*luc*-mRNA complex was 89.4 nm, indicating their susceptibility to various surface particle activities with the cells contributing to the toxic effects seen in the HEK293 and Caco-2 cell lines at higher concentrations.

In general, the cell viability results show that treatment with these complexes are concentration or dose dependent and cell type specific. Overall, both nanocomplexes performed similarly in all cell lines with cell viability over 50% at all ratios.

#### 4.5.4.3 Luciferase reporter gene assay

PLL-AuNPs have been proven as highly efficacious for the delivery of plasmid DNA and surpasses most commercial vectors (Ghosh *et al*., 2008). However, their efficacy for the delivery of mRNA has not yet been evaluated. This study hopes to answer some of these questions. The luciferase reporter gene assay is based upon the bioluminescent measurement of firefly luciferase (*Photinus pyralis*) activity which catalyses the conversion of the substrate luciferin to an enzyme-bound intermediate luciferyl-AMP *via* an ATP-dependent reaction (Fan and Wood, 2007).

This intermediate then undergoes an oxidative decarboxylation reaction to generate the final product oxyluciferin in a high-energy state producing a yellow-green light or bioluminescence. Only successfully transfected cells will emit luminescence. The intensity of light emission is directly proportional to the level of luciferase activity and is measured as relative light units (RLU) at 560 nm. The RLU measurements are normalized against the soluble protein content in the cell lysates determined using the BCA assay.

In all three cell lines, the best transgene activity was observed at the sub-optimal ratios (ratio 1) for both the PLL and PLL-AuNP:mRNA complexes ( Figures 4.11 A-C). Maximum recorded luciferase activity for the PLL and PLL-AuNP:mRNA complexes were $1.07 \times 10^5$ and $1.5 \times 10^5$ RLU/mg protein in the HEK293 cell line (Figure 4.11 A), $4.7 \times 10^5$ and $6.4 \times 10^5$ RLU/mg protein in the Caco-2 cell line (Figure 4.11 B) and $5.3 \times 10^3$ and $6.9 \times 10^3$ RLU/mg protein in the MCF-7 cell line (Figure 4.11 C).

In all cell lines, a general trend was seen wherein the luciferase activity decreased as the ratio of PLL and PLL-AuNP to F*luc*-mRNA increased, indicating that transfection efficiency was concentration dependent. This observation may be related to the high compaction and restricted release of F*luc*-mRNA which is due to the high binding efficiency of PLL and PLL-AuNP, as established by the band shift and dye displacement assays.

Overall, PLL-AuNP:F*luc*-mRNA complexes displayed significantly higher trangene activity than PLL:F*luc*-mRNA complexes, indicating that the transfection efficiency of PLL was

improved due to its conjugation with the AuNPs, as previously reported (Joshi *et al*., 2004). The transfection and binding efficiency of PLL to nucleic acids are linearly correlated to the length and molecular weight of PLL (Segura and Shea, 2001).

Functionalised AuNPs have been reported to be taken up voluntarily by cells by passive mechanisms with their intracellular uptake and distribution being dependent on characteristics such as zeta potential, surface modification, shape and size (Huefner *et al*., 2014). For positively charged amine functionalised AuNPs the mechanism of internalization involves their interaction with the negatively charged cell membrane (Sandhu *et al*., 2002). In this study, all nanocomplexes were less than 100 nm in size, allowing for easier uptake by the cells. Furthermore, the higher transgene expression obtained for the PLL-AuNP:F*luc*-mRNA compared to the PLL-AuNP complexes could be related to the zeta potential differences with the latter having a negative zeta potential and was also less stable. The PLL-AuNP:F*luc*-mRNA nanocomplexes had a high positive zeta potential, allowing for increased interaction with the negatively charged cellular membrane and better stability overall.

It has been proposed that the formation of a protein corona on the AuNP surface may be a possible mechanism for the recognition and subsequent internalisation of the AuNPs into the cells by receptor-mediated endocytosis (Giljohann *et al*., 2007). Experimental procedures and parameters such as concentration and exposure time also influence their cellular uptake and distribution (Mironava *et al*., 2010).

From the results, it can be concluded that transfection activity, similar to the cytotoxicity, was cell specific with Caco-2 cells producing the highest gene expression for both nanocomplexes. Interestingly, Caco-2 cells also best tolerated these nanocomplexes which correlated into a better transfection efficiency. The synthesized PLL-AuNPs properties such as excellent colloidal stability, ability to protect the F*luc*-mRNA and inherent low cytotoxicity all contributed in enhancing the transfection efficiency of the complex.

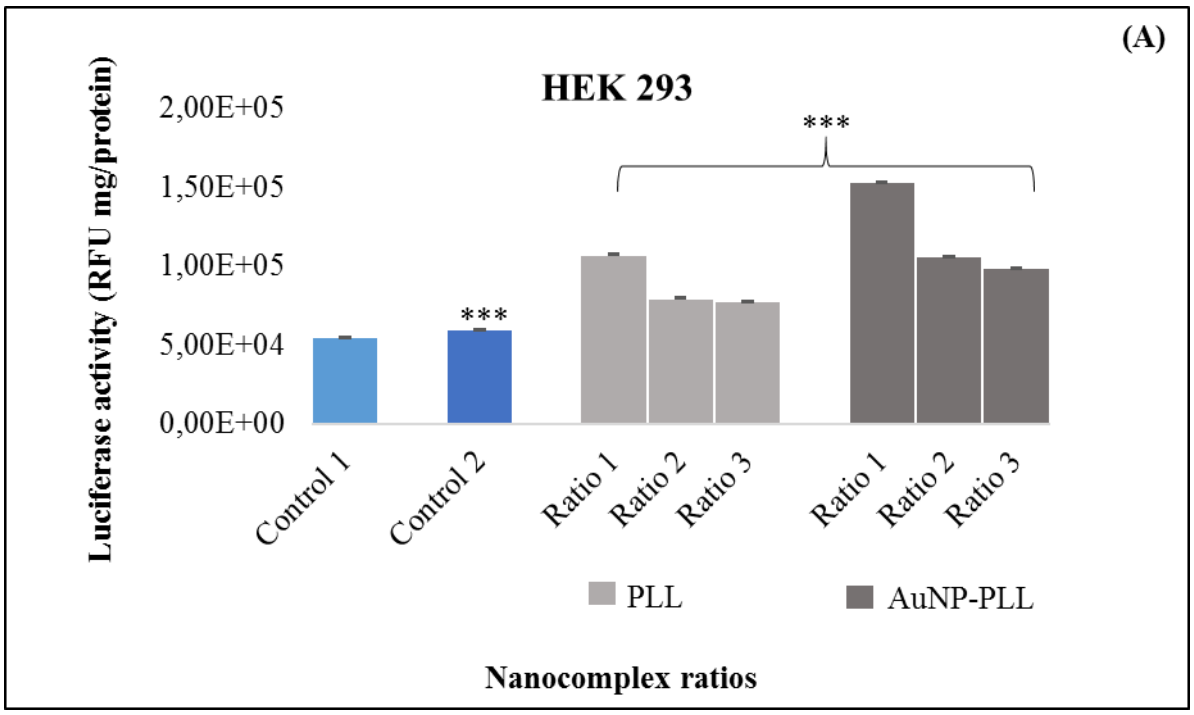
(A)
HEK 293
Luciferase activity (RFU mg/protein)
2,00E+05
1,50E+05
1,00E+05
5,00E+04
0,00E+00
***
***
Control 1
Control 2
Ratio 1
Ratio 2
Ratio 3
Ratio 1
Ratio 2
Ratio 3
PLL
AuNP-PLL
Nanocomplex ratios

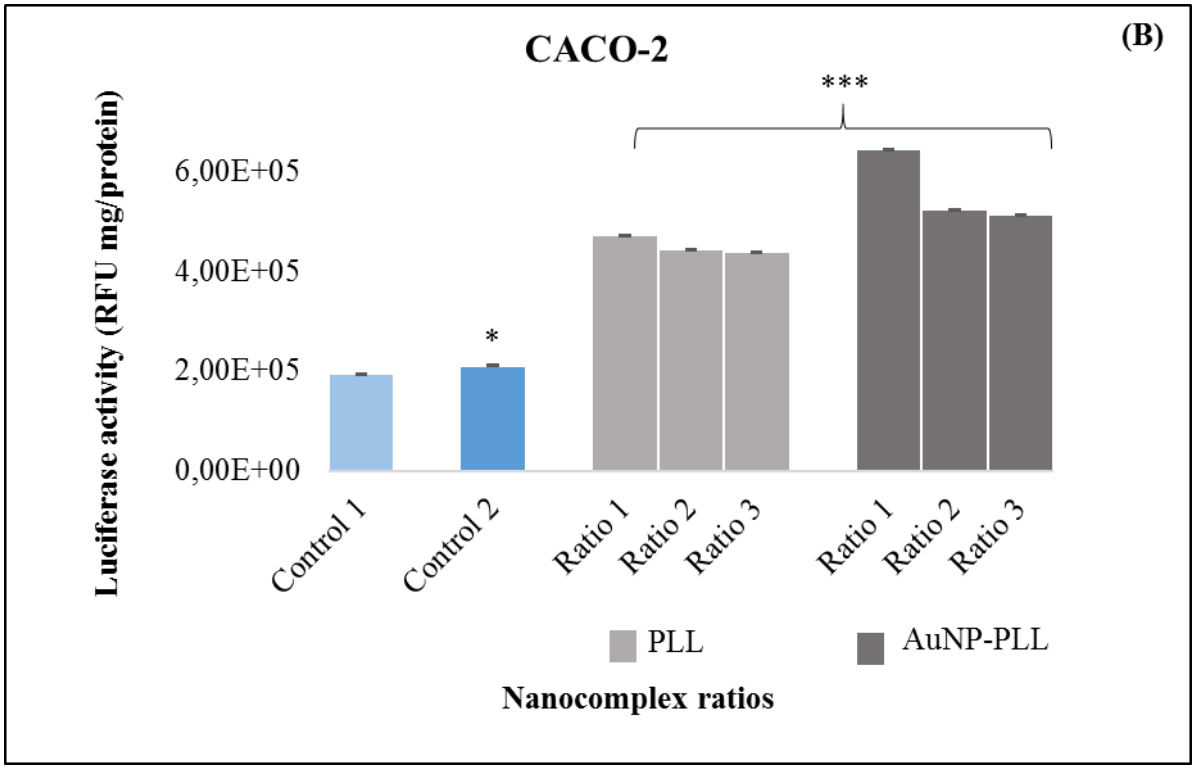
(B)
CACO-2
Luciferase activity (RFU mg/protein)
6,00E+05
4,00E+05
2,00E+05
0,00E+00
***
*
Control 1
Control 2
Ratio 1
Ratio 2
Ratio 3
Ratio 1
Ratio 2
Ratio 3
PLL
AuNP-PLL
Nanocomplex ratios

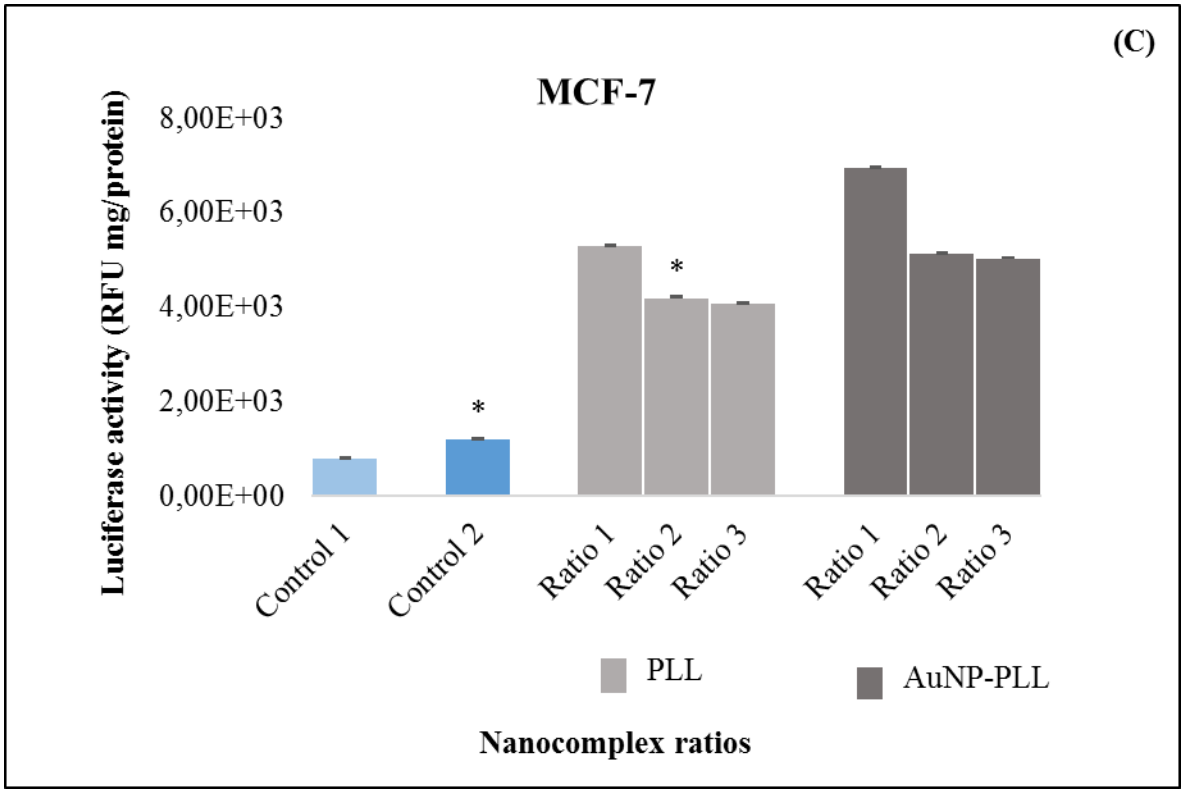


**Figure 4.11:** Luciferase gene expression activity of nanocomplexes in RLU/mg protein in cell lines: (A) HEK293, (B) Caco-2 and (C) MCF-7. Data represented as mean ± SD (n=3), * $p<0.05$, ** $p<0.01$ and *** $p<0.001$ were considered statistically significant as determined by the Tukey-Kramer test.

#### 4.5.4.4 Acridine Orange/Ethidium Bromide (AO/EB) apoptosis assay

There is an array of detrimental effects which can be induced upon exposure to nanoparticles to cells which include mitochondrial damage, genotoxicity, oxidative stress, radical production, glutathione depletion, lipid peroxidation, protein oxidation and apoptosis (Ramakrishna and Rao, 2011). Apoptosis is a programmed cell death that is genetically regulated to control the development of tissues by eliminating physiologically defective, damaged and abnormal cells (Liu *et al.*, 2015) and is, hence, an effective defence mechanism of the body in eliminating tumour cells. The balance between cell proliferation and apoptosis is maintained in normal cells. However, cancer cells have been known to inhibit these pathways, thus ensuring their uncontrolled proliferation (Lodish *et al.*, 2000). Apoptosis induces a number of morphological changes which are used for characterization purposes. These include cell shrinkage, condensed chromatin, formation of cytoplasmic protrusions and fragmentation of DNA (Abou-Ghali and Stiban, 2015). The cell membrane protrusions eventually separate from the cells to form apoptotic bodies. In contrast, necrosis results from

physical and chemical injury wherein cells die slowly by the progression of swelling and rupturing (Elmore, 2007).

The AO/EB dual staining method is a useful technique to distinguish and characterise apoptotic cells based on morphology, colour of fluorescence emission and organization of chromatin condensation (Ciniglia *et al*., 2010). Acridine orange acts by permeating living cells and causing them to fluoresce green while cells which have lost their cytoplasmic membrane integrity selectively take up the EtBr stain as well as initiating the nucleus to fluoresce red (Liu *et al*., 2015). The nucleus of live cells will fluoresce green, apoptotic cells which has fragmented chromatin fluoresce red and necrotic cells orange (Ribble *et al*., 2005). All control cells fluoresced green, indicating the absence of apoptosis and necrosis (Figure 4.12). The number of apoptotic cells after treatment with the PLL-AuNP:F*luc*-mRNA complex was far greater than that of the PLL:F*luc*-mRNAcomplex, indicating the ability of the PLL-AuNP:F*luc*-mRNA to induce apoptosis. The distinct morphological characteristics of red apoptotic cells (‘A”) [which included cellular shrinking and blebbing (Figure 4.12), and orange necrotic cells (‘N’) which showed swelling (Figure 4.12)] were seen.

The apoptotic index (Table 4.5) for the PLL:F*luc*-mRNA complex was lower than that for the PLL-AuNP:F*luc*-mRNA complexes in all cell lines correlating to the fluorescent intensity (Figure 4.13) measurements. PLL and its complexes has been proven to cause stress-induced apoptosis by mitochondrial permeabilization which has been proved by the detection of the activation of pro-apoptotic Bax channels forming protein cytochrome C release, activation of executioner caspases and alterations of membrane potential in the mitochondria of endothelial and hepatocyte-like cells (Symonds *et al*., 2005). AuNPs, by themselves, facilitate apoptosis by inducing morphological changes, loss of membrane potential and the production of reactive oxygen species in mitochondria (Kodiha *et al*., 2015). Hence, functionalisation of AuNPs with PLL combined their apoptosis-inducing effects, resulting in a greater apoptotic index compared to PLL on its own.

The greater apoptotic index for the PLL-AuNP:F*luc*-mRNA complex further indicates a normal cellular apoptosis defence mechanism which may be correlated to their excellent transfection efficiency and cytotoxicity. It has previously been reported that an increase in size, concentration and exposure time of cells to AuNPs results in a higher percentage of cells undergoing apoptosis (Mironava *et al*., 2010). It has been reported that concentrations of AuNPs up to 200 µg/ml exposed to MCF-7 cells displayed concentration-dependent

cytotoxicity through apoptosis detected by the upregulatated mRNA expression of p53, bax, caspase-3 and caspase-9 whereas the expression of anti-apoptotic bcl-2 mRNA was down-regulated (Selim and Hendi, 2012). Additionally, AuNPs show cell-type specificity for the induction of apoptosis as seen between the HEK293, Caco-2 and MCF-7 cell lines with the highest apoptotic index values seen in the Caco-2 cell line.

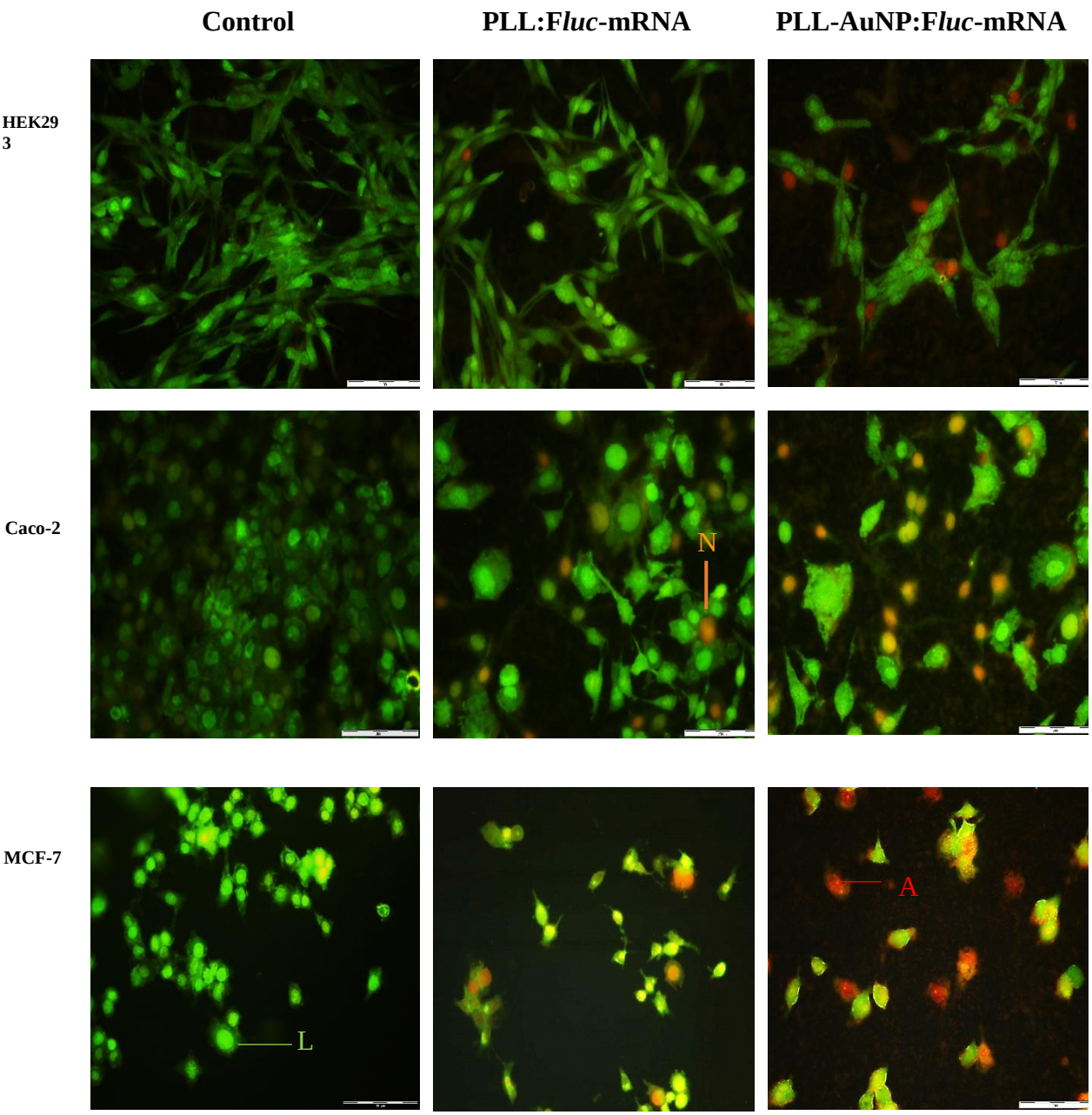


**Figure 4.12:** Fluorescence images obtained for the AO/EB apoptosis assay on HEK293, Caco-2 and MCF-7 cell lines at 20× magnification. A= apoptotic cells, N= necrotic cells, L= live cells.

**Table 4.5.** Apoptotic index values for each nanocomplex in the three cell lines.

| Cell line | Sample | Number of apoptotic cells | Total number of cells | Apoptotic index |
|---|---|---|---|---|
| **HEK293** | 1. PLL:F*luc*-mRNA | 1 | 83 | 0.012 |
| | 2. PLL-AuNP:F*luc*-mRNA | 9 | 68 | 0.132 |
| **Caco-2** | 1. PLL:F*luc*-mRNA | 12 | 62 | 0.194 |
| | 2. PLL-AuNP:F*luc*-mRNA | 21 | 44 | 0.477 |
| **MCF-7** | 1. PLL:F*luc*-mRNA | 5 | 31 | 0.161 |
| | 2. PLL-AuNP:F*luc*-mRNA | 11 | 26 | 0.423 |

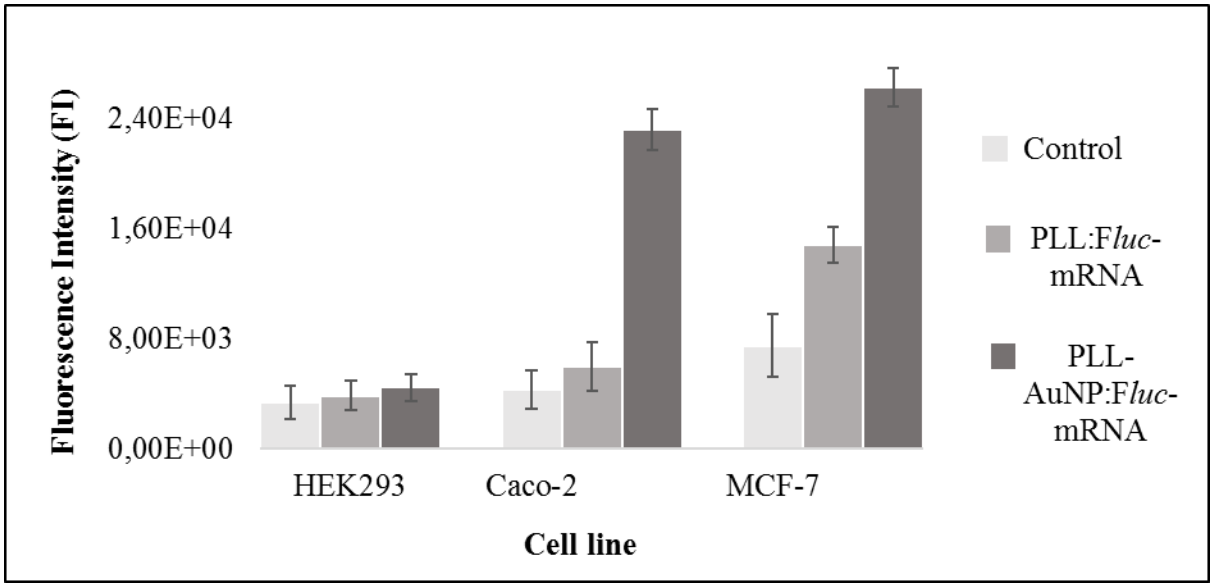


**Figure 4.13:** Fluorescence intensity (FI) in cell lines HEK293, Caco-2 and MCF-7 with and without treatment of the complexes. Data represented as mean ± SD (n=3).

## 4.6 Conclusion

The design and successful synthesis of PLL functionalised AuNP-based gene carriers have been shown to significantly influence transgene expression in the three cell lines tested. Gel retardation and florescence-based dye displacement assays demonstrated that these nanocomplexes were able to efficiently bind and condense F*luc*-mRNA at low concentrations. The small size excellent colloidal stability and "flower-like" morphology of the nanocomplexes resulted in a highly compact structure capable of efficiently protecting the mRNA against nucleases, facilitated safe delivery of the cargo with low cytotoxicity and

significant reporter gene expression. Furthermore, these nanocomplexes were able to induce apoptosis more so in the cancer cell lines (Caco-2 and MCF-7) than in the normal HEK293 cell line, indicating their potential as anti-tumour agents. These results indicate that these PLL-AuNPs have the potential to be effective gene delivery vectors, especially for cancer therapy. Since cytotoxicity, transfection efficiency and apoptosis induction are highly dependent on the formulation characteristics of the nanoparticles, a factor that will have to be seriously considered in future studies. It is recommended that formulations of the PLL-AuNPs of various concentrations, sizes, shapes and surface charges be prepared. Furthermore, studies of different environmental parameters such as exposure time and pH levels for the optimization of protocols could be critical in addition to assessing their biological activities in more cells lines *in vitro*.

## REFERENCES


Abou-Ghali, M., and Stiban, J. (2015). Regulation of ceramide channel formation and disassembly: Insights on the initiation of apoptosis. *Saudi journal of biological sciences, 22*(6), 760-772.

Amendola, V., and Meneghetti, M. (2009). Size evaluation of gold nanoparticles by UV− vis spectroscopy. *The Journal of Physical Chemistry C, 113*(11), 4277-4285.

Arjmandi, N., Van Roy, W., Lagae, L., and Borghs, G. (2012). Measuring the electric charge and zeta potential of nanometer-sized objects using pyramidal-shaped nanopores. *Analytical chemistry, 84*(20), 8490-8496.

Banerjee, A., Majumder, P., Sanyal, S., Singh, J., Jana, K., Das, C., and Dasgupta, D. (2014). The DNA intercalators ethidium bromide and propidium iodide also bind to core histones. *FEBS open bio, 4*(1), 251-259.

Bathrinarayanan, P. V., Thangavelu, D., Muthukumarasamy, V. K., Munusamy, C., and Gurunathan, B. (2013). Biological synthesis and characterization of intracellular gold nanoparticles using biomass of Aspergillus fumigatus. *Bulletin of Materials Science, 36*(7), 1201-1205.

Cancer Association of South Africa. (2016). Fact Sheet on a Health Profile of South Africa and Related Information.

Carr, B., and Wright, M. (2008). Nanoparticle tracking analysis. *Innovations in Pharmaceutical Technology, 26*, 38-40.

Chen, Y.-C., Lee, I.-L., Sung, Y.-M., and Wu, S.-P. (2013). Triazole functionalized gold nanoparticles for colorimetric Cr 3+ sensing. *Sensors and Actuators B: Chemical, 188*, 354-359.

Ciniglia, C., Pinto, G., Sansone, C., and Pollio, A. (2010). Acridine orange/Ethidium bromide double staining test: a simple in-vitro assay to detect apoptosis induced by phenolic compounds in plant cells. *Allelopathy J, 26*(2), 301-308.

Das, S. K., Dickinson, C., Lafir, F., Brougham, D. F., and Marsili, E. (2012). Synthesis, characterization and catalytic activity of gold nanoparticles biosynthesized with Rhizopus oryzae protein extract. *Green Chemistry, 14*(5), 1322-1334.

De Long, R. K., Reynolds, C. M., Malcolm, Y., Schaeffer, A., Severs, T., and Wanekaya, A. (2010). Functionalized gold nanoparticles for the binding, stabilization, and delivery of therapeutic DNA, RNA, and other biological macromolecules. *Nanotechnol Sci Appl, 3*(1), 53-63.

Elmore, S. (2007). Apoptosis: a review of programmed cell death. *Toxicologic pathology, 35*(4), 495-516.

Fan, F., and Wood, K. V. (2007). Bioluminescent assays for high-throughput screening. *Assay and drug development technologies, 5*(1), 127-136.

Filipe, V., Hawe, A., and Jiskoot, W. (2010). Critical evaluation of Nanoparticle Tracking Analysis (NTA) by NanoSight for the measurement of nanoparticles and protein aggregates. *Pharmaceutical research, 27*(5), 796-810.

Gascón, A. R., Pozo-Rodríguez, A. d., and Solinís, M. (2013). Non-viral delivery systems in gene therapy. *Gene therapy–tools and potential application*.

Ghosh, P., Han, G., De, M., Kim, C. K., and Rotello, V. M. (2008). Gold nanoparticles in delivery applications. *Advanced drug delivery reviews, 60*(11), 1307-1315.

Giljohann, D. A., Seferos, D. S., Patel, P. C., Millstone, J. E., Rosi, N. L., and Mirkin, C. A. (2007). Oligonucleotide loading determines cellular uptake of DNA-modified gold nanoparticles. *Nano letters, 7*(12), 3818-3821.

Giljohann, D. A., Seferos, D. S., Prigodich, A. E., Patel, P. C., and Mirkin, C. A. (2009). Gene regulation with polyvalent siRNA− nanoparticle conjugates. *Journal of the American Chemical Society, 131*(6), 2072-2073.

Hasenoehrl, C., Alexander, C. M., Azzarelli, N. N., and Dabrowiak, J. C. (2012). Enhanced detection of gold nanoparticles in agarose gel electrophoresis. *Electrophoresis, 33*(8), 1251-1254.

Huefner, A., Septiadi, D., Wilts, B. D., Patel, I. I., Kuan, W.-L., Fragniere, A., Mahajan, S. (2014). Gold nanoparticles explore cells: Cellular uptake and their use as intracellular probes. *Methods, 68*(2), 354-363.

Ivanov, M. R. (2011). Covalently functionalized gold nanoparticles: synthesis, characterization, and integration into capillary electrophoresis.

Jain, P. K., Lee, K. S., El-Sayed, I. H., and El-Sayed, M. A. (2006). Calculated absorption and scattering properties of gold nanoparticles of different size, shape, and composition: applications in biological imaging and biomedicine. *The Journal of Physical Chemistry B, 110*(14), 7238-7248.

Jang, K. J., Lee, H., Jin, H. L., Park, Y., and Nam, J. M. (2009). Restriction-Enzyme-Coded Gold-Nanoparticle Probes for Multiplexed DNA Detection. *Small, 5*(23), 2665-2668.

Jin, L., Zeng, X., Liu, M., Deng, Y., and He, N. (2014). Current progress in gene delivery technology based on chemical methods and nano-carriers. *Theranostics, 4*(3), 240-255.

Joshi, H., Shirude, P. S., Bansal, V., Ganesh, K., and Sastry, M. (2004). Isothermal titration calorimetry studies on the binding of amino acids to gold nanoparticles. *The Journal of Physical Chemistry B, 108*(31), 11535-11540.

Kodiha, M., Wang, Y. M., Hutter, E., Maysinger, D., and Stochaj, U. (2015). Off to the organelles—killing cancer cells with targeted gold nano-particles. *Theranostics, 5*(4), 357-370.

Liu, K., Liu, P.-c., Liu, R., and Wu, X. (2015). Dual AO/EB staining to detect apoptosis in osteosarcoma cells compared with flow cytometry. *Medical science monitor basic research, 21*, 15.

Lodish, H., Berk, A., Zipursky, S. L., Matsudaira, P., Baltimore, D., and Darnell, J. (2000). DNA Damage and Repair and Their Role in Carcinogenesis.

Lonza Rockland Inc. (2007). Instructions for using SYBR® Green II Nucleic Acid Gel Stain

Manjila, S. B., Baby, J. N., Bijin, E. N., Constantine, I., Pramod, K., and Valsalakumari, J. (2013). Novel gene delivery systems. *International journal of pharmaceutical investigation, 3*(1), 1.

Matsui, A., Uchida, S., Ishii, T., Itaka, K., and Kataoka, K. (2015). Messenger RNA-based therapeutics for the treatment of apoptosis-associated diseases. *Scientific reports, 5*.

Mironava, T., Hadjiargyrou, M., Simon, M., Jurukovski, V., and Rafailovich, M. H. (2010). Gold nanoparticles cellular toxicity and recovery: effect of size, concentration and exposure time. *Nanotoxicology, 4*(1), 120-137.

Nayerossadat, N., Maedeh, T., and Ali, P. A. (2012). Viral and nonviral delivery systems for gene delivery. *Advanced biomedical research, 1*(1), 27.

Pedrosa, P., Vinhas, R., Fernandes, A., and Baptista, P. V. (2015). Gold nanotheranostics: proof-of-concept or clinical tool? *Nanomaterials, 5*(4), 1853-1879.

Philip, D. (2008). Synthesis and spectroscopic characterization of gold nanoparticles. *Spectrochimica Acta Part A: Molecular and Biomolecular Spectroscopy, 71*(1), 80-85.

Polte, J. (2015). Fundamental growth principles of colloidal metal nanoparticles–a new perspective. *CrystEngComm, 17*(36), 6809-6830.

Radwan, S. H., and Azzazy, H. M. (2009). Gold nanoparticles for molecular diagnostics. *Expert review of molecular diagnostics, 9*(5), 511-524.

Ramakrishna, D., and Rao, P. (2011). Nanoparticles: Is Toxicity a Concern? *EJIFCC, 22*(4), 92.

Ribble, D., Goldstein, N. B., Norris, D. A., and Shellman, Y. G. (2005). A simple technique for quantifying apoptosis in 96-well plates. *BMC biotechnology, 5*(1), 12.

Rozenberg, M., and Shoham, G. (2007). FTIR spectra of solid poly-l-lysine in the stretching NH mode range. *Biophysical chemistry, 125*(1), 166-171.

Sandhu, K. K., McIntosh, C. M., Simard, J. M., Smith, S. W., and Rotello, V. M. (2002). Gold nanoparticle-mediated transfection of mammalian cells. *Bioconjugate chemistry, 13*(1), 3-6.

Sau, S. P., Kumar, P., Sharma, P. K., and Hrdlicka, P. J. (2012). Fluorescent intercalator displacement replacement (FIDR) assay: determination of relative thermodynamic and kinetic parameters in triplex formation—a case study using triplex-forming LNAs. *Nucleic acids research, 40*(21), e162-e162.

Segura, T., and Shea, L. D. (2001). Materials for non-viral gene delivery. *Annual Review of Materials Research, 31*(1), 25-46.

Selim, M. E., and Hendi, A. A. (2012). Gold nanoparticles induce apoptosis in MCF-7 human breast cancer cells. *Asian Pacific Journal of Cancer Prevention, 13*(4), 1617-1620.

Shan, Y., Luo, T., Peng, C., Sheng, R., Cao, A., Cao, X., Shi, X. (2012). Gene delivery using dendrimer-entrapped gold nanoparticles as nonviral vectors. *Biomaterials, 33*(10), 3025-3035.

Shen, L., Rapenne, L., Chaudouet, P., Ji, J., and Picart, C. (2012). In situ synthesis of gold nanoparticles in exponentially-growing layer-by-layer films. *Journal of colloid and interface science, 388*(1), 56-66.

Sivaramakrishnan, C., Jositta S. J., and Yadavalli, T. (2014). Surface functionalization of gold nanoparticles for targeted drug delivery. *International Journal of ChemTech Research, 7*(3), 1198-1205.

Stefanneli, C., Maddalena, Z., Bonavita, F., Flamigini, F., Zambonin, L., Landi, L., Calderera, C. M. (2000). Polyamines directly induce release of cytochrome c from heart mitochondria. *Biochemical Journal, 347*(3), 875-880.

Stobiecka, M., and Hepel, M. (2011). Double-shell gold nanoparticle-based DNA-carriers with poly-L-lysine binding surface. *Biomaterials, 32*(12), 3312-3321.

Symonds, P., Murray, J. C., Hunter, A. C., Debska, G., Szewczyk, A., and Moghimi, S. M. (2005). Low and high molecular weight poly (l-lysine) s/poly (l-lysine)–DNA complexes initiate mitochondrial-mediated apoptosis differently. *FEBS letters, 579*(27), 6191-6198.

Szpunar, J. (2005). Advances in analytical methodology for bioinorganic speciation analysis: metallomics, metalloproteomics and heteroatom-tagged proteomics and metabolomics. *Analyst, 130*(4), 442-465.

Turkevich, J., Stevenson, P. C., and Hillier, J. (1951). A study of the nucleation and growth processes in the synthesis of colloidal gold. *Discussions of the Faraday Society, 11*, 55-75.

Van Doren, E. A., De Temmerman, P.-J. R., Francisco, M. A. D., and Mast, J. (2011). Determination of the volume-specific surface area by using transmission electron tomography for characterization and definition of nanomaterials. *Journal of nanobiotechnology, 9*(1), 1.

Verma, H. N., Singh, P., and Chavan, R. (2014). Gold nanoparticle: synthesis and characterization. *Veterinary world, 7*(2), 72-77.

Wu, Y., Hussain, M., and Fassihi, R. (2005). Development of a simple analytical methodology for determination of glucosamine release from modified release matrix tablets. *Journal of pharmaceutical and biomedical analysis, 38*(2), 263-269.

Yeh, Y.-C., Creran, B., and Rotello, V. M. (2012). Gold nanoparticles: preparation, properties, and applications in bionanotechnology. *Nanoscale, 4*(6), 1871-1880.

Zhou, J., Ralston, J., Sedev, R., and Beattie, D. A. (2009). Functionalized gold nanoparticles: synthesis, structure and colloid stability. *Journal of colloid and interface science, 331*(2), 251-262.

Zhuang, B., Li, Z., Pang, J., Li, W., Huang, P., Wang, J., Ye, X. (2015). Nanocomplexation of thrombin with cationic amylose derivative for improved stability and hemostatic efficacy. *Int J Nanomedicine, 10,* 939-947.

# CHAPTER FIVE

## CONCLUSION

The use of non-viral gene carriers for the treatment of heterogenous diseases such as cancer is an exponentially growing field. Despite significant efforts made towards the development of these carriers, their biological safety, stability and delivery efficiency are limited. Hence, the need for novel gene delivery strategies that will overcome the challenges faced by current systems. Gold nanoparticles (AuNPs) have been applied in diagnostic and photothermal treatment of cancer, showing great promise as a gene delivery vehicle as they provide multi-functional platforms for the delivery of a variety of therapeutic biomolecules. In addition, AuNPs are biocompatible, allowing for surface modification of cationic polymers which ensure electrostatic binding of nucleic acids without compromising their function, cellular uptake and release of the therapeutic cargo through endocytotic mechanisms. This study, investigated the delivery of mRNAs as opposed to the conventional pDNA since mRNA molecules have been reported as being more advantageous in terms of safety and their ability to overcome intracellular barriers. This study encompassed the development of chitosan (CS) and poly-l-lysine (PLL) functionalised AuNPs to effect electrostatic binding of mRNA molecules (F*luc*-mRNA) and to investigate gene delivery and transgene expression in three mammalian cell lines. The outcomes of this study clearly indicate the potential of these delivery systems for future use in genetic vaccination and immunotherapy of cancer.

Overall, AuNPs were successfully synthesized and functionalised with CS and PLL. Morphologically, the AuNPs appeared disperse, homogenous, spherical and formed agglomerates upon functionalization. All nanoparticle and nanocomplexes were less than 100 nm in size, ensuring efficient cellular uptake. Furthermore, zeta potential analysis indicated the high colloidal stability of the AuNPs after functionalisation, attributing to their efficient cellular uptake and intracellular processing. Gel retardation and dye displacement assays, confirmed the good binding and compacting of the mRNA by the nanoparticles. Furthermore, the nanocomplexes did not lose their integrity after being subjected to nuclease digestion.

*In vitro* cytotoxicity studies indicated that the functionalized nanocomplexes were relatively non-toxic and well tolerated in all three cell lines. Furthermore, they were able to elicit significant transgene expression in the three cell lines tested with highest expression recorded in the Caco-2 cell line.

These functionalised nanocomplexes were able to induce greater apoptosis in the cancer cell lines (Caco-2 and MCF-7) than in the normal HEK293 cell line, confirming their cell specificity. Overall, the functionalised nanocomplexes proved to be more stable, less toxic and more efficient than the individual cationic polymer:mRNA complexes, indicating that AuNPs functionalisation with CS and PLL enhanced the properties and biological functions of the nanocomplexes. Hence, these CS/PLL-AuNPs have the potential to be effective gene delivery systems especially for cancer treatment and results obtained thus far augur well for their use in future *in vivo* studies.

Overall, the aims and objectives of this study were successfully achieved. However, further optimizations need to be considered before these nanocomplexes can be translated into clinical applications. There are several possible recommendations that can be addressed in future studies in this area.

## 5.1 Future recommendations

- To fully investigate the functionalisation of AuNPs with other CPs at different CP molecular weights and in different ratio formulations.
- To improve the pharmacokinetics of the nanocomplexes by grafting with the steric stabilizing polymer, polyethylenegycol (PEG) or other suitable ligands.
- Cytotoxicity and transfection studies revealed that the CP-AuNPs exhibited dose-dependent and cell-type specific effects, indicating the requirement for broader concentration ranges and more cell types to be tested.
- In depth studies of the fate of the nanoparticles, their mechanisms of cellular uptake, bio-distribution and biodegradability should be undertaken.
- Since these nanocomplexes showed cell specificity with respect to transfection efficiency, the conjugation of targeting ligands or antibodies could be investigated.

# APPENDIX A1: ICP results

Method: Hari gold 27052016 Page 29 Date: 5/27/2016 5:30:33 PM

Logged In Analyst (Original) : Administrator
Initial Sample Wt: Initial Sample Vol:
Dilution: Sample Prep Vol:

Replicate Data: 2.5ppm

| Repl# | Analyte | Net Intensity | Corrected Intensity | Calib. Conc. | Units | Analysis Time |
|---|---|---|---|---|---|---|
| 1 | Au 267.595 | 26685.8 | 26707.7 | [2.5] | mg/L | 15:24:16 |
| 1 | Au 242.795 | 54380.6 | 54576.9 | [2.5] | mg/L | 15:24:16 |
| 1 | Au 208.209 | 6612.7 | 6570.5 | [2.5] | mg/L | 15:24:16 |
| 2 | Au 267.595 | 26329.8 | 26351.8 | [2.5] | mg/L | 15:24:17 |
| 2 | Au 242.795 | 53686.9 | 53883.3 | [2.5] | mg/L | 15:24:17 |
| 2 | Au 208.209 | 6556.9 | 6514.7 | [2.5] | mg/L | 15:24:17 |
| 3 | Au 267.595 | 26219.8 | 26241.7 | [2.5] | mg/L | 15:24:19 |
| 3 | Au 242.795 | 53688.7 | 53885.1 | [2.5] | mg/L | 15:24:19 |
| 3 | Au 208.209 | 6594.0 | 6551.8 | [2.5] | mg/L | 15:24:19 |

Mean Data: 2.5ppm

| Analyte | Mean Corrected Intensity | Std.Dev. | RSD | Calib Conc. | Units |
|---|---|---|---|---|---|
| Au 267.595 | 26433.7 | 243.58 | 0.92% | [2.5] | mg/L |
| Au 242.795 | 54115.1 | 399.97 | 0.74% | [2.5] | mg/L |
| Au 208.209 | 6545.7 | 28.41 | 0.43% | [2.5] | mg/L |

Calibration Summary

| Analyte | Stds. | Equation | Intercept | Slope | Curvature | Corr. Coef. | Reslope |
|---|---|---|---|---|---|---|---|
| Au 267.595 | 5 | Lin, Calc Int | -7.0 | 10560 | 0.00000 | 0.999863 | |
| Au 242.795 | 5 | Lin, Calc Int | -183.0 | 21630 | 0.00000 | 0.999874 | |
| Au 208.209 | 5 | Lin, Calc Int | -44.3 | 2631 | 0.00000 | 0.999762 | |

Analysis Begun

Start Time: 5/27/2016 5:26:50 PM Plasma On Time: 5/27/2016 4:57:51 PM
Logged In Analyst: Administrator Technique: ICP Continuous
Spectrometer Model: Optima 5300 DV, S/N 077N5111401Autosampler Model: AS-93plus

Sample Information File: C:\pe\Administrator\Sample Information\Hari\Hari gold 27052016new.sif
Batch ID: Hari gold sample new
Results Data Set: Hari 27052016 new
Results Library: C:\pe\Administrator\Results\Results.mdb

Sequence No.: 1 Autosampler Location: 10
Sample ID: Gold sample new 27052016 Date Collected: 5/27/2016 5:26:50 PM
Analyst: Data Type: Original
Initial Sample Wt: Initial Sample Vol:
Dilution: Sample Prep Vol:

Replicate Data: Gold sample new 27052016

| Repl# | Analyte | Net Intensity | Corrected Intensity | Calib. Conc. | Units | Sample Conc. | Units | Analysis Time |
|---|---|---|---|---|---|---|---|---|
| 1 | Au 267.595 | 95894.2 | 95916.1 | 9.081 | mg/L | 9.081 | mg/L | 17:27:58 |
| 1 | Au 242.795 | 191092.8 | 191289.1 | 8.850 | mg/L | 8.850 | mg/L | 17:27:58 |
| 1 | Au 208.209 | 23415.6 | 23373.4 | 8.902 | mg/L | 8.902 | mg/L | 17:27:58 |

Mean Data: Gold sample new 27052016

| Analyte | Mean Corrected Intensity | Calib. Conc. | Units | Std.Dev. | Sample Conc. | Units | Std.Dev. | RSD |
|---|---|---|---|---|---|---|---|---|
| Au 267.595 | 95916.1 | 9.081 | mg/L | | 9.081 | mg/L | | |
| Au 242.795 | 191289.1 | 8.850 | mg/L | | 8.850 | mg/L | | |
| Au 208.209 | 23373.4 | 8.902 | mg/L | | 8.902 | mg/L | | |

**ICP spectroscopy analysis report of synthesized AuNP solution**

# APPENDIX A2: FTIR spectra

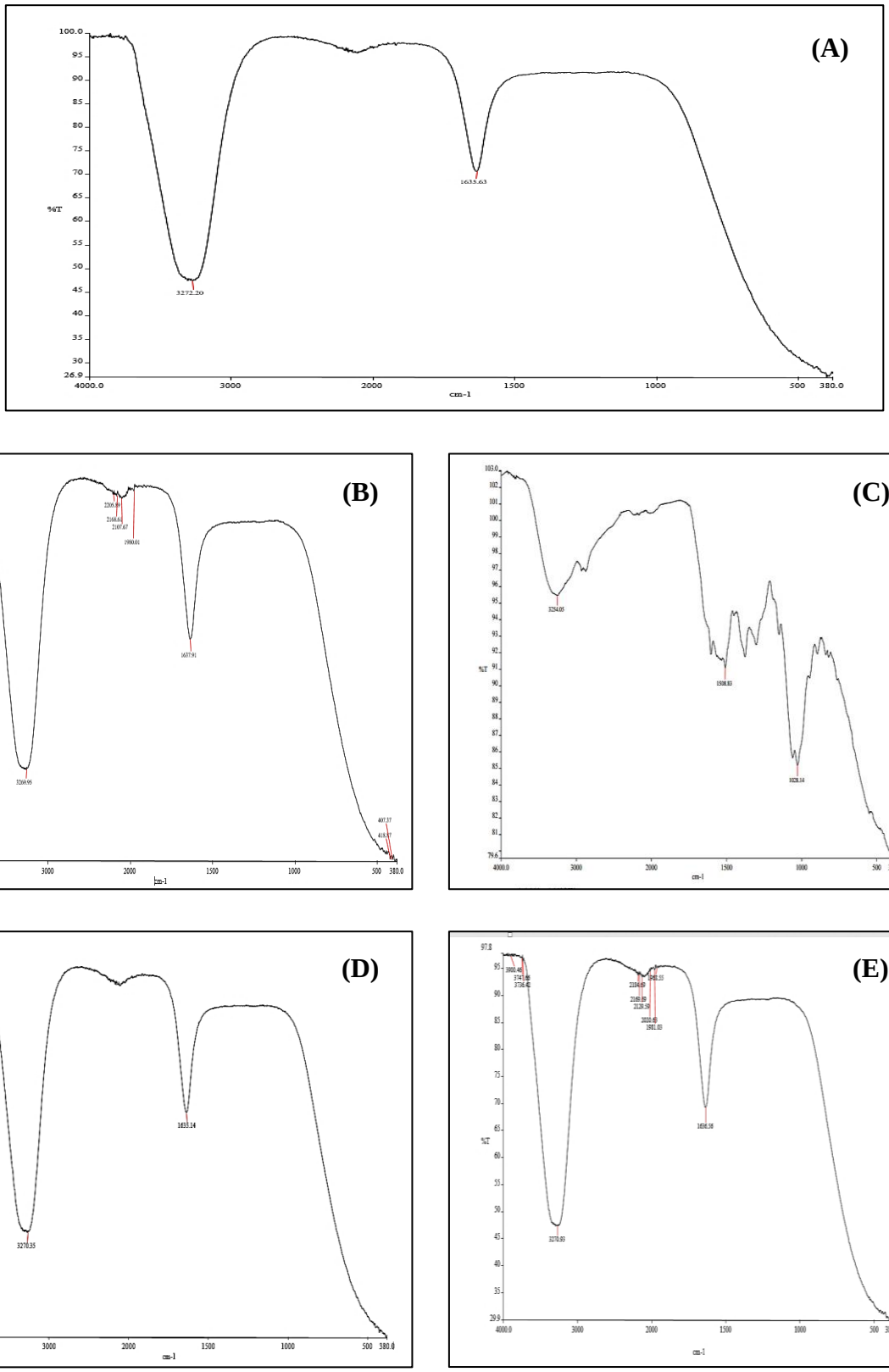


**FTIR absorption spectra of (A) AuNP, (B) CS, (C) CS-AuNP, (D) PLL and (E) PLL-AuNP solutions**

# APPENDIX B: NTA results

NANOSIGHT

Gold 1 2015-08-19 14-25-43

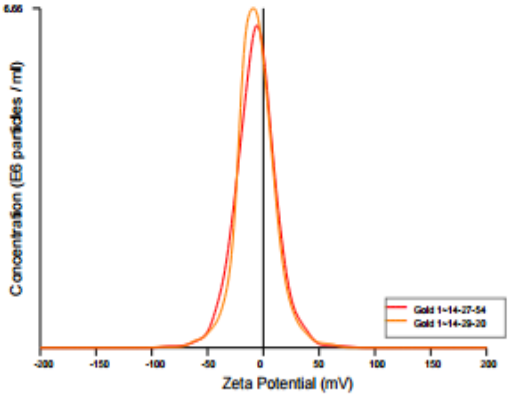


Zeta Potential / Concentration graph for Experiment:
Gold 1 2015-08-19 14-25-43

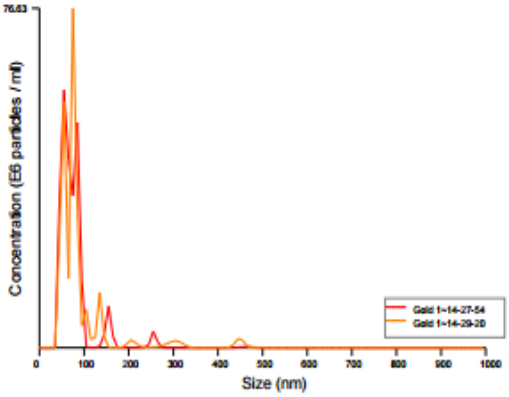


Size / Concentration graph for Experiment:
Gold 1 2015-08-19 14-25-43

**Included Files**

Gold 1 2015-08-19 14-27-54
Gold 1 2015-08-19 14-29-20

**Details**

| | |
|---|---|
| NTA Version: | NTA 3.0 0069 |
| Script Used: | SOP Zeta Measurement 02-25-43PM 19Aug2015.txt |
| Time Captured: | 14:25:43 19/08/2015 |
| Operator: | MSc |
| Pre-treatment: | |
| Sample Name: | Gold |
| Diluent: | Water |
| Remarks: | |

**Capture Settings**

| | |
|---|---|
| Camera Type: | SCMOS |
| Camera Level: | 12 |
| Slider Shutter: | 600 |
| Slider Gain: | 350 |
| FPS | 25.0 |
| Number of Frames: | 1498 |
| Temperature: | 25.0 - 25.0 °C |
| Viscosity: | (Water) 0.9 cP |
| Dilution factor: | Dilution not recorded |

**Analysis Settings**

| | |
|---|---|
| Detect Threshold: | 5 |
| Blur Size: | Auto |
| Max Jump Distance: | Auto: 17.4 - 19.4 pix |

**Results**

Stats: Mean +/- Standard Error

| | |
|---|---|
| Mean: | 78.8 +/- 5.7 nm |
| Mode: | 65.9 +/- 9.8 nm |
| SD: | 55.5 +/- 12.7 nm |
| D10: | 38.7 +/- 1.1 nm |
| D50: | 61.2 +/- 2.6 nm |
| D90: | 106.2 +/- 18.5 nm |
| Concentration: | 2.55e+008 +/- 1.69e+006 particles/ml |
| | 13.0 +/- 0.1 particles/frame |
| | 14.4 +/- 0.1 centres/frame |

**Zeta Settings and Results**

Parabola fit complete

| | |
|---|---|
| Adjusted r-square: | 1.00 |
| Applied Voltage: | 24.0 V |
| Dielectric Constant: | 80.00 |
| AverageCurrent: | 0.55 - 0.59 µA |

Stats: Mean +/- Standard Error

| | |
|---|---|
| Mean: | -7.1 +/- 0.0 mV |
| Mode: | -7.3 +/- 1.6 mV |
| SD: | 18.2 +/- 0.6 mV |
| D10: | -28.7 +/- 1.8 mV |
| D50: | -7.9 +/- 0.4 mV |
| D90: | 14.0 +/- 0.8 mV |

**NTA and zeta potential analysis report of AuNP solution**

**NANOSIGHT**

## Gold chitosan 1 2015-08-19 15-35-34

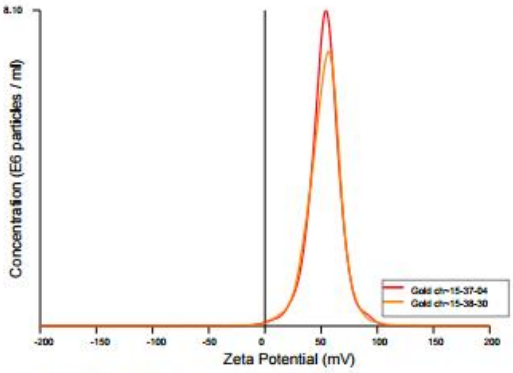


Zeta Potential / Concentration graph for Experiment:
Gold chitosan 1 2015-08-19 15-35-34

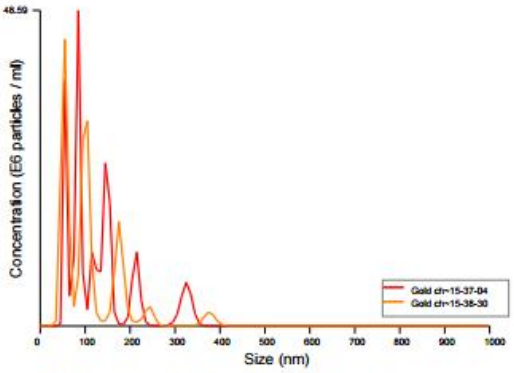


FTLA Size / Concentration graph for Experiment:
Gold chitosan 1 2015-08-19 15-35-34

**Included Files**

Gold chitosan 1 2015-08-19 15-37-04
Gold chitosan 1 2015-08-19 15-38-30

**Details**

| | |
|---|---|
| NTA Version: | NTA 3.0 0069 |
| Script Used: | SOP Zeta Measurement 03-35-34PM 19Aug2015.txt |
| Time Captured: | 15:35:34 19/08/2015 |
| Operator: | MSc |
| Pre-treatment: | |
| Sample Name: | Gold chitosan |
| Diluent: | Water |
| Remarks: | |

**Capture Settings**

| | |
|---|---|
| Camera Type: | SCMOS |
| Camera Level: | 12 |
| Slider Shutter: | 600 |
| Slider Gain: | 350 |
| FPS | 25.0 |
| Number of Frames: | 1498 |
| Temperature: | 25.0 ºC |
| Viscosity: | (Water) 0.889 - 0.889 cP |
| Dilution factor: | Dilution not recorded |

**Analysis Settings**

| | |
|---|---|
| Detect Threshold: | 3 |
| Blur Size: | Auto |
| Max Jump Distance: | Auto: 15.5 - 18.5 pix |

**Results**

| | |
|---|---|
| Stats: Mean +/- Standard Error | |
| Mean: | 116.7 +/- 11.1 nm |
| Mode: | 69.6 +/- 15.2 nm |
| SD: | 73.3 +/- 3.3 nm |
| D10: | 42.9 +/- 3.2 nm |
| D50: | 94.9 +/- 8.8 nm |
| D90: | 196.2 +/- 19.9 nm |
| Concentration: | 2.28e+008 +/- 5.38e+006 particles/ml |
| | 11.6 +/- 0.3 particles/frame |
| | 13.5 +/- 0.6 centres/frame |

**Zeta Settings and Results**

| | |
|---|---|
| Parabola fit complete | |
| Adjusted r-square: | 0.99 |
| Applied Voltage: | 24.0 V |
| Dielectric Constant: | 80.00 |
| AverageCurrent: | 1.92 - 1.95 µA |
| Stats: Mean +/- Standard Error | |
| Mean: | 52.7 +/- 0.1 mV |
| Mode: | 55.5 +/- 1.2 mV |
| SD: | 15.5 +/- 0.3 mV |
| D10: | 34.2 +/- 0.8 mV |
| D50: | 52.9 +/- 0.2 mV |
| D90: | 68.9 +/- 0.1 mV |

**NTA and zeta potential analysis report of CS-AuNP solution**

NANOSIGHT

Capture 2015-10-01 11-28-11

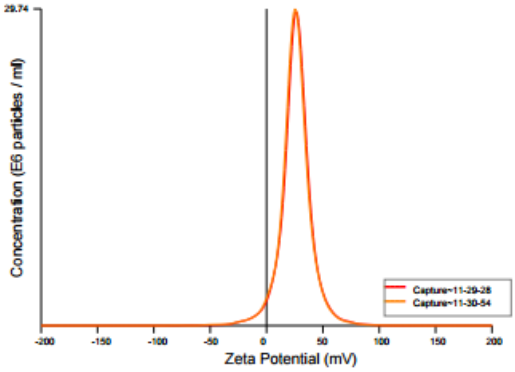


Zeta Potential / Concentration graph for Experiment:
Capture 2015-10-01 11-28-11

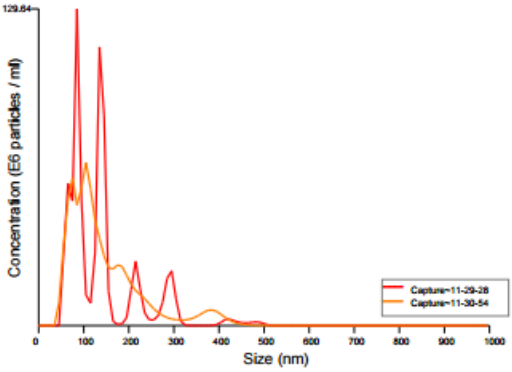


Size / Concentration graph for Experiment:
Capture 2015-10-01 11-28-11

**Included Files**

Capture 2015-10-01 11-29-28
Capture 2015-10-01 11-30-54

**Details**

| | |
|---|---|
| NTA Version: | NTA 3.0 0069 |
| Script Used: | SOP Zeta Measurement 11-28-11AM 01Oct2015.txt |
| Time Captured: | 11:28:11 01/10/2015 |
| Operator: | Shandre |
| Pre-treatment: | |
| Sample Name: | |
| Diluent: | WATER |
| Remarks: | |

**Capture Settings**

| | |
|---|---|
| Camera Type: | SCMOS |
| Camera Level: | 12 |
| Slider Shutter: | 600 |
| Slider Gain: | 350 |
| FPS | 25.0 |
| Number of Frames: | 1498 |
| Temperature: | 25.0 ºC |
| Viscosity: | (Water) 0.9 cP |
| Dilution factor: | Dilution not recorded |

**Analysis Settings**

| | |
|---|---|
| Detect Threshold: | 7 |
| Blur Size: | Auto |
| Max Jump Distance: | Auto: 12.8 - 14.5 pix |

**Results**

Stats: Mean +/- Standard Error

| | |
|---|---|
| Mean: | 137.6 +/- 2.2 nm |
| Mode: | 95.0 +/- 9.9 nm |
| SD: | 82.3 +/- 1.5 nm |
| D10: | 57.1 +/- 0.7 nm |
| D50: | 114.2 +/- 5.9 nm |
| D90: | 254.2 +/- 12.8 nm |
| Concentration: | 7.43e+008 +/- 1.99e+006 particles/ml |
| | 37.7 +/- 0.1 particles/frame |
| | 44.2 +/- 0.5 centres/frame |

**Zeta Settings and Results**

Parabola fit complete

| | |
|---|---|
| Adjusted r-square: | 1.00 |
| Applied Voltage: | 24.0 V |
| Dielectric Constant: | 80.00 |
| AverageCurrent: | 1.05 - 1.10 µA |

Stats: Mean +/- Standard Error

| | |
|---|---|
| Mean: | 25.4 +/- 0.4 mV |
| Mode: | 25.9 +/- 0.5 mV |
| SD: | 14.5 +/- 0.1 mV |
| D10: | 9.5 +/- 0.3 mV |
| D50: | 25.1 +/- 0.4 mV |
| D90: | 40.5 +/- 0.3 mV |

**NTA and zeta potential analysis report of CS-AuNP:F*luc*-mRNA solution**

NANOSIGHT

AuNP-PLL 2015-10-09 12-54-36

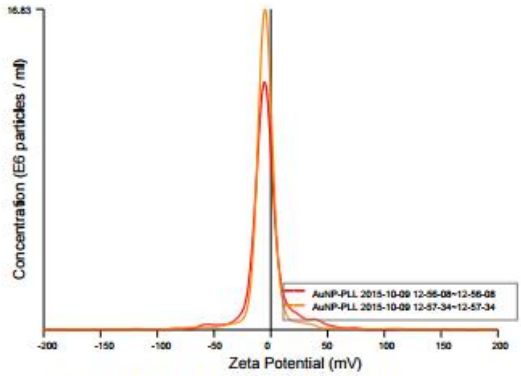


Zeta Potential / Concentration graph for Experiment:
AuNP-PLL 2015-10-09 12-54-36

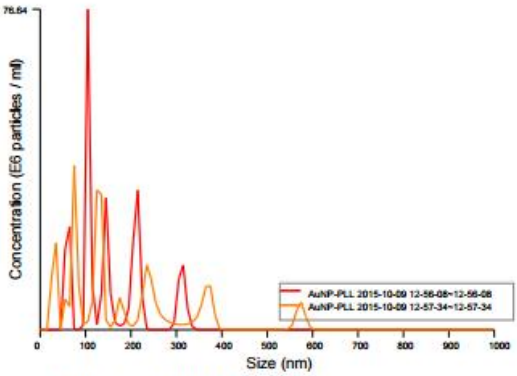


Size / Concentration graph for Experiment:
AuNP-PLL 2015-10-09 12-54-36

**Included Files**

AuNP-PLL 2015-10-09 12-56-08
AuNP-PLL 2015-10-09 12-57-34

**Details**

| | |
|---|---|
| NTA Version: | NTA 3.0 0069 |
| Script Used: | SOP Zeta Measurement 12-54-36PM 09Oct2015.txt |
| Time Captured: | 12:54:36 09/10/2015 |
| Operator: | Shandre |
| Pre-treatment: | |
| Sample Name: | AuNP-PLL |
| Diluent: | water |
| Remarks: | |

**Capture Settings**

| | |
|---|---|
| Camera Type: | SCMOS |
| Camera Level: | 7 |
| Slider Shutter: | 250 |
| Slider Gain: | 250 |
| FPS | 25.0 |
| Number of Frames: | 1498 |
| Temperature: | 25.0 - 25.0 ºC |
| Viscosity: | (Water) 0.9 cP |
| Dilution factor: | Dilution not recorded |

**Analysis Settings**

| | |
|---|---|
| Detect Threshold: | 3 |
| Blur Size: | Auto |
| Max Jump Distance: | Auto: 13.7 - 19.0 pix |

**Results**

Stats: Mean +/- Standard Error

| | |
|---|---|
| Mean: | 165.3 +/- 14.1 nm |
| Mode: | 90.4 +/- 15.0 nm |
| SD: | 107.4 +/- 30.8 nm |
| D10: | 41.3 +/- 12.6 nm |
| D50: | 127.0 +/- 3.6 nm |
| D90: | 327.1 +/- 33.7 nm |
| Concentration: | 2.94e+008 +/- 5.93e+006 particles/ml |
| | 14.9 +/- 0.3 particles/frame |
| | 90.3 +/- 21.8 centres/frame |

**Zeta Settings and Results**

Parabola fit complete (poor quality fit)

| | |
|---|---|
| Adjusted r-square: | 0.82 |
| Applied Voltage: | 24.0 V |
| Dielectric Constant: | 80.00 |
| AverageCurrent: | 11.31 - 12.73 µA |

Stats: Mean +/- Standard Error

| | |
|---|---|
| Mean: | -4.9 +/- 0.3 mV |
| Mode: | -5.3 +/- 0.2 mV |
| SD: | 20.1 +/- 0.7 mV |
| D10: | -17.7 +/- 1.6 mV |
| D50: | -5.9 +/- 0.1 mV |
| D90: | 9.0 +/- 3.9 mV |

**NTA and zeta potential analysis report of PLL-AuNP solution**

NANOSIGHT

AuNP-PLL mRNA 2015-11-11 12-38-09

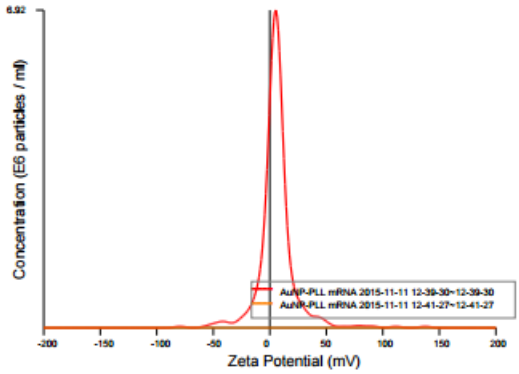


Zeta Potential / Concentration graph for Experiment:
AuNP-PLL mRNA 2015-11-11 12-38-09

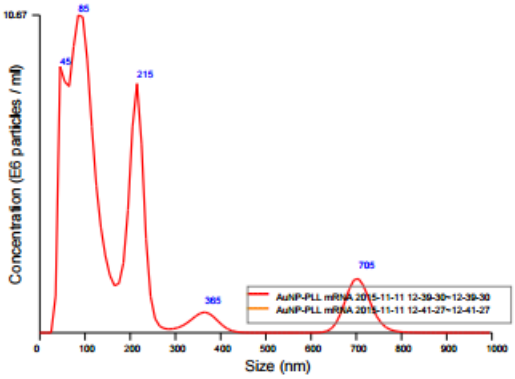


Size / Concentration graph for Experiment:
AuNP-PLL mRNA 2015-11-11 12-38-09

**Included Files**

AuNP-PLL mRNA 2015-11-11 12-39-30
AuNP-PLL mRNA 2015-11-11 12-41-27

**Details**

| | |
|---|---|
| NTA Version: | NTA 3.0 0069 |
| Script Used: | SOP Zeta Measurement 12-38-09PM 11Nov2015.txt |
| Time Captured: | 12:38:09 11/11/2015 |
| Operator: | Shandre |
| Pre-treatment: | |
| Sample Name: | AuNP-PLL mRNA |
| Diluent: | Water |
| Remarks: | |

**Capture Settings**

| | |
|---|---|
| Camera Type: | SCMOS |
| Camera Level: | 9 |
| Slider Shutter: | 450 |
| Slider Gain: | 250 |
| FPS | 25.0 |
| Number of Frames: | 2248 |
| Temperature: | 25.0 - 25.0 ºC |
| Viscosity: | (Water) 0.9 cP |
| Dilution factor: | Dilution not recorded |

**Analysis Settings**

| | |
|---|---|
| Detect Threshold: | 22 |
| Blur Size: | Auto |
| Max Jump Distance: | Auto: 14.0 pix |

**Results**

Stats: Mean +/- Standard Error

| | |
|---|---|
| Mean: | 178.7 +/- 0.0 nm |
| Mode: | 89.4 +/- 0.0 nm |
| SD: | 177.7 +/- 0.0 nm |
| D10: | 44.7 +/- 0.0 nm |
| D50: | 105.2 +/- 0.0 nm |
| D90: | 363.9 +/- 0.0 nm |
| Concentration: | 7.25e+007 +/- 6.86e+007 particles/ml |
| | 3.7 +/- 3.5 particles/frame |
| | 9.1 +/- 8.4 centres/frame |

**Zeta Settings and Results**

Parabola fit complete (poor quality fit)

| | |
|---|---|
| Adjusted r-square: | 0.84 |
| Applied Voltage: | 24.0 V |
| Dielectric Constant: | 80.00 |
| AverageCurrent: | 0.60 - 0.68 µA |

Stats: Mean +/- Standard Error

| | |
|---|---|
| Mean: | 2.9 +/- 2.9 mV |
| Mode: | -97.1 +/- 102.4 mV |
| SD: | 9.1 +/- 9.1 mV |
| D10: | -4.6 +/- 4.6 mV |
| D50: | 2.2 +/- 2.2 mV |
| D90: | 9.8 +/- 9.8 mV |

**NTA and zeta potential analysis report of PLL-AuNP:F*luc*-mRNA solution**

# APPENDIX C: Conference Presentation


**Certificate of attendance for the 25th South African Society of Biochemistry and Molecular Biology (SASBMB) congress, East London, Eastern Cape 10th-14th July 2016.**

**First place poster prize in biotechnology awarded at the 25th SASBMB congress, East London, Eastern Cape 10th-14th July 2016.**